



GREDER

Green RE-usable DEbris Remover



Authors :

Tim **Lewis**

Alina **Trifunovic**

Lukas **Krause**

Alexis **Rolin**

Julien **Huynh**

Supervising professor :

Prof. Dr.-Ing. Uwe *Apel*

Version 1.0.0
February 27, 2020

Contents

1 Schedule	2
1.1 Initial Schedule	2
1.2 Final schedule – comparison as planned and as achieved	3
2 Requirements	5
3 Launcher requirements and launch envelope	7
4 Mission analysis	9
4.1 Mission Summary	9
4.1.1 Phase 1	9
4.1.2 Phase 2	11
4.2 Delta-V reduction	11
5 Satellite capturing process	16
5.1 Choice of the process	16
5.2 Magnetic solution	17
5.2.1 Assumptions	17
5.3 Sketching and Calculations	17
6 Heat shield	21
6.1 Thermal protection system	21
6.2 First estimation	21
6.3 Material choice	22
6.4 Lift and drag	23
6.5 Aerobraking altitude	25
6.6 Simplifications	26
6.7 Heat shield interface	27
6.8 Radiative cooling	28
6.9 Final heat shield mass	29

7 Propellant selection	31
7.1 Options overview	32
7.2 Detailed comparison between MON/MMH and H ₂ O ₂ /RP-1	33
7.3 H ₂ O ₂ /RP-1 feasibility check	36
7.4 Summary	37
8 Vehicle architecture	38
9 Mass model and burning times	41
9.1 Mass Budget - First Iteration	41
9.1.1 Coefficients & Masses after steps	41
9.1.2 Global equation between m_{UP} and $m_{initial}$	41
9.1.3 First iteration of mass budget	42
9.2 Mass Budget - Second iteration	45
9.2.1 Coefficients & Masses after steps	45
9.2.2 Global equation between m_{UP} and $m_{initial}$	45
9.2.3 Second iteration of mass budget	46
9.3 Frozen information	48
9.3.1 Frozen points	48
9.4 Mass Budget - Final iteration	49
9.4.1 Coefficients & Masses after steps	49
9.4.2 Global equation between m_{UP} and $m_{initial}$	49
9.4.3 Detailed contributors	50
9.4.4 Final mass budget	51
9.5 Burn times	52
10 Propulsion system	53
10.1 Engine cycle	53
10.2 RCS / ACS	56
10.3 Multi-usage of hydrogen peroxide	59
10.4 Propellant tanks	62
10.4.1 Requirements and specification	62
10.4.2 Materials	65
10.4.3 Concepts and options	66
10.4.4 Final design	67
10.4.5 Expulsion principle	69
10.4.6 Stresses	72
10.4.7 Liner tanks	74
10.5 Catalyzer	74
10.6 Injectors	77
10.7 Feeding system	78

10.7.1 Line diameters	81
10.7.2 Fuel feeding system	81
10.7.3 Oxidizer feeding system	82
10.8 Turbo pumps	83
10.9 Pressure evolution summary	86
10.9.1 Fuel side	86
10.9.2 Oxidizer side	87
10.10 Engine	88
10.11 Nozzle	88
11 Simulations	89
11.1 Engine performance simulation	89
11.2 Regenerative cooling simulation	93
11.3 Hydrogen peroxide decomposition simulation	95
12 Evaluation	98
12.1 Requirement verification	98
12.2 Lessons learnt	99

Introduction

Ever since the launch of Sputnik 1, the first artificial satellite in October 1957, the number of satellites launched has sharply risen and as of 2020, thousands of satellites are orbiting around the Earth. However, each of every one of those spacecrafts will eventually see their mission being stopped, usually due to a lack of resources from the satellite itself as it reaches the end of its life.

Those who are at the end of their lives will turn into a simple uncontrolled object that keeps orbiting around the Earth and should be avoided as another functioning satellite could take their slot as some of the most important orbits around our planet are starting to get overcrowded and the demand keeps rising.

Moreover, such uncontrolled objects in space can become dangerous as collisions could potentially happen and at such high velocity, those can heavily damage other spacecrafts and create even more debris.

As public awareness grows towards the space debris problem, our mission, Green Debris Remover (GREDER), is looking to contribute to a solution to this problem in a particular orbit, the geo stationary orbit, which is particularly overcrowded due to the many different kinds of satellite operating there.

This mission has been started with the following context :

Design of a LEO-GEO transfer vehicle for removal of suspended satellites

The transfer vehicle is aimed to transport a 3500 kg satellite from GEO to atmospheric re-entry. It will be stationed and refueled in LEO orbit (400 km altitude 55° inclination). A single-stage design using a bi-propellant propulsion system has to be implemented. The design and modeling task shall include the preliminary design and analysis of the vehicle and its propulsion system.

Chapter 1

Schedule

At the start of the project a dedicated group meeting was performed in order to agree on a common project sequence, tasks and challenges as well as work distribution. This group meeting was deemed essential to structure the work packages and to achieve a consolidated baseline for the whole project including time line.

The result is a complex MS project Gantt diagram, which can be found in Annex I - Gantt Schedule.

1.1 Initial Schedule

The first version of the schedule starts with a project Kick-Off in October which is afterwards followed by a short planning phase. In this planning phase issues as scheduling, work distribution and scope of the project were addressed.

Subsequently, the definition phase started. Within this phase, the vehicle requirements were defined and the mission was planned, calculated and visualized in MATLAB. The outcomes of the definition phase are the boundary requirements which are set to provide a frame for both: the vehicle itself as well as the propulsion system. The requirements were defined at the beginning of the project and were verified after project completion.

Upon definition of the boundary requirements, the specification phase started. Within this phase, different propellant combinations were identified, discussed and compared. Additionally a first mass budget was calculated. The result of this phase is the system specification.

The sequence of the project includes several presentations. The first one was performed in October for a quick overview on the project planning. The second one after the bound-

ary requirements and system specification was set. After this presentation, the vehicle and sub system design phase started. This phase included major parts of the work packages including propulsion system design with all sub-assemblies as RACS/ACS, propellant tanks, feeding and pressurization system, turbo pumps, catalyzer, engine, injector and nozzle. The outcome of this phase is a preliminary vehicle design and sub system design which was presented in the mid-term presentation.

As a last major work package the simulation phase started. The whole system was simulated including all sub systems and additionally the complex H₂O₂ decomposition regulation. The final presentation was performed after all tasks were completed and the simulation was finalized.

An overview the compressed initial schedule is shown in Figure 1.1. The detailed Gantt schedule can be found in Annex 1.

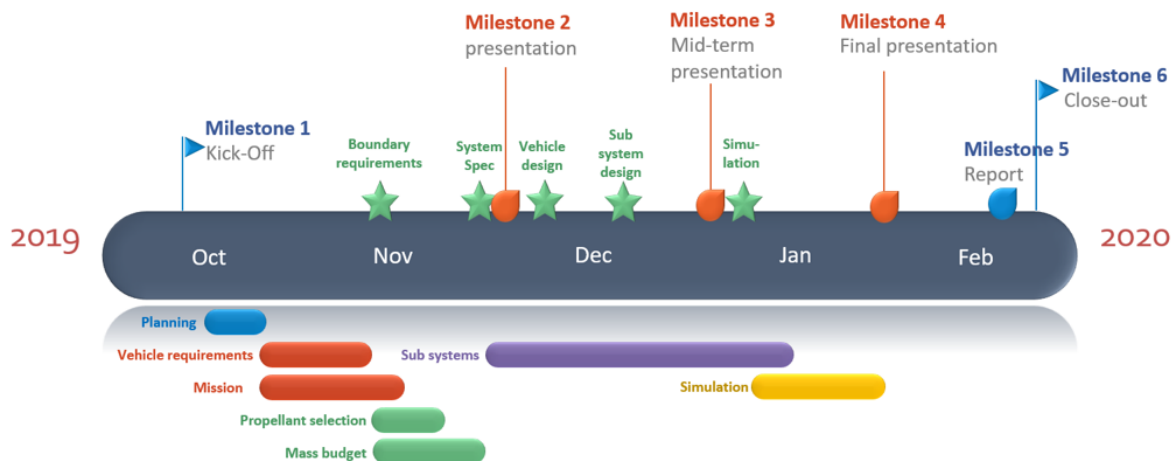


Figure 1.1: Initial schedule

1.2 Final schedule – comparison as planned and as achieved

As usual in project management and project work, not all milestones were achieved in time. As it is shown in the compressed final schedule in Figure 1.2, the finalized vehicle design, the finalized sub system design and the corresponding simulation shifted within the project schedule (Figure 1.2, shown in red). Nevertheless all work packages have been successfully completed until Milestone 4, the final presentation.

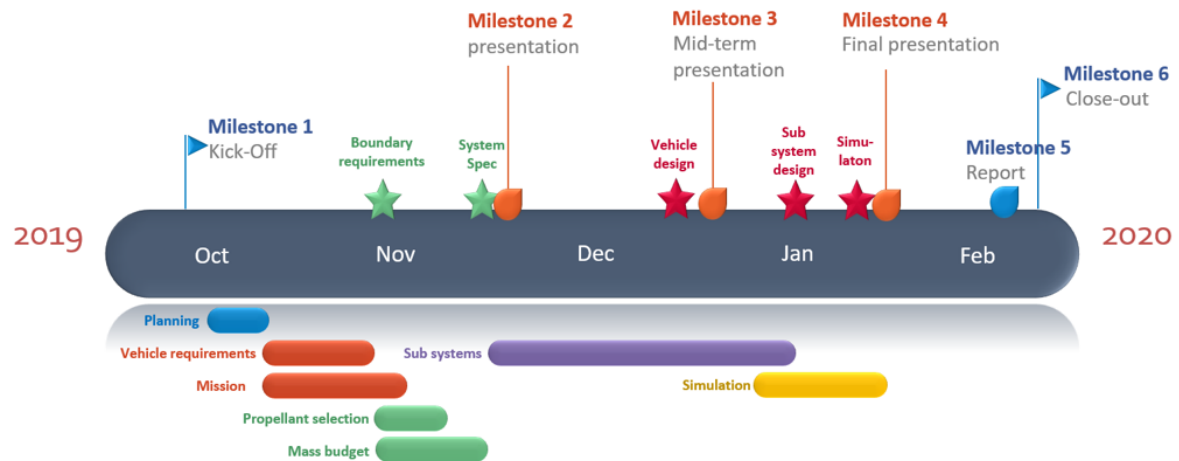


Figure 1.2: Final schedule - comparison as planned and as achieved

Chapter 2

Requirements

The top level requirements for the vehicle and propulsion system are divided in three categories: operation, environment and vehicle. The operation requirements are related to the propulsion system and its applicability for the planned missions. The environmental requirements are defined to ensure that both the vehicle and propulsion system is capable of operating and sustaining during launch, mission and in space environment. The scope of the vehicle requirements is to cover the major parts of the planned mission as refuel-ability, aero braking or accuracy.

Operation
TL-1 Provide sufficient thrust for completion of the mission profile including a safety margin
TL-2 Re-ignitable at least 1000 times
TL-3 Service life time of at least 100 missions or 25 years in orbit
TL-4 Ignition and functional reliability shall be higher than 99,5%
Environment
TL-5 Withstand the launch phase
TL-6 Operate in vacuum
TL-7 Withstand the temperature gradients resulting from areas turned towards or away
TL-8 Sustain space-related radiation throughout it's complete life time
TL-9 Withstand debris impact of under 1cm diameter with a max relative speed of 15 km/s
Vehicle
TL-10 The engine shall be the main propulsion system of a GEO satellite recovery vehicle
TL-11 Refuelable between missions
TL-12 Perform aerobrake maneuvers in Earth's atmosphere.
TL-13 Control flight path in Earth's atmosphere using non-propulsive flight control systems
TL-14 Remain within the ARIANE 6/Falcon 9 payload launch capabilities to LEO.
TL-15 Remain on it's guided trajectory with less than 0.1% deviation.

Table 2.1: Requirements for the vehicle

Chapter 3

Launcher requirements and launch envelope

From our initial requirements we set to stay within certain margins of size and mass. These two parameters create constraint for the launch. Indeed, we have to analyze the different launcher on the market and their capabilities. Thus, we chose to stay within the capabilities of two of the most used actual launchers: Ariane 6.4 and Falcon 9.

These launchers have almost the same launch capability; the Falcon 9 can send 22.8 t in LEO and Ariane 6.4 can send 21.6 t to LEO. The other important characteristic is the dimension of the fairing. Here we have two different launchers with almost identical size; the Falcon 9 can carry a payload up to 11.4 m long and 4.6 m wide, whereas Ariane 6.4 can carry up to 18 m long and 4.57 m wide but as the Ariane's fairing is very elongated the true usable size will be more around 12 m by 4.57 m.

To allow us to correctly design our spacecraft we need to create a theoretical envelope based on these two launchers. For that we set the following dimension: a diameter of 4.5 m and a total length of 11.4 m. These dimensions are lower than the two launchers to unsure to have a safety margin.

To sum up, here is the 3 fairing we spoke about:

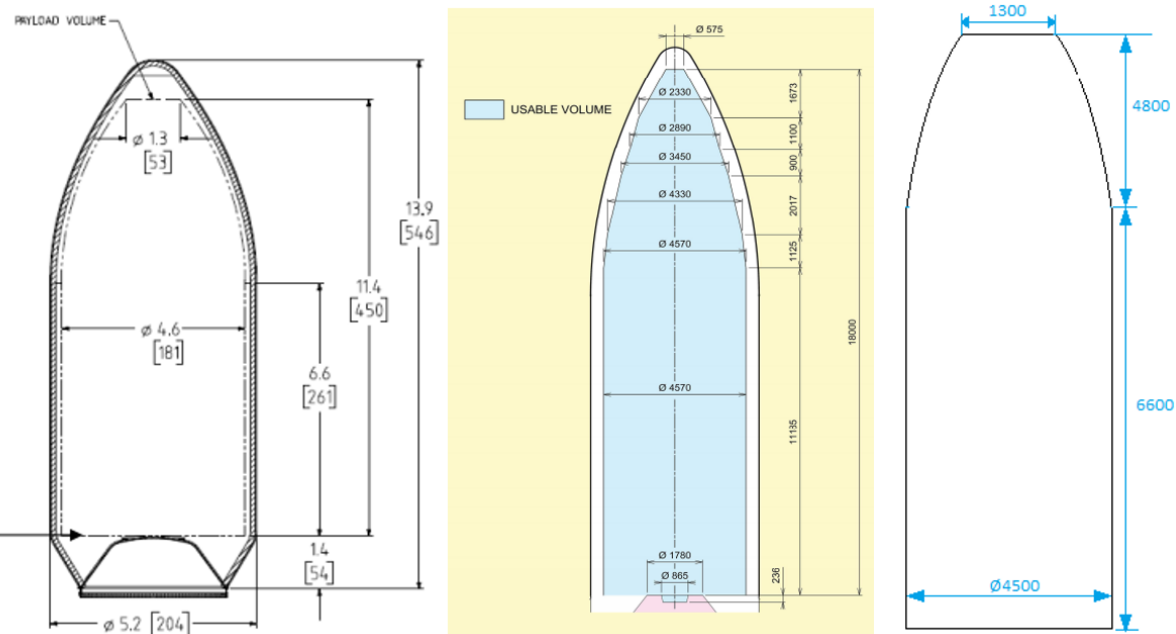


Figure 3.1: Falcon 9 - Ariane 6 - combined fairing

In case, during the design process, the spacecraft cannot stay behind the 22t to LEO launch capability of the Falcon 9, we plan to use the bigger Falcon Heavy which can send 60t to LEO. This launcher will be the last choice, we want at most to stay within our pre-requirement.

We first think to use the structure of our spacecraft, which is aerodynamic, as a fairing so we have less constraint on the size but as it has wings and tail it will generate a small lift but sufficient to destabilize the launcher and might cause a crash. So we decided to forget this idea and to stay within a classic fairing.

Through our project we are going to see if our requirements can meet our calculations and we will make a choice of launcher.

Chapter 4

Mission analysis

4.1 Mission Summary

The objective of the mission is the deorbiting of a GEO satellite. The first step to developing the propulsion system is to break down the mission segments and calculate the delta-V for each of them. Then after the Δv and some mission constraints are clear the detailed mission profile needs to be chosen and optimized.

The mission is broken down into two major phases. Phase 1 is to reach the satellites orbit and match its velocity to enable the capturing process. Phase 2 is deorbitng te satellite and retuning to the original LEO orbit.

4.1.1 Phase 1

Transferring the spacecraft from LEO at 55° inclination to GEO at 0° inclination

First concept :

- Burn 1.1 : LEO to GTO at 55°
- Burn 1.2 : Inclination change to 0° at Apogee of GTO
- Burn 1.3 : GTO to GEO at 0°

To calculate the required delta-V for a burn to change the velocity without changing the direction of the spacecraft is simply identifying the difference in value of the starting and target vector. So for Burn 1.1 the orbital speed of LEO at 400 km needs to be calculated as well as the perigee speed of an elliptic orbit with 400 km as perigee and GEO altitude as apogee. To calculate these values several Matlab functions were written:

```

1 function a = v(r) % velocity of a circular orbit with Radius r
2 a = sqrt(mu/r);
3 end

```

Then the function was used for the calculation with $R_{LEO} = 6778$ km

$$v_{LEO} = v(R_{LEO}) = 7669 \text{ m/s} \quad (4.1)$$

The target velocity for the perigee of the GTO is calculated with the following function:

```

1 function a = vp(r, R) % perigee velocity of elliptical orbit with perigee r and apogee
2   ↪   R
2 if r<R %if clause to prevent mistaken input
3 a = sqrt(2*mu/r-2*mu/(r+R));
4 end
5 end

```

With $R_{GEO} = 42164$ km, the speed is calculated:

$$v_{gto_p} = v_p(R_{le}, R_{geo}) = 10066 \text{ m/s} \quad (4.2)$$

The difference between the two values is the required Δv , $\Delta v_1 = 2398$ m/s.

To calculate the delta-V needed for an inclination change the following function was used:

```

1 function a= dVi(i, v) % delta-V required for inclination change of i (deg) and velocity
2   ↪   v
2 a= 2*v*sin(deg2rad(i)/2);
3 end

```

The velocity passed to the function is the velocity at which the inclination change shall be performed. Here the apogee velocity of the GTO $v_{gto_a} = 1618$ m/s was used:

$$\Delta v_{inc1} = \Delta v_i(i, v_{gto_a}) \quad (4.3)$$

Lastly, the velocity change from the apogee of the GTO v_{gto_a} and the velocity at GEO $v_{geo} = 3075 \text{ m/s}$ needs to be calculated. The difference between the two values is $\Delta v_2 = 1457$ m/s.

Now all the three delta-Vs are added to the delta-V requirement of phase 1:

$$\Delta v_{phase1} = \Delta v_1 + \Delta v_2 + \Delta v_{inc1} = 5348 \text{ m/s} \quad (4.4)$$

4.1.2 Phase 2

Transferring the captured satellite to a deorbiting trajectory and returning to LEO at 55° inclination

First concept :

After capture the satellite needs to be deorbited. Therefore it needs to be set to a drop trajectory. But since the spacecraft shall not deorbit but stay in LEO it needs to make short correction burn to slightly increase the targeted perigee.

- Burn 2.1 : GEO to GTO with (with DROP altitude as perigee, afterwards detaching the satellite)
- Burn 2.2 : Inclination change to 55°
- Burn 2.3 : GTO(DROP) to GTO(LEO as perigee)
- Burn 2.4 : GTO(LEO) to LEO

These Δv are calculated in the same way as described above. The total Δv for phase 2 with $v_{drop_a} = 1587$ m/s, $v_{aero_{a1}} = 1592$ m/s, $v_{aero_{p1}} = 10283$ m/s, $v_{lto_p} = 7887$ m/s and $v_{lto_a} = 7596$ m/s.

$$\Delta v_3 = \Delta v(v_{GEO}, v_{drop_a}) = 1488 \text{ m/s} \quad (4.5)$$

$$\Delta v_4 = \Delta v(v_{drop_a}, v_{aero_{a1}}) = 5 \text{ m/s} \quad (4.6)$$

$$\Delta v_5 = \Delta v(v_{aero_{p1}}, v_{lto_p}) = 2396 \text{ m/s} \quad (4.7)$$

$$\Delta v_{inc_2} = \Delta v_i(i, v_{drop_a}) = 1465 \text{ m/s} \quad (4.8)$$

$$\Delta v_6 = \Delta v(v_{lto_a}, v_{leo}) = 72 \text{ m/s} \quad (4.9)$$

$$\Delta v_{Phase_2} = \Delta v_3 + \Delta v_4 + \Delta v_{inc_2} + \Delta v_6 = 3031 \text{ m/s} \quad (4.10)$$

Since this maneuver is very costly in terms of fuel consumption the concept of aerobraking was introduced. An aerobrake is using the atmospheric drag in the upper atmosphere to brake and reduce velocity. For this mission an aerobrake can save a large amount of delta-V and fuel respectively. in that case, Δv_5 does not need to be included in the sum, saving 2396 m/s.

4.2 Delta-V reduction

There are further means which enable the reduction of delta-V. The ones applied will be discussed in the following.

Combining burns

It can make sense to combine burns. Since Inclination changes require burns perpendicular to the flight direction they can be combined with accelerating or decelerating burns in flight direction. The resulting vector is of shorter length than the sum of the separate burns. Thus, less fuel needs to be burnt. To combine inclination and velocity changing burns the following function was used:

```

1 function a = cosl(v1, v2, i) % combined maneuver of velocity change v1 -> v2 and
  ↪ inclination i change
2 a = sqrt(v1^2+v2^2-2*v1*v2*cos(deg2rad(i)));
3 end

```

The function uses the Cosine-law to calculate the magnitude of the vector between the original velocity vector and the target vector rotated by the required inclination.

Splitting inclination change burns

Mostly it makes most sense to make the inclination change at the lowest possible velocity, since the velocity vector needs to be rotated and this is easier with a shorter vector. However, when the inclination change is split up to combine with further necessary burns the fuel consumption be reduced even further. For the GREDER spacecraft the burns were optimized to reduce the ΔV to the lowest feasible. The outcome of various optimization loops was to split the inclination change into 1.7° , 52.6° and 1.7° as shown in Table 4.1 below.

Overshooting the apogee for inclination change

Since the inclination change is most efficient at lowest velocities it can make sense to overshoot the targeted apogee and adding a burn to reach the targeted orbit with the inclination already changed. The inclination change is then performed combined with the added burn to get to the originally targeted orbit.

Compare options 3 and 5 in the Table 4.1 below. The higher the orbit the lower is the required Δv . However, since increasing the apogee by too much could result in reaching the sphere of influence of the moon and also increase the mission duration by more than tolerable. Also, the increments by which the delta-V decreases get smaller by a constant increase of apogee. So as a compromise roughly double the altitude of GEO was chosen at an orbit radius of 90000 km.

Inclination change during aerobrake

Atmospheric drag can help in reducing the velocity of a spacecraft. In addition, it can be used to generate lift and if directed in the right direction this can reduce or even replace a necessary inclination change burn. An aerobrake strongly influences the architecture of a spacecraft though, since some kind of heat shield is mostly necessary. This is discussed in

Option	Phase 1	Burns	Δv (km/s)	Remarks
1	LEO - GTO - INC55 - GEO	3	5.3483	
2	LEO - GTO - INC55/GEO	2	4.9203	
3	LEO - INC3/GTO - INC52/GEO	2	4.8796	
4	LEO - LETo90k - INC55 - 90ktoGEO - GEO	4	4.9241	
5	LEO - LETo90k - INC55/90ktoGEO - GEO	3	4.6916	
6	LEO - INC1.7/LETo90k - INC51.6/90ktoGEO - INC1.7/GEO	3	4.6674	
7	LEO - LETo90k - INC55 - 90ktoAERO - AEROTOGEO - GEO	5	5.0133	
8	LEO - LETo90k - INC55/90ktoAERO - AEROTOGEO - GEO	4	4.9935	
	Phase 2			
9	GEO - GEOTO DROP - INC55 - GEOTOAERO - AEROTOLEO	4	3.0309	
10	GEO - GEOTO DROP - GEOTOAERO - AEROTOLEO	3	1.5655	inclination change through aerobrake

Table 4.1: Mission planning options

Chapter 6. Also adding wings to the spacecraft increase its mass and structural behaviour.

To estimate the best mission profile several different combinations of these strategies were calculated and compared to each other. The following Table 4.1 shows the considered missions, the number of burns as well as the total necessary delta-V. To reach the best possible delta-V all the different optimization concepts of the team members were taken into account and combined to settle for a final mission profile.

Changing the inclination at the perigee with the highest velocity requires a lot more energy than at GEO altitude. However, if this is achieved without burning fuel and with a lifting body instead a considerable amount of fuel and ΔV is saved. This resulted in the team decision to settle for the combination of option 6 and 10. The complete mission Δv is composed by the following parts:

Phase 1 :

- $\Delta v = 4.67$ km/s

Phase 1 savings :

- Combined burns : ≈ 430 m/s
- Overshooting the apogee : ≈ 230 m/s

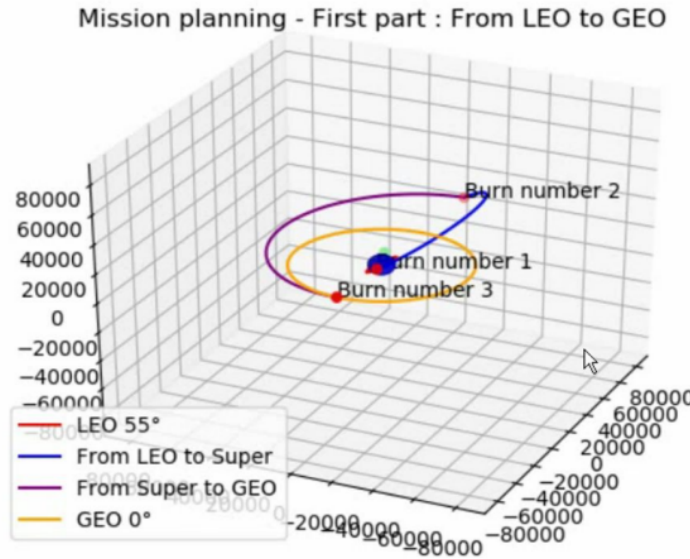


Figure 4.1: Mission planning - First part

Phase 2 :

- $\Delta v = 1.57 \text{ km/s}$

Further secondary burns :

- Steering, rotation : $\approx 80 \text{ m/s}$
- Reserve, correction : $\approx 200 \text{ m/s}$
- Capture : $\approx 100 \text{ m/s}$

Total Δv for the whole mission : 6.61 km/s Phase 2 savings :

- Aerobrake : $\approx 390 \text{ m/s}$
- Inclination change during aerobrake : 1470 m/s

Total savings in both phases : 2.95 km/s

Figure 4.2 shows the paths of the second part of the mission. Here only one exemplary aerobrake orbit is shown as a simplification.

Mission planning - Second part : From GEO back to LEO

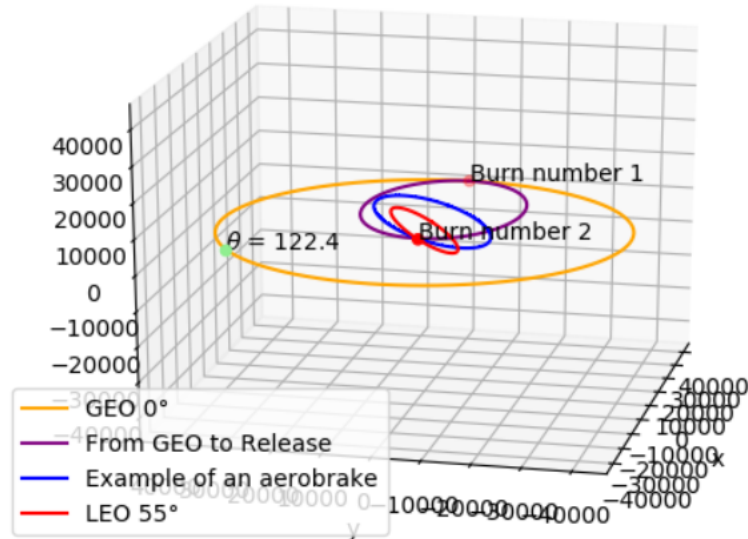


Figure 4.2: Mission planning - Second part

Chapter 5

Satellite capturing process

5.1 Choice of the process

In order to capture and de-orbit a satellite in GEO, we considered the following usable tools :

- Net
- Harpoon
- Claw
- Magnet

Other solutions such as towing the satellite or simply removing them from GEO were not considered as they either did not fit our program or would create too much strain on our spacecraft.

We then took a closer look at the feasibility of each solution and compared the advantages and disadvantages :

Solution	Advantages	Drawbacks	Feasibility
Net	Cheap, simple, low mass	Slow, hard to handle	Yes (JAXA, ESA)
Harpoon	Fairly cheap	Can create more debris	Yes (ESA)
Claw	Safer	Mechanical, moving parts	WIP (CleanSpace One)
Magnet	Adjustable, no moving parts	Higher mass, needs power	Research State

As the main focus of our mission is reliability and re-usability, we made the choice of using magnets to capture and hold the satellite we would like to de-orbit.

5.2 Magnetic solution

Even though we decided that we would use magnets, we needed to make sure it was feasible and to lower the drawbacks related to this solution as much as possible. The first precision we need to make is that we will be using electromagnets in order to regulate the intensity of the current in the coil of it, thus, modulating the attraction force so the contact between our spacecraft and the satellite will not be made at high velocity, avoiding damages and space debris creation.

Even though it is still at the state of research, we believe that using electromagnets as our capturing solution is realistic as both ESA (with ISAE SupAero) and the NASA have been considering and studying this solution since 2017.

However, as a matter of complexity, we will have to make assumptions in order to simplify the problem. The objective in this part is to prove that, with assumptions, this solution can be applied to our mission and to find the required energy to both capture and hold the satellite until its release.

5.2.1 Assumptions

In our calculations, we assumed that :

1. We can consider the magnetic circuit between GREDER and the nozzle of the satellite is a closed one (no air gaps)
2. About 0.1% of the satellite's mass is magnetically operable
3. Mutual attraction is relatively low compared to the magnetic force
4. Residuals in the alloy of the magnets' cores are neglectable

5.3 Sketching and Calculations

Using the first assumption, we can use the formula for the magnetic force in a magnetic circuit with no air gap :

$$F = \frac{(\mu NI)^2 A}{2\mu_0 L^2} \quad (5.1)$$

With :

- μ the magnetic permeability of the core of our magnet (determined by the alloy)
- N the number of turns of the coil around the core

- I the current running through the coil
- A the cross section area of the core
- μ_0 the magnetic constant
- L the length of the mean magnetic circuit

In order to have a good balance between thermal properties and magnetic properties we decided to use an alloy made of 90% of iron and 10% of cobalt for our core. We decided to use this alloy as iron has the best magnetic properties (high relative magnetic permeability) and added cobalt as it has a higher Curie Temperature than iron but has a lower relative magnetic permeability.

In terms of magnet design, we chose to use a squared cross section of $5\text{cm} \times 5\text{cm}$ for the magnet core and with a length of 15cm , made of an iron-cobalt alloy and a copper coil around it. We decided to have 135 turns of the coil around the core with a coil diameter of 1mm in order to not have the wire revolutions stuck to each other. We also want to run a current of 10A through the coil.

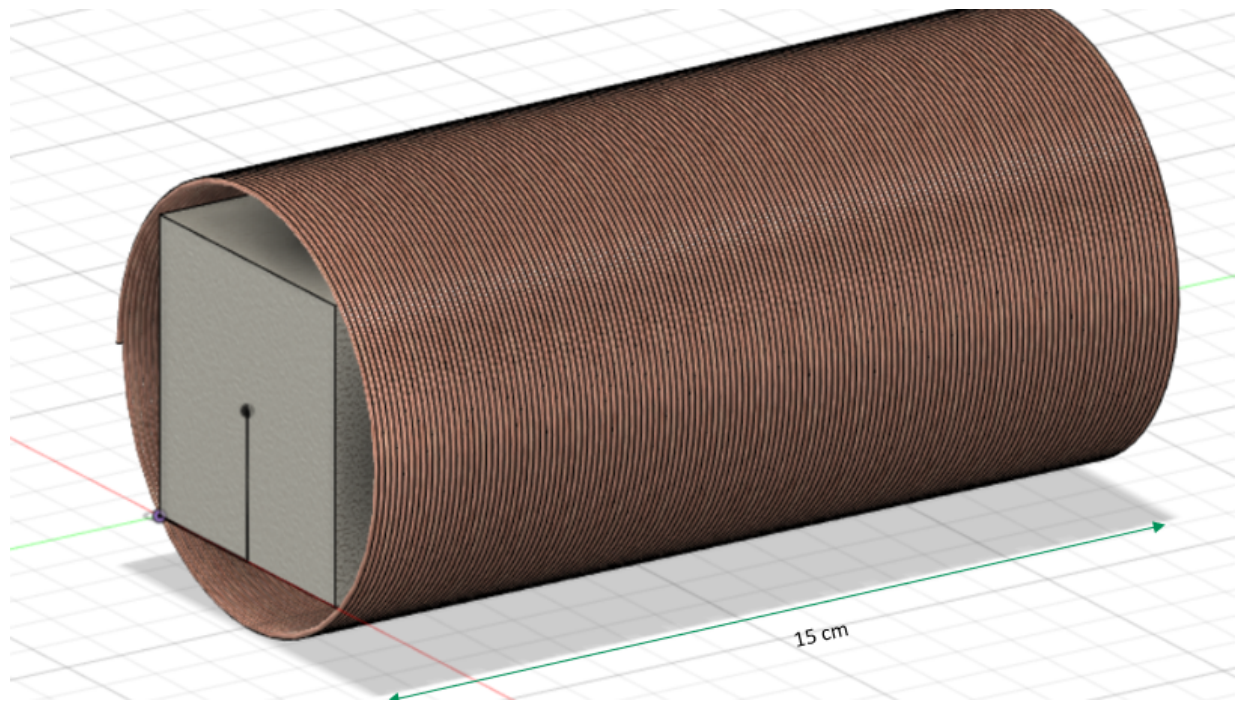


Figure 5.1: CAD of a capturing magnet

With those design choices we get the following parameters while taking into consideration that there should not be any kind of residuals in the core alloy :

- $\mu_0 = 4\pi \times 10^{-7} \text{ H/m}$
 - $\mu = \left(\frac{\mu_{iron} + \mu_{cobalt}}{2} \right) \times \mu_0 = 5.868 \times 10^{-3} \text{ H/m}$
 - $N = 135$ turns
 - $I = 10 \text{ A}$
 - $A = 25\text{cm}^2 = 2.5 \times 10^{-3} \text{ m}^2$
 - $\rho_{core} = \rho_{iron} \times 0.9 + \rho_{cobalt} \times 0.1 = 7.9726 \text{ g/cm}^3$
 - $\rho_{coil} = \rho_{copper} = 8.96 \text{ g/cm}^3$

We then need to find the length L of the mean magnetic circuit. In order to do so, we decided to start the capturing sequence at 10 m from the satellite and that the target has an exploitable nozzle of 40 cm of diameters which is realistic for spacecrafts in the mass range of $3\,500\text{ kg}$. We could then sketch the capturing sequence as so (not to scale) :

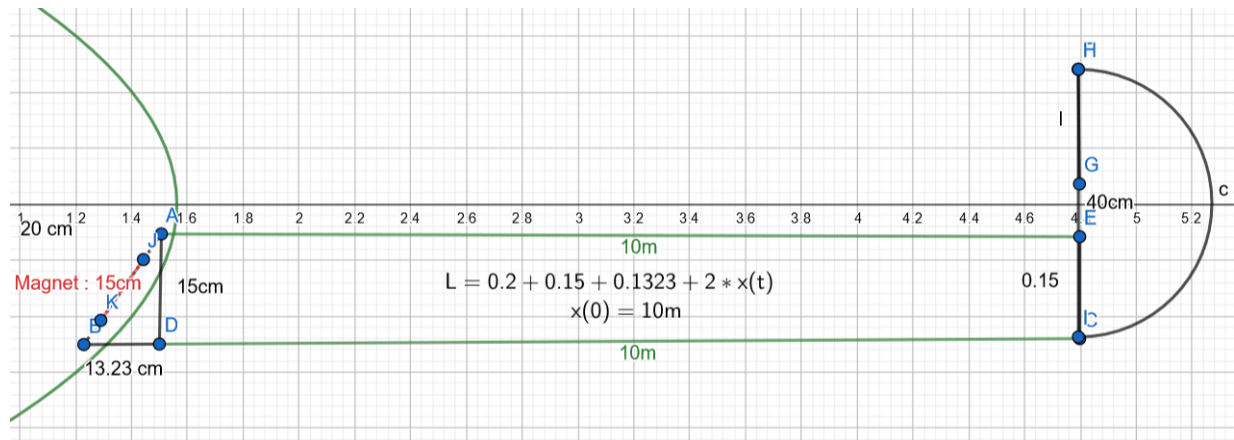


Figure 5.2: Capturing sequence (not to scale)

We can then have the length L as a function of the distance between the tip of our spacecraft and the nozzle of our target. As a result we can proceed to find the feasibility of our solution with this magnet design by finding the time it would require at this state to attract the target. However, in this case, the current modulation when the target is close has not been modeled due to its complexity.

Considering that the force will be on one axis only and $m = 0.001 \times m_{target} = 3.5 \text{ kg}$:

$$\vec{F} = m\vec{a} \quad (5.2)$$

$$\frac{(\mu NI)^2 A}{2\mu_0 L(x)^2} = m \times \ddot{x} \quad (5.3)$$

$$\frac{(\mu NI)^2 A}{2\mu_0[0.2 + 0.15 + 0.1323 + 2x(t)]^2} = m\ddot{x}(t) \quad (5.4)$$

$$\frac{(\mu NI)^2 A}{2\mu_0[0.4823 + 2x(t)]^2} = m\ddot{x}(t) \quad (5.5)$$

The capturing time can then be found using *ode45* on Matlab :

```

1 clearvars; clc;
2 catchtime = 1;
3 x0 = 10;
4 while 1
5     [t,x] = ode45(@f3,[0:1:catchtime], [x0; 0; 0; 0]);
6     if (x(catchtime ,1) >= 2 * x0)
7         break
8     else
9         catchtime = catchtime +1;
10    end
11 end

```

And the function used for the *ode* solver :

```

1 function [Xdot] = f3(t, X)
2 mu = 5.686e-3; mu0 = 4 * pi * 10 ^(-7);
3 N = 135; I = 10; A = 0.05 ^ 2; m = 3500 ;
4 x = X(1); y = X(2); vx = X(3); vy = X(4);
5 Fmag = (mu * N * I) ^2 * A / (2 * mu0 *(2 * norm(X(1:2)) + 0.4823) ^ 2 );
6 Xdot = [vx; vy; 0.001 * Fmag / m; 0];
7 end

```

We then get a capture time of 812 seconds. As a result, we can determine the energy required to operate the magnets aswell as their masses and volumes. We are considering a holding time for approximately half an hour and we also need to verify that the magnets will be able to hold the target while we are de-orbiting.

Chapter 6

Heat shield

6.1 Thermal protection system

A complete deorbiting mission from LEO to GEO and returning to LEO has a very high delta-V requirement of roughly 8.5 km/s. To reduce this delta-V the GREDER spacecraft will use atmospheric drag in the upper atmosphere at an altitude of 70 – 120 km to reduce its relative velocity when returning from GEO to LEO. This kind of maneuver is called an aerobrake and has the potential to save a significant amount of fuel and total spacecraft mass. Aerobrakes are commonly used for reentry vehicles. However, these experience very high thermal loads since the kinetic energy is converted to heat through friction with the atmosphere in a single reentry trajectory. Thus, a high mass for a heat shield is necessary. For a reusable spacecraft ablative heat shields are not useful. Instead, a passively cooled thermal protection system (TPS) was chosen. This allows to radiate the heat away. When the velocity is reduced into small increments the spacecraft can radiate the heat away in the time between the aerobrakes. The advantage is, that fuel is only required for trimming maneuvers to set the targeted perigee radius and not for the deceleration itself. A high number of aerobrakes can be performed with relatively small heat loads if extended mission time is not of a large concern.

Since the GREDER spacecraft is unmanned and does not utilize cryogenic fuels the extended mission time is not as critical. A heat shield needs to be developed for the spacecraft to protect it at the areas with the highest heat loads.

6.2 First estimation

For first rough calculations the total velocity reduced by the aerobrakes was determined as 2.4 km/s. This is the difference in velocity between the perigee velocity of the transfer orbit from GEO to aerobraking altitude and the velocity of the perigee of the transfer orbit

Property	Reinforced Carbon-Carbon	Aluminium (2024-T8XX)	Steel Type 321	Titanium (6A1-4V)
Density (kg/m^3)	1578	2803	8027	4437
Thermal conductivity ($\text{W/m} - \text{K}$)	3.9*	145.4	14.7	69
Specific heat ($\text{J/kg} - \text{K}$)	711.8	816.4	565.2	523.4
Multipule Use Temperature Limit (K)	1922	425**	872**	662**
Single Use Temperature Limit (K)	2033	450	922	700
$T_{cond} \times M_{TempLim}(E + 6)$	1.41	0.35	0.49	0.35

(*thru-the-thickness not isotropic; **values extrapolated by ratio of single/multiple use of CFRC)

Table 6.1: Comparison of materials for heat shield

from the last aerobrake to LEO. The mass of the spacecraft after deorbiting was estimated at 3500 kg. This results in a kinetic energy of:

$$E_{kinetic} = \frac{m_{sc}\Delta v^2}{2} = 10.04 \text{ GJ} \quad (6.1)$$

For a number of 15 aerobrakes this kinetic energy needs to be divided by 15 assuming the temperature at the beginning of each aerobrake will be the same. This kinetic energy was then assumed to be completely converted to thermal energy and distributed evenly over the mass of a heat shield. With the maximum allowable temperature of the chosen material a rough required heat shield mass could be estimated.

6.3 Material choice

$$E_{kinetic} = \frac{mv^2}{2} \quad (6.2)$$

$$m_{shield} = \frac{E_{kinetic}}{c \times dT} \quad (6.3)$$

The table above is a comparison of possible TPS materials. The values are taken from the TPSX NASA Material Properties Database. Multiple Use Temperature values were not available for the chosen metals but were extrapolated based on the ratio of the multiple and single use temperature limits of CFRC. The last row shows the product of the values of the lines Specific Heat and Multiple Use Temperature Limit. This relative value allows to quickly compare the materials with each other regarding the required mass for a heat shield. The unit is J/kg showing that a high value is favorable to store as much energy as possible per mass.

Carbon Fibre Reinforced Carbon quickly proves as the material of choice for a low heat shield mass. Several metals were also taken into account since the manufacturing and integration into the spacecraft struture would be a lot easier. But the low mass for a CFRC TPS in combination with the low thermal conductivity made this the material of choice. CFRC was utilised in the space shuttle heat shield and was found to be the cause of the columbia catastrophe since it is quite brittle and thus sensitive to impact (Columbia Accident Investigation Board Report¹). But since the GREDER spacecraft will be launched inside a rocket launcher fairing no high velocity impacts are to be expected. The capturing of the satellite on the nose cone will be done at very low relative velocities since the force applied by the magnets is controllable with the applied current and can be carefully adjusted (compare Chapter 5).

$$m_{shield_{cc}} = \frac{m_{sc} \times (\Delta v_5 \times 1000)^2}{2n_{ab}c_{cc}(T_{max_{cc}} - T_0)} \quad (6.4)$$

With :

- Δv_5 : Required Δv
- m_{sc} : Spacecraft mass
- n_{ab} : Number of aerobrakes
- T_{max} : Maximum allowable temperature of CFRC
- T_0 : Temperature at beginning of aerobrakes

6.4 Lift and drag

An aerobrake can also be used to change the inclination of the orbital plane. To achieve this the spacecraft needs to be a lifting body. To increase the lift wings can be attached to increase the projected area of the spacecraft. This area affects both the lift and drag of the spacecraft.

$$F_l = C_l \times \frac{\rho}{2} \times v_1^2 \times A_h \quad (6.5)$$

$$\Rightarrow F_l = 13.9 \text{ kN} \quad (6.6)$$

$$F_d = C_d \times \frac{\rho}{2} \times v_1^2 \times A_h \quad (6.7)$$

$$\Rightarrow F_d = 3.5 \text{ kN} \quad (6.8)$$

¹https://www.nasa.gov/columbia/home/CAIB_Vol1.html

The angle of attack influences the lift and drag coefficients. Since both forces are perpendicular to each other the resulting force and the angle of the direction are calculated by:

$$F_{res} = \sqrt{F_l^2 + F_d^2} \quad (6.9)$$

$$F_{res} = 14.3 \text{ kN} \quad (6.10)$$

$$\beta_{F_{res}} = \arctan\left(\frac{F_l}{F_d}\right) \times \frac{180}{\pi} \quad (6.11)$$

$$\beta_{F_{res}} = 76^\circ \quad (6.12)$$

It may be noted that unlike an aircraft the lift vector does not point "upwards" but rather parallel to ground and perpendicular to the orbital plane. Thus, the altitude is not affected by the "lift".

The lift and drag coefficient are typically experimental values. For the drag similar shapes can be used as a reference. For the GREDER spacecraft a value of 0.3 is assumed to be reasonable because of its similarity to the bullet shape (compare Figure 6.2 and fig xafter). The delta wing should have a significantly lower drag coefficient and is therefore not taken into account.

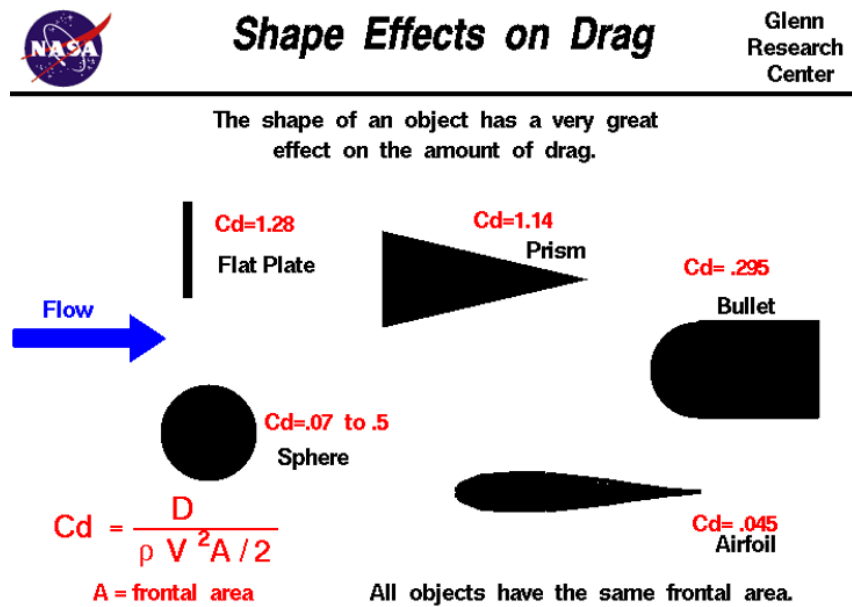


Figure 6.1: Shape effect on drag

Regarding the lift coefficient a strong simplification as made. For a flat plate the lift

coefficient can be approximated with the following formula based on the angle of attack² :

$$C_L = 2\pi \sin(\alpha) \quad (6.13)$$

For an angle of attack of 11° the result for the lift coefficient is 1.2.

To reduce fuel consumption for attitude control a constant angle of attack would be beneficial. To achieve this, the angle between the resulting vector of lift and drag and the velocity vector needs to be the same as the angle between the resulting vector of decelerating and inclination changing vector and the velocity vector. The required delta-Vs for decelerating and inclination change are perpendicular to each other and the angle between them is given by:

$$\beta_{\Delta v_{res}} = \arctan \left(\frac{\Delta v_{inc2p}}{\Delta v_5} \right) = 76^\circ \quad (6.14)$$

$$\beta_{F_{res}} = \arctan \left(\frac{C_L}{C_D} \right) \quad (6.15)$$

To compute the angle of attack these formulas need to be equated and the formula for C_L included.

$$\alpha = \arcsin \left(\frac{\Delta v_{inc2p}}{\Delta v_5} \times \frac{C_D}{2\pi} \right) \quad (6.16)$$

For an angle of attack of 11° the angle of the resulting vector of lift and drag is 76° . This results in a balance of both forces during each aerobrake.

6.5 Aerobraking altitude

To estimate the altitude of the aerobrakes, the Matlab function atmoscoesa was used. Here the density of the atmosphere is calculated by altitude between 0 and roughly 84000 m. The values for higher altitudes are extrapolated. A higher altitude results in a longer necessary time in the atmosphere. This has the benefit of a slower heating up of the spacecraft and low values for lift and drag forces. However this could require a higher number of aerobrakes. Weighing these parameters against each other an altitude of 82 km was chosen for the aerobrakes. At this altitude the total aerobraking time is 30.4 minutes. At a number of 20 aerobrakes each would take roughly 91 seconds. During the first aerobrake the distance traveled would be roughly 937 km and during the last roughly 730 km. The forces acted upon the spacecraft are 13.9 kN for lift and 3.5 kN for drag.

²<http://brennen.caltech.edu/fluidbook/externalflows/lift/flatplateairfoil.pdf>

At a remaining spacecraft mass of 3000 kg this adds up to an acceleration of 4.8 km/s^2 so roughly 0.5 Gs. These values seemed reasonable since this would keep the mechanical stress relatively low allowing for reusability of the GREDER spacecraft.

6.6 Simplifications

Regarding the thermal loads on the spacecraft the heat shield needs a little more detail. Modeling the heat flux and conductance within the heat shield is simplified due to complexity. Since the even distribution of the heat over the shield is inaccurate several conservative assumptions shall leave a margin for this. CFRC retains its mechanical properties up to 2400° C ³. The maximum allowable temperature used for the heat shield modeling is 2000 Kelvin. Also, the assumed temperature at the beginning of the aerorakes is 400 Kelvin. Furthermore It is assumed that the entire kinetic energy is converted to thermal energy and this is completely distributed onto the spacecraft. In reality however not only the spacecraft but also the atmosphere would be heated through friction. This is highly dependent on the geometry of the body. Most reentry vehicles use blunt front faces to "push" a protective shock wave heat shield in front of them. This keeps the highest heat loads away from the surface. This affect can be seen in Figure 6.2 below.

³<https://www.makeitfrom.com/material-properties/Carbon-Carbon>

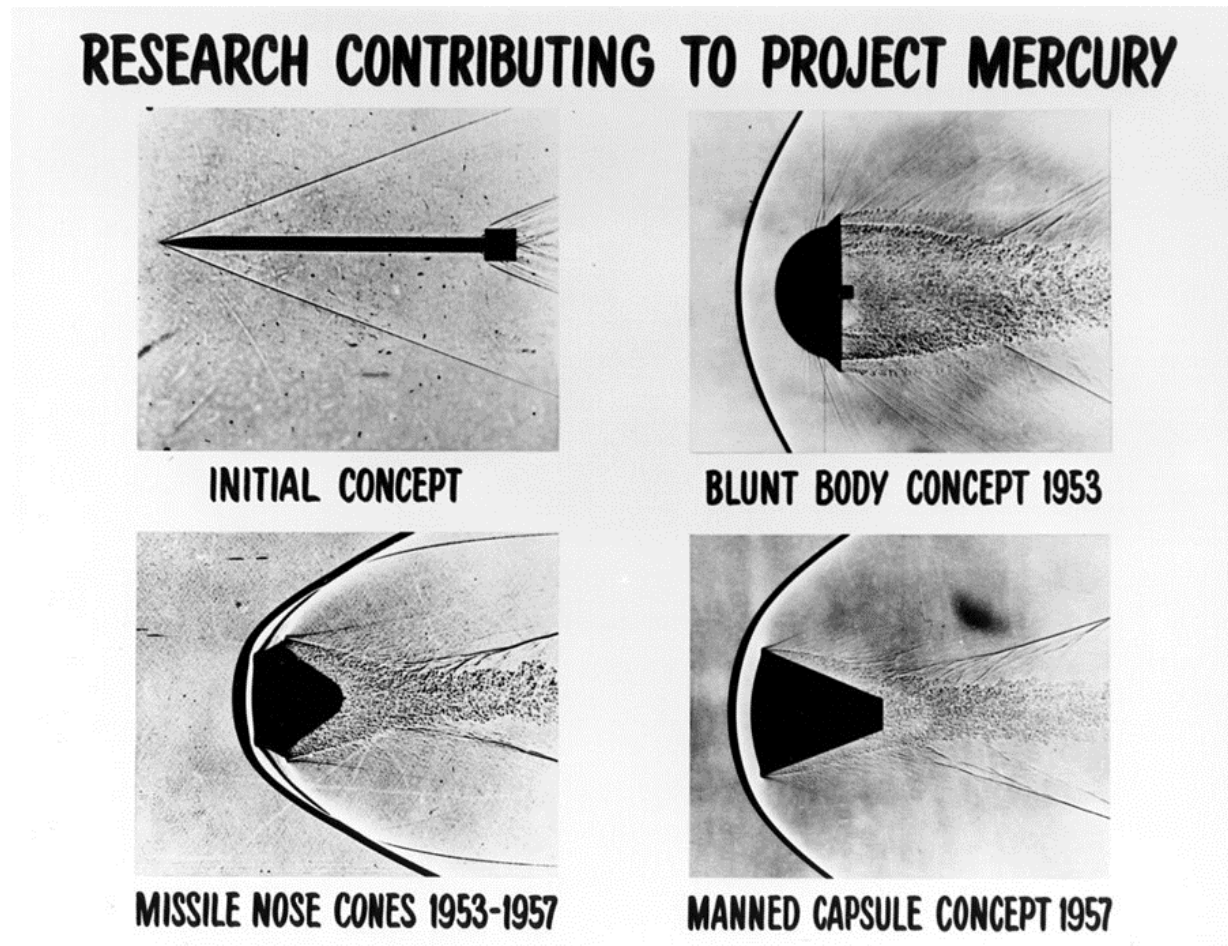


Figure 6.2: Shadowgraph images of Reentry vehicles

As a further simplification, heat transfer is considered solely through convection during the aerobrake maneuver and solely through radiation during the completion of each orbit. The short duration of the aerobrakes is not very significant compared to the duration of a completed orbit (90 s vs. roughly 90 minutes). Furthermore the heat capacity of CFRC increases with increasing temperature. At 750 Kelvin the specific heat capacity is roughly double the value compared to ambient temperature (Specific Heat of Carbon/Carbon Composites ⁴) This leaves an increased margin during the peak heat loads of the atmospheric breaking.

6.7 Heat shield interface

To avoid mechanical failure of the spacecraft's hull beneath the heat shield an insulating blanket will be applied underneath the CFRC heat shield. Herefore, the flight proven

⁴<https://apps.dtic.mil/dtic/tr/fulltext/u2/a106709.pdf>

AFRSI Blanket was chosen due to its excellent isolating properties and very low density. Here a 10 mm layer of the silica blanket at a density of $\rho_A F = 9.6 \text{ kg/m}^3$ and an additive aereal weight of $m_{add} = 1 \text{ kg/m}^2$ is utilized.⁵

The thermal loads are expected to be highest on the leading edges of the spacecraft's wings and the nose of the spacecraft. In these areas the heat shield shall have the largest thickness. Figure 6.2 shows the areas where the heat shield will be applied. roughly half of the GREDER spacecraft will be covered by the heat shield. This includes the lower faces and leading faces. The upper side and rear of the spacecraft is not expected to endure high thermal loads during the aerobraking maneuvers since the nose will be tilted upwards exposing the lower side.

6.8 Radiative cooling

To verify that the radiative cooling of the CFRC shield is sufficient, an interactive model of the radiated heat was created. To calculate the Power radiated by a gray body in space the following formula was used:

$$P = A j^* = A \varepsilon \sigma T^4 \quad (6.17)$$

The emissivity of CFRC is $\varepsilon = 0.78$ and σ is the Stefan-Boltzmann constant.⁶ As a starting temperature the maximum allowable temperature of 1982 K was used and for the simulation time the period of the shortest and last orbit with a period of roughly 80 minutes or 4800 seconds. The surface area of the heat shield is half of the total spacecraft surface area.

Calculating the emitted energy could be transferred into a temperature delta for each second of the simulation. after 4800 iterations the temperature is plotted. The last value of 233 K is lower than the assumed 400 K and thus leaves some safety margin.

```

1 sigma=5.6703E-8 %W/m2K4 stefan boltzmann constant
2 eps_cc=0.78;
3 T1=zeros(1,4800); %K
4 T1(1)=1982; %K
5 for k=1:1:length(T1)-1
6 T_rad=sigma*T1(k)^4*eps_cc*A_sc_tot/2*c_cc/m_tps_cc;
7 T1(k+1)=T1(k)-T_rad;
8 end
9 plot(T1);

```

⁵<https://tpsx.arc.nasa.gov/material.html?matid=12>

⁶<https://tpsx.arc.nasa.gov/material.html?matid=24&units=si>

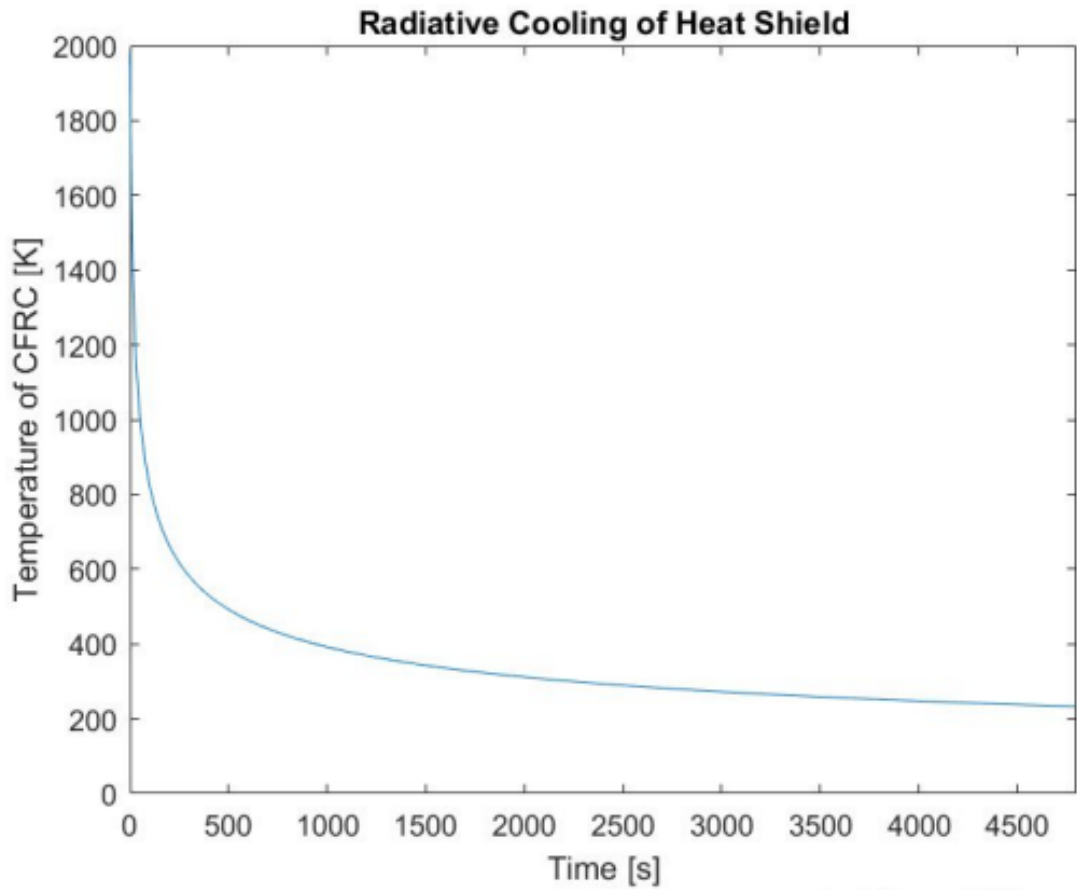


Figure 6.3: Radiative cooling of the heat shield

6.9 Final heat shield mass

For the final mass of the TPS a specific heat capacity for CFRP of $c_{cc} = 840 \text{ kJ/kg-K}$ was assumed. Moreover :

- $\Delta v_5 = 2.396 \text{ km/s}$
- Spacecraft mass $m_{sc} = 3000 \text{ kg}$
- Number of aerobrakes $n_{ab} = 20$
- Maximum allowable temperature $T_{Max_{cc}} = 1982 \text{ K}$
- Starting temperature $T_0 = 400 \text{ K}$

At a surface area of the total spacecraft of $A_{sc_{tot}} = 67.4 \text{ m}^2$ and half of the surface covered with the TPS also the AFRSI blanket mass can be calculated.

$$m_{tps_{cc}} = \frac{(\Delta v_5 \times 1000)^2 m_{sc}}{2n_{ab}c_{cc}(T_{max_{cc}} - T_0)} = 323.9 \text{ kg} \quad (6.18)$$

$$m_{blanket} = \frac{\rho_{AF} A_{sc_{tot}}}{2 * 0.01} + \frac{A_{sc_{tot}}}{m_{add}} = 37 \text{ kg} \quad (6.19)$$

$$m_{tps} = m_{blanket} + m_{tps_{cc}} = 360.9 \text{ kg} \quad (6.20)$$

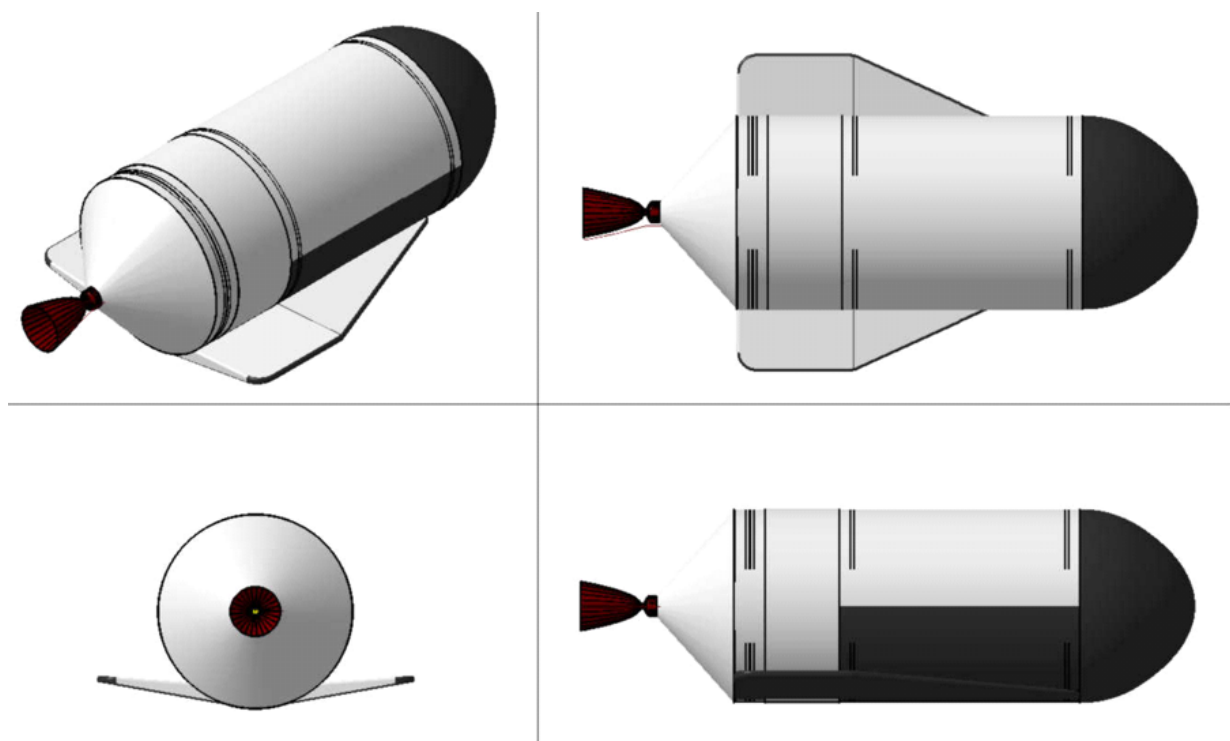


Figure 6.4: GREDER Spacecraft (various views) - Heat shield shown in gray

Chapter 7

Propellant selection

For the propellant selection for our vehicle, several important aspects have to be taken into account including:

- Specific impulse in vacuum (Isp) of the propellant
- Storability
- Toxicity including ground handling
- Costs (while the main cost driver is not the propellant itself more its toxicity)
- Reasonable refueling options due to the desired mission profile of the vehicle
- Space flight heritage of the propellant (e.g. flight proven, ground proven or in development)
- Density specific impulse
- Corrosive behavior and compatibility with typical light weight tank materials as titanium or aluminum
- and many more

At first several possible and typical flight proven propellant combinations were analyzed and the most promising combinations were selected and then compared in detail. Afterwards a feasibility study for the chosen propellant combination was deemed necessary in order to check whether the desired propellant combination is able to perform the required mission and de-risk the next development steps.

7.1 Options overview

In literature and historical research several reasonable and flight proven propellant combinations have been found. The propellant combinations are divided in three sub-categories: petroleum, cryogenics and hypergolic. These combinations are all bipropellant combinations, the monopropellants have already been excluded at the beginning due considerably low specific impulse in comparison to bipropellants and therefore not suitable for the intended mission profile.

Petroleum fuels are containing a combination of complex hydrocarbons and have been refined from mineral oil. The typical petroleum used as rocket fuel is a highly refined kerosene, called RP-1 (rocket propellant 1). In bipropellant use an oxidizer is necessary and therefore petroleum is often mixed with LOX (liquid oxygen). The specific impulse of a petroleum fuel and cryogenic oxidizer combination is higher than for hypergolic propellant combinations but lower than for fully cryogenic options.

The cryogenics are gaseous bipropellants stored at very low temperatures and usually stand out due to their high specific impulse. The most common cryogenics are liquid hydrogen and liquid oxygen which have to be stored at -253°C for LH₂ and -183°C for LOX. Recently, cryogenic combinations with liquid methane (LCH₄) as fuel are receiving more attention due to availability methane on mars and therefore it might become attractive for future mars missions.

The last group in this option overview are the hypergolics. The hypergolics are bipropellants that ignite spontaneously when in contact. The main advantage of hypergolics is the storability. Hypergolics are liquid at room temperature and therefore no additional heating or cooling is necessary during the mission. Nevertheless the hypergolics provide less specific impulses than cryogenics and they are mostly highly toxic.

Table 7.1 shows a comparison of different bipropellants divided in the three above mentioned categories. In the initial comparison of this chapters the propellant combinations are compared with regards to their major characteristics: specific impulse, flight evidence and therefore technical risk, storability and their reasonability for our application.

It is clearly visible that most propellant combinations have not been found reasonable for our application due to low temperature storage. Our vehicle is designed to perform several missions with several ignitions permission and refueling at an in orbit refueling station – this mission profile is not conformable with constant low temperature storage.

In contrast to that the group of hypergolics offers great storability and good specific impulse for the mission profile and a storage of these propellants at an in orbit refueling

station is feasible. Since the two options MON/MMH and H₂O₂/RP-1 are promising, further in depth analysis was deemed necessary.

Type	Combination	Isp [s] vacuum	Flight proven	Storability	Toxicity	Reasonable for our application
Petroleum	LOX / RP-1	300-353	Used for the lower stages of the Soyuz boosters, and the first stage of the U.S. Saturn V, Atlas, and Falcon 9 boosters. Very similar to Robert Goddard's first rocket.	LOX low temperature storage	non-toxic	NO
Cryogenic	LOX / LH ₂	420-453	Used in the stages of the Space Shuttle, Space Launch System, Ariane 5, Delta IV, New Shepard, H-IIB, GSLV and Centaur.	low temperature storage	non-toxic	NO
	LOX / LCH ₄ (methane)	355	NO	low temperature storage	non-toxic	NO
	LF ₂ (flourine) / LH ₂	470	NO	low temperature storage	highly toxic	NO
Hypergolic	MON / MMH	321-336	three first stages Proton booster, Indian Vikas engine for PSLV and GSLV rockets, most Chinese boosters, a number of military, orbital and deep space rockets	storables	highly toxic	YES
	H ₂ O ₂ / RP-1	313	British gamma rocket engines (65kN 2nd stage for example)	storables	non-toxic	YES

Table 7.1: Propellant combinations overview

7.2 Detailed comparison between MON/MMH and H₂O₂/RP-1

The hypergolic propellant combination MON/MMH and H₂O₂/RP-1 have been found reasonable for our mission and application. Table 7.2 shows a detailed comparison of the propellant combinations. Several characteristics were found to be minor and others were found to be major for our application. The major characteristics are the vacuum specific impulse, the tank volume ration, the combined density, the density specific impulse and the toxicity and storability (highlighted in yellow).

Both propellant combinations have a comparable specific impulse. Therefore no favor

for either MON/MMH or H₂O₂/RP-1.

The tank volume ratio is better for MON/MMH because the ratio is nearly one to one, therefore both oxidizer and fuel tank could share the same tank design. This would significantly decrease the development costs since no second tank design and second qualification tank is necessary. Also the manufacturing costs would decreased due to more possibilities of batch production. Especially production costs of forged tank hemispheres are a huge cost driver and these would decrease due to non-recurring costs being distributed on a larger number of hemispheres. Also the costs for jigs and tools would decrease. This favors MON/MMH.

The combined density for H₂O₂/RP-1 is slightly better than for MON/MMH. Nevertheless the combined density is not a significant value without taking the specific impulse into account. Calculating the density specific impulse, which is basically the specific impulse per mass, H₂O₂/RP-1 exceeds MON/MMH by 12%. In this category H₂O₂/RP-1 is the winner because it can provide more specific impulse per mass.

Comparing toxicity of MON/MMH to H₂O₂/RP-1 it can be stated that MON/MMH is highly toxic and has to be handled with extreme care which increases the ground handling costs of this propellant combination. In contrast to that is the toxicity of H₂O₂/RP-1. This propellant combination is non-toxic and can be considered as “green” propellant. Nevertheless careful ground-handling is also necessary for this combination because it is prone to reaction with trace elements. H₂O₂/RP-1 succeeds in this category.

The last category is the storability. Since both propellant combinations are storable in liquid/liquid condition both propellants are suitable for the application.

Taking all criteria and results into account H₂O₂/RP-1 is the preferred propellant combination for our application. The main reasons are:

- comparable specific impulse to MON/MMH
- better density specific impulse
- non-toxic advantage for maintenance at refuel station
- good on-ground handling
- possibility of R&D funds by ESA for green debris remover

The main reason against MON/MMH is the toxicity.

	MON / MMH	H ₂ O ₂ / RP-1
Isp vacuum [s]	321-336	335
state at 20 °C	liquid / liquid	liquid / liquid
phase transus solid/gaseous	[-52 °C; 87 °C] / [-11 °C; 21 °C]	[-0,4 °C; 142 °C] / [-60 °C; 300 °C]
Densities [kg/m ³]	1450 / 900	1440 / 900
Viscosity [mPa·s]	0,86 / 0,48	1,19 / 0,8
Vapor pressure at 20 °C [bar]	0,05 / 1,1	0,003 / 7,5
Mixture ratio [Parts of Oxidator]	1,6	7
Tank volumes per 1000kg propellant [l]	424,4 / 427,4 total 851,6	607,6 / 138,9 total 746,5
Tank volume ratio	1 to 1,007	1 to 0,23
Combined density [kg/m ³]	1240	1370
Density specific impulse [Kg*s/m ³]	409200	458950
Chamber temperature [K]	3330	2900
Toxicity	highly toxic	non-toxic
Storability	storable	storable
Corrosion	highly corrosive	slightly corrosive
Compatible materials	for example Titanium, Aluminum	High purity aluminum (Al95), stainless steel (304, 304L, 316, 316L)
Isp mono propellant mode [s]	250 / N/A	160 / N/A
Flight proven	3 first stages Proton booster, Indian Vikas engine for PSLV and GSLV rockets, most Chinese boosters, a number of military, orbital and deep space rockets	British gamma rocket engines (65kN 2nd stage for example)

Table 7.2: Detailed propellant comparison MON/MMH and H₂O₂/RP-1

Propellants	Engine name	Engine type	Engine status	F _{vac} (kN) Vacuum thrust	OF Ox to fuel ratio	I _{svac} (N-s/kg) Specific vacuum impulse	[ms/mp] Ratio stage empty mass (ms) over total propellant mass (mp)	Calculated Δv [km/s]
H ₂ O ₂ (~0.97)-RP1	RD161P	Upper stage, unknown	Development	24.5 to 14.7	5,9	3128	[--]	[--]
H ₂ O ₂ (~0.83)-RP1	Gamma-2	Upper stage, Pump fed	Flown	68.2	8,23	2599	0.18	4,46
H ₂ O ₂ (--)-RP1	BA-44	Upper stage, Pressure fed	Development	196 to 98	7,5	2941	0.08	7,43
H ₂ O ₂ (--)-RP1	BA-810	Upper stage, Pressure fed	Development	3600 to 1800	7,5	2765	0.08	6,98
								required $\Delta v=6,61$

Table 7.3: Historical data of flight H₂O₂/RP-1 engines

7.3 H₂O₂/RP-1 feasibility check

Since H₂O₂/RP-1 is not a common propellant combination and not as frequently used space industry as MON/MHH a further feasibility study has to be performed:

- to de-risk the next development steps
- to check whether the desired propellant combination is able to perform the required mission

In 7.3 historical data of flight H₂O₂/RP-1 engines is analyzed. One of the engines “Gamma-2” was flown, the others were in development. The thrusts of all engines are comparable or higher than foreseen for our application and two engines also operate in comparable delta-v ranges. This leads to the conclusion that a H₂O₂/RP-1 engine is generally speaking feasible.

7.4 Summary

In summary H₂O₂/RP-1 is a viable non-toxic hypergolic propellant combination with a good density specific impulse. Additionally the propellant combination is supported by historical flight data. Therefore all further steps will be based on this combination.

Chapter 8

Vehicle architecture

This chapter aims to describe the vehicle system architecture. As the space craft needs to be able to perform an aerobreak within earth's atmosphere, the design is relatively constrained towards a space shuttle-related architecture, with a heat shield in the front, some form of lifting devices and a length to diameter ratio greater than 1. As the satellite capturing system GREDER uses needs to be situated in the front of the vehicle and the propellant choices dictated the performance, the tank volumes were defined by mission requirements and the mass budget. After defining the system diameter to be 2.5 m, the complete system design was basically finalized. The complete 3D-render can be seen in Figure 8.1.

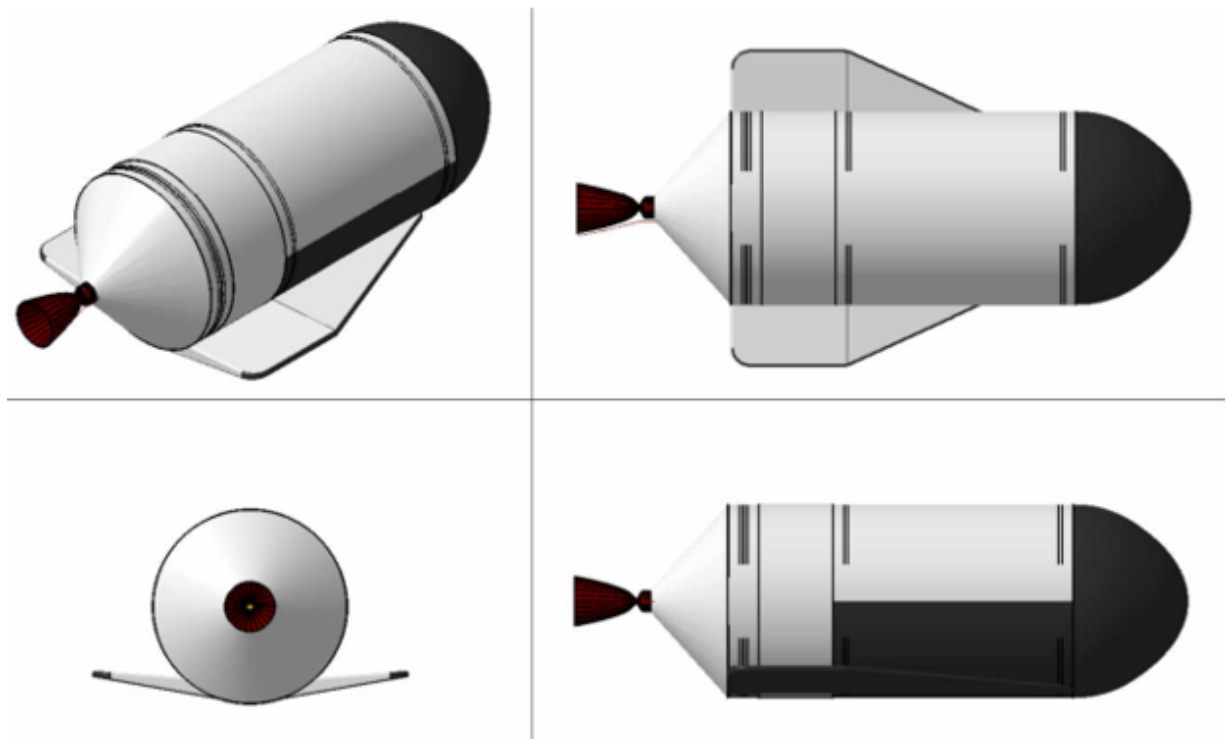


Figure 8.1: Vehicle design 3D-Render

The vehicle consists of 3 zones, which are highlighted in the 3D view as the frontal black zone, the middle white zone and the engine, which is colored in black. The frontal zone houses the battery, fuel cell and capturing equipment as well as the heat shield. A detailed CAD of this area has not been created, as all the equipment was only calculated based on its function and performance. The engine zone, which is the main component of this assignment, will be described in detail, including CAD, calculations and simulations, in Chapter 10 and Chapter 11.

The tank zone, which consists of the oxidizer tank in the upper part of the cylindric vehicle section and the fuel tank in the lower end, is shown in Figure 8.2.

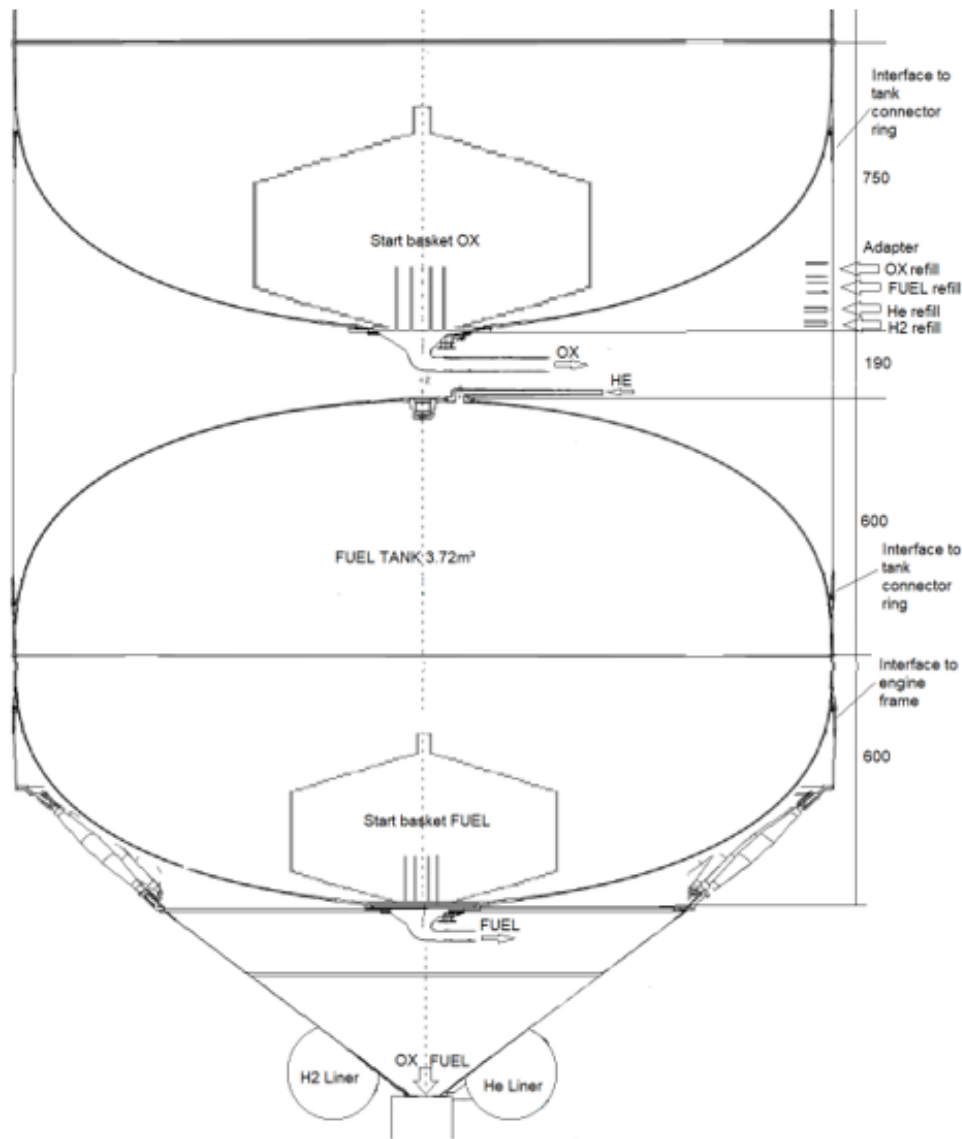


Figure 8.2: Vehicle architecture - Tank section

As Figure 8.2 shows, the tanks and the outer wall are the same structure throughout the cylindrical sections of the propellant tanks. Both tanks are shapes as cylinders will elliptical bulkheads, between which the oxidizer tank outlet is situated. The refueling ports are located between the tanks as well. The oxidizer as well as liner tank lines are funneled through the wing, which extends down until the engine section, where the engine is structurally supported by a conically shaped engine frame, which is connected to the cylindrical structure by axial dampers.

Chapter 9

Mass model and burning times

9.1 Mass Budget - First Iteration

Before actually going into our mass budget, we wanted to get a reference idea for the propellant mass so that we would be sure to be able to achieve our Δv . In order to get this, we decided to find a relation between the usable propellant mass and the mass of the rest as a ratio. This is then fixed and will also allow us to know roughly how much propellant we need depending on the dry mass. Let m_{UP} be the mass of usable propellant. Moreover, we would be aiming for a total initial mass of roughly 20 to 25t on our last iteration. This first iteration was done with another magnet design, presented in November which consisted in two large discs of 600 kg each and have then been abandoned for the second iteration.

9.1.1 Coefficients & Masses after steps

Considering that $ISP = 295s$ and annotating $\frac{m_{UP_i}}{m_{total_i}} = K_i$ with i the burn number :

Step	Required Δv in m/s	K_i	Mass after step
1	2802.4	0.620	$0.38 m_{initial}$
2	1342.2	0.371	$0.239 m_{initial}$
3	522.9	0.165	$0.200 m_{initial}$
Satellite caught	NA	NA	$0.2m_{initial} + 3500$
4	1487.8	0.402	$0.1196m_{initial} + 2093$
Satellite release	NA	NA	$0.1196m_{initial} - 1407$
5	5.3	0.002	$0.1194m_{initial} - 1404.186$
6	72.4	0.0247	

9.1.2 Global equation between m_{UP} and $m_{initial}$

Step	$\frac{m_{UP}}{m_{initial}}$	Bias due to debris
1	0.620	0
2	0.141	0
3	0.039	0
4	0.0804	1407
5	0.00024	-2.814
6	0.00295	-36.68
TOTAL	0.88359	+1369.506

We then get our general relation between the usable propellant mass and the initial mass

$$m_{prop} = 0.88359m_{init} + 1369.506$$

And as $m_{initial} = m_{UP} + m_{rest}$:

$$m_{prop} = \frac{1}{0.11641} [0.88359m_{rest} + 1369.506]$$

m_{rest} includes the dry mass and the propellant required for the ACS.

9.1.3 First iteration of mass budget

Sub systems

Contributor	Mass in kg
EPS	-
Fuel cells	165.6727
H2 for fuel cell (tank included)	10
Cables	20
GNC	5
Batteries	61.3333
Actuators (for flaps)	10
Servos	1
On board computer	5
Telecommunications	10
Thermal control	10
ACS/RCS	-
Reaction wheels	106
ACS (without propellant)	36.16
Total	440.166

Payload

Contributor	Mass in kg
Magnet	1200

Structure

Contributor	Mass in kg
Hull	509
Wing	54
Engine	60
Engine frame	51
Connectors	25
Tanks	350
Heat shield	472
<u>Total</u>	1521

Others

Contributor	Mass in kg
Catalyzer	10
Lines	25
ACS including Propellant	672
Non usable propellant (Residuals, transient, etc.)	200
Helium (including tank)	30
<u>Total</u>	937

We then get

$$m_{rest} = m_{Subsystems} + m_{Payload} + m_{Structure} + m_{Others} = 4098.166 \text{ kg}$$

Which, with the previously obtained equation :

$$m_{UP} = 42\ 870.926 \text{ kg}$$

As the mixture ratio is $MR = 7.07$ and $m_{UP} = m_{UF} + m_{UOP}$

$$m_{UsableFuel} = \frac{m_{UP}}{1 + MR} = 5\ 312\text{kg}$$

$$m_{UsableOxidizer} = MR \times m_{UsableFuel} = 37\ 559\text{kg}$$

Results

We can sum this first iteration up with the following table :

Contributor	Mass (kg)
Structure	1 521
Magnets	1 200
Sub Systems	440.166
Tank Pressurization	30
Engine	60
Catalyzer	10
Lines	25
Dry mass	3 286.166
Non usable propellant	200
ACS/RCS Propellant	142.12
Usable propellant	42 870.926
Total initial mass	46 969.092

Table 9.7: Initial mass budget

This first initial mass is way over what we are targeting and there are many parameters to be refined during the next iteration.

9.2 Mass Budget - Second iteration

After refining multiple parameters and fixing others to get more accurate values, we went into the second iteration of our mass budget. Having our I_{SP} changed also required another iteration in our calculation formula between the usable propellant mass the the rest of the mass.

9.2.1 Coefficients & Masses after steps

Considering that $ISP = 315s$ and annotating $\frac{m_{UP_i}}{m_{total_i}} = K_i$ with i the burn number :

Step	Required Δv in m/s	K_i	Mass after step
1	2802.4	0.596	$0.404 m_{initial}$
2	1342.2	0.352	$0.261792 m_{initial}$
3	522.9	0.156	$0.221 m_{initial}$
Satellite caught	NA	NA	$0.221 m_{initial} + 3500$
4	1487.8	0.382	$0.137 m_{initial} + 2163$
Satellite release	NA	NA	$0.137 m_{initial} - 1337$
5	5.3	0.0017	$0.1368 m_{initial} - 1334.73$
6	72.4	0.023	

9.2.2 Global equation between m_{UP} and $m_{initial}$

Step	$\frac{m_{UP}}{m_{initial}}$	Bias due to debris
1	0.596	0
2	0.142	0
3	0.041	0
4	0.084	1337
5	0.0002	-2.273
6	0.0032	-30.699
TOTAL	0.8664	+1304.028

This time our equation between those two masses is given by

$$m_{UsableProp} = \frac{1}{0.1336} \left[0.8664 m_{rest} + 1304.028 \right] \quad (9.1)$$

9.2.3 Second iteration of mass budget

As our way of presenting our first iteration of the mass budget didn't seem clear enough to us, we decided to present it in another, more logical way : **Structure**

Contributor	Mass (kg)
Hull	192
Tanks (including non usable propellant)	700
Wings	136
Lines	60
Connectors	16
H_2 tank	12
Structure	1 116

Electrical related contributors

Contributor	Mass (kg)
Batteries	241
Fuel cells	202
On Board Computer	5
Cables	20
H_2 for fuel cells	5
Wing actuators	10
Telecommunications	10
GNC	5
Thermal Control	10
Magnets (Payload)	25.65
Electrical related contributors	533.65

ACS and RCS

Contributor	Mass (kg)
Thrusters	36
H_2O_2	90
Reaction wheels	106
ACS & RCS	232

Propulsion

Contributor	Mass (kg)
Engine	93
Turbopumps	25
Pressurization (He)	1.3
Catalyzer	30
Propulsion	149.3

With those tables, we can deduce m_{rest} :

$$m_{rest} = m_{Structure} + m_{Elec} + m_{ACS\&RCS} + m_{Propulsion} \quad (9.2)$$

$$m_{rest} = 2\ 030.95\text{kg} \quad (9.3)$$

Thus,

$$m_{UsableProp} = \frac{1}{0.1336} \left[0.8664m_{rest} + 1304.028 \right] \quad (9.4)$$

$$m_{UsableProp} = 22\ 931\text{kg} \quad (9.5)$$

$$m_{Fuel} = \frac{m_{UsableProp}}{MR + 1} \quad (9.6)$$

$$m_{Fuel} = 2841.6\text{kg} \quad (9.7)$$

$$m_{Ox} = m_{UsableProp} - m_{Fuel} \quad (9.8)$$

$$m_{Ox} = 20\ 089.89\text{kg} \quad (9.9)$$

$$m_0 = 24\ 962.41\text{kg} \quad (9.10)$$

In this second iteration with a better I_{sp} and refined values for all of the contributors, we have a large improvement as our initial mass decreased drastically.

Data	Value	Unit
Empty raw mass	2 031	kg
Usable propellant	22 931	kg
Total mass	24 962	kg
Flowrate	10	kg/s
Rocket diameter	2	m
$I_{spvacuum}$	335	s
Thrust $F = \dot{m}I_{sp}g_0$	32863.5	N
Mixture Ratio	7.07	-
Wall thickness	TBA	m
H_2O_2 internal pressure	1.35	bar

Table 9.10: Frozen information

9.3 Frozen information

[H] After our second iteration of the mass budget, we decided to make a list of the fixed values that we will work around in our further design.

9.3.1 Frozen points

- We will do 20 aerobrakes
- We will have a separate tank design
- H_2O_2 will be pressurized by its decomposition
- The decomposition control will be managed by rotation of the spacecraft
- ACS/RCS Layout similar to the Space Shuttle
- H_2O_2 catalyzers separate
- H_2O_2/O_2 separation via thermodynamic properties
- H_2/O_2 will be used in fuel cells to produce energy

9.4 Mass Budget - Final iteration

As the fixed I_{sp} has been refined as well as other parameters, we went into our final iteration of the mass budget with the same process as the two previous ones.

9.4.1 Coefficients & Masses after steps

Considering that $ISP = 335s$ and annotating $\frac{m_{UP_i}}{m_{total_i}} = K_i$ with i the burn number :

Step	Required Δv in m/s	K_i	Mass after step
1	2802.4	0.574	$0.426 m_{initial}$
2	1342.2	0.335	$0.283 m_{initial}$
3	522.9	0.148	$0.241 m_{initial}$
Satellite caught	NA	NA	$0.241 m_{initial} + 3500$
4	1487.8	0.364	$0.153 m_{initial} + 2226$
Satellite release	NA	NA	$0.153 m_{initial} - 1274$
5	5.3	0.0016	$0.1528 m_{initial} - 1271.96$
6	72.4	0.0218	$(0.1495 m_{initial} - 1244.23)$

Table 9.11: Coefficients and masses after steps

9.4.2 Global equation between m_{UP} and $m_{initial}$

Step	$\frac{m_{UP}}{m_{initial}}$	Bias due to debris
1	0.574	0
2	0.143	0
3	0.042	0
4	0.088	1274
5	0.0002	-2.038
6	0.0033	-27.73
TOTAL	0.8505	+1244.232

Thus,

$$m_{UsablePropellant} = \frac{1}{0.1495} [0.8505 m_{rest} + 1244.232]$$

Contributor	Mass (kg)
Hull	192
Tanks	700
Wings	136
Lines	70
Connectors	16
Brackets	35
H_2 Tanks	12
Structure	1161

Contributor	Mass (kg)
Batteries	388.66
Fuel cell	202
OBC	10
Cables	57
H_2 for fuel cells	5
Wing actuators	10
Data transmission	10
GNC	10
Thermal control	20
Magnets	25.65
Electrical systems	738.31

Table 9.13: Mass budget - Electrical systems

9.4.3 Detailed contributors

Structure

Electrical systems

The mass of the batteries is given by $m_{Bat} = \frac{E_{pumps} + E_{magnet}}{ED_{Lithium}}$ with a considered energy density of $100Wh/kg$

Contributor	Mass (kg)
Thrusters	36
H_2O_2 for the ACS	90
Reaction wheels	106
Attitude control	232

Table 9.14: Mass Budget - Attitude Control

Contributor	Mass (kg)
Engine	93
Turbopumps + Electric motors	170
He for pressurization	1.3
Catalyzer	40.86
Propulsion	305.16

Table 9.15: Mass Budget - Propulsion

Attitude control

Propulsion

9.4.4 Final mass budget

Contributor	Mass (kg)
Structure	1161
Electrical systems	738.31
Attitude control	232
Heat shield	360
Propulsion	305.16
m_{rest}	2796.5
m_{UP} with a 5% performance window	25 505
m_{Fuel}	3160.5
m_{Ox}	22 345
Initial wet mass	28 302

Table 9.16: Final mass budget

Step	Mass after step (kg)
1	12 056.652
2	8 009.466
3	6 820.782
Catch	9 754.742
4	6 556.206
Release	3 056.206
5	3 052.586
6	2 986.039

Table 9.17: Masses after step

9.5 Burn times

From the tables of Δv and related mass-ratios (from the Tsiolkovsky Equation), we can get the burn times as, for each step, the burn time is defined by :

$$t_{burn} = \frac{\Delta m_{step}}{\dot{m}} \quad (9.11)$$

With \dot{m} being the general mass flow of 10 kg/s. We separate our first step into two different burns.

$$\Delta m_j = m_{j-1} \quad (9.12)$$

Step	$\Delta v_{step}(m/s)$	$\Delta m_{step}(kg)$	$t_{burn}(s)$
1	2802.4	16 245.35	1 624.535 (separate into two burns)
2	1342.2	4 047.19	404.719
3	522.9	1 188.684	118.868
4	1487.8	3 198.536	319.854
5	5.3	3.62	0.362
6	72.4	66.817	6.682
TOTAL	6 233		2 475.02

Chapter 10

Propulsion system

10.1 Engine cycle

The spacecraft uses electrically-driven turbo pumps to feed the oxidizer as well as the fuel to the engine. The propellant and oxidizer are each driven out of their tanks at low pressure, where after a turbo pump in each propellant line strain raises their pressures. As the oxidizer strain has a higher mass flow rate and faces a large pressure drop in the catalyzer, the respective pump is also more powerful as a result. The turbo pumps are driven electrically by electric motors which use large batteries for their power intake. These batteries offer enough charge for one maximum burn time of 900 seconds, after which they are re-powered by a fuel cell which runs on hydrogen and the hydrogen peroxide decomposition product oxygen. This will be explained further in section 10.3. In order to demonstrate how exactly the engine cycle is made up, a flow schematic is shown in the following. Firstly, the pressurization system is shown in Figure 11.1.

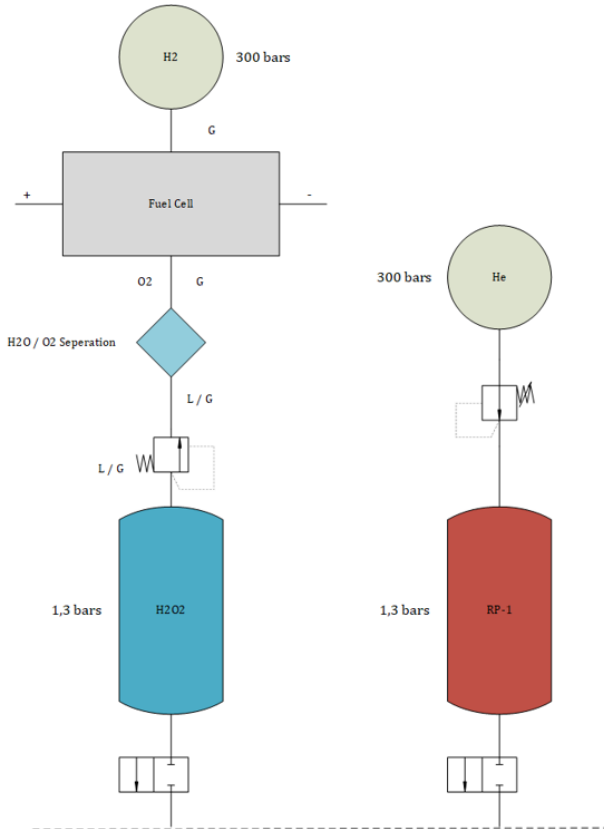


Figure 10.1: Flow Schematic - Pressurization system

As the figure shows, only the RP-1 tank is pressurized by pressurization gas, using a 300 bars helium tank. The hydrogen peroxide has certain decomposition characteristics which enable it to self-pressure due to the rising pressure upon vaporization. The critical point of hydrogen peroxide is at around 150 degrees Celsius and 1.5 bars, meaning that if the thermal control is sufficiently reliable, a tank pressure of around 1.3 bars can be maintained by self-pressure. The control system and more details will be explained in section 10.3. The 300 bars H₂ Tank that can be seen in the pressurization system flow schematic is therefore not a pressurization tank, but a tank for the sole purpose of running the fuel cell in combination with the oxygen which is separated from water, which is the second decomposition product of hydrogen peroxide. The separation works by simply condensing the water and allowing the gaseous oxygen to pass through a filter. Both the RP-1 tank and the H₂O₂ tank have a main valve after their outlets, which are visible in Figure 11.1. The remaining feeding system is shown in the second part of the flow schematic, depicted in Figure 11.2.

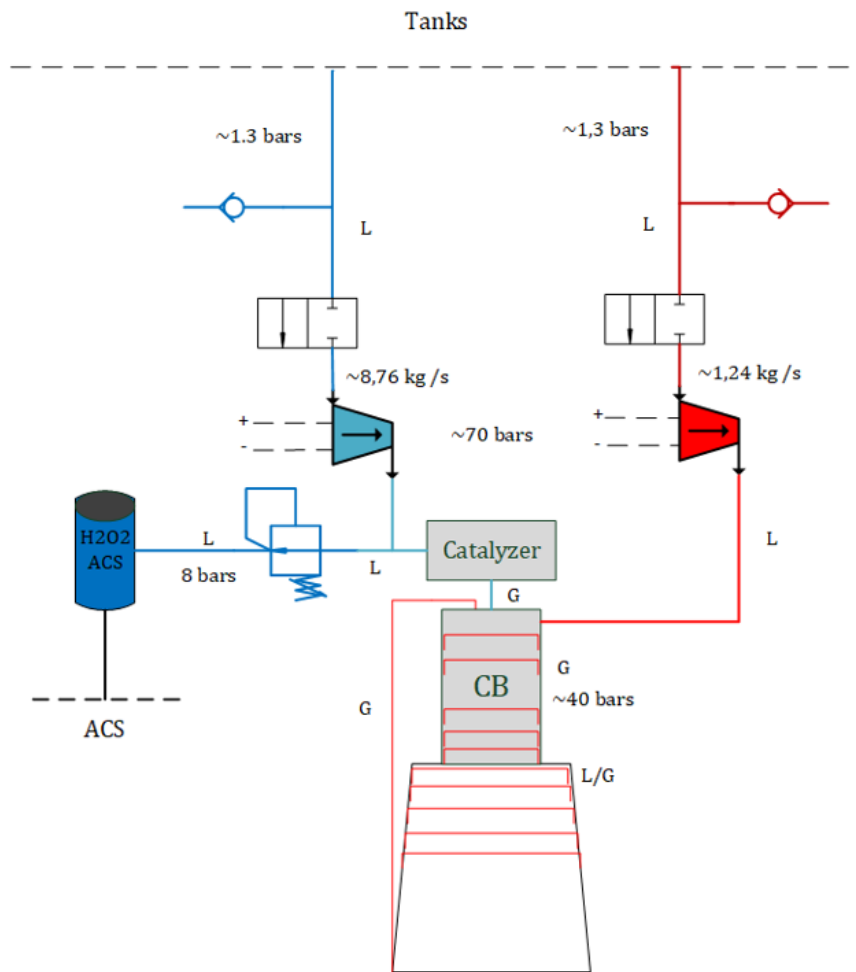


Figure 10.2: Flow Schematic - Engine section

The fueling ports for RP-1 as well as hydrogen peroxide extend to the left- and right-hand-side of the top of the figure. Check valves are situated at these points to only allow propellant flowing in. A second main valve for both propellants is installed just before the turbopumps, which are closed during refueling. While the RP-1 is then funneled through cooling channels in the regenerative cooling system, the oxidizer runs into a catalyzer, where a rapid decomposition reaction splits the hydrogen peroxide into its reactive products for combustion. A second oxidizer strain is guided towards a pressure regulation valve, behind which it continues into a buffer tank of hydrogen peroxide for monopropellant use in the ACS. The catalyzers for ACS thrusters are located in close proximity to their respective combustion chambers. The ACS is not depicted as a flow schematic.

10.2 RCS / ACS

In the previous section we mention that we are going to use hydrogen peroxide as a monopropellant for our Reaction Control System. Indeed, hydrogen peroxide can be used as a quite good RCS propellant.

At the moment, the biggest part of the monopropellant thruster using H_2O_2 are test bench engine. This is because of the difficulty to characterize the engine and its parameters.

Hydrogen peroxide is usable as a monopropellant because of its natural decomposition. As we are going to see on the Catalyzer part further on the report H_2O_2 can be decomposed in H_2 and H_2O . That's this decomposition we are going to use inside our thruster. When hydrogen peroxide goes through a catalyser it decomposes and generates a great amount of heat, up to 1000K. This two factors create steam at a very high temperature and pressure; it's this steam that creates our thrust.

Before designing the engine and its characteristics we need to choose the positioning of the thrusters. In order to do that, we based our design on the American Space Shuttle which use cluster of small thrusters all around the spacecraft to allow a good maneuverability.

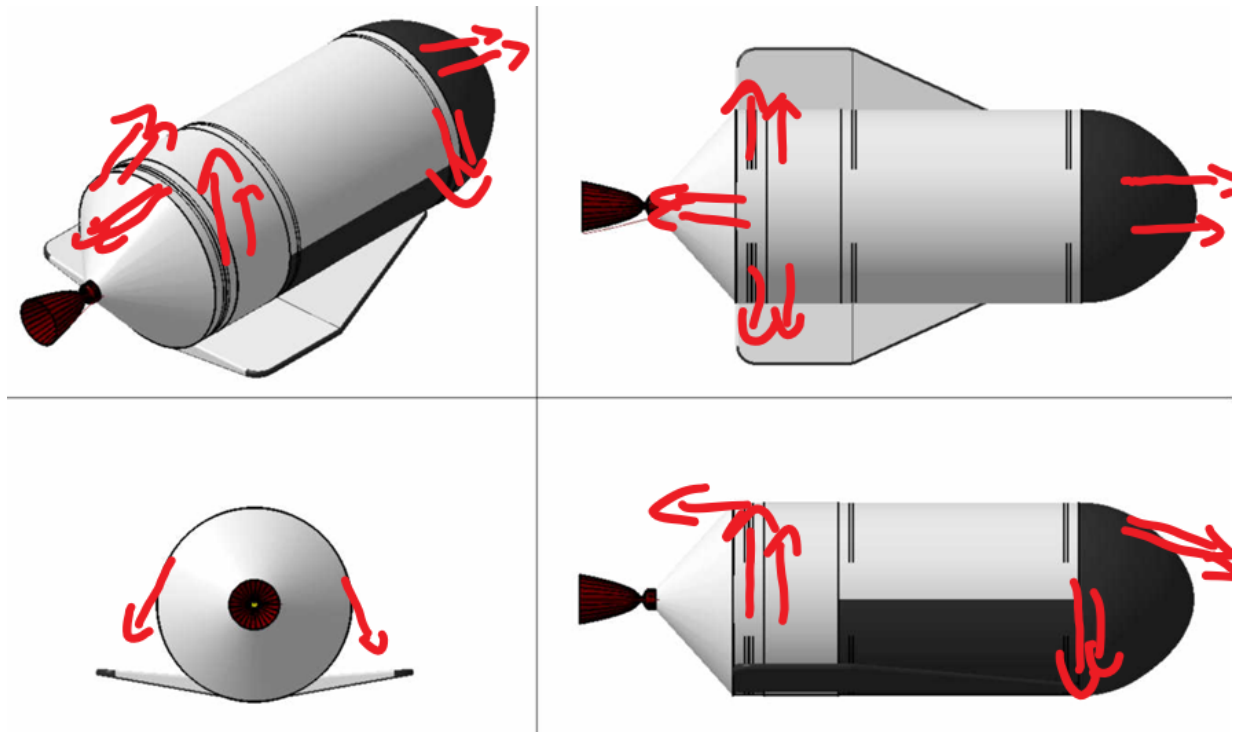


Figure 10.3: RCS thruster repartition

We are going to use 6 different clusters spread over the craft, each cluster is composed of 2 thrusters for a total of 12. This disposition allow to manipulate every axis.

Now we need to compute the characteristic of the thruster, to do so we used RPA (a NASA software to compute the parameters of a thruster based on the propellant and several other characteristics) and some papers of recent studies about hydrogen peroxide thruster.

We assumed a chamber pressure of 10bars and a thrust of 100N , then we use RPA to get the other parameters.

- Combustion temperature: $1223K$
- Ejection temperature: $424K$
- Ejection pressure : 0.094bars
- $\gamma = 1.335$
- $R = 368.6$
- $ISP = 140s$

With these parameters we can then compute every other parameters we want for the thruster and especially the mass flow rate which is necessary to have a correct mass budget.

$$c^* = \sqrt{\frac{RT_c}{\gamma}} \times \frac{\gamma + 1}{2}^{\frac{\gamma+1}{2(\gamma-1)}}$$

Throat characteristics:

$$T_t = T_c \left(\frac{2}{\gamma + 1} \right) \quad P_t = P_c \left(\frac{2}{\gamma + 1} \right)^{\frac{\gamma}{\gamma-1}} \quad \rho = \frac{P_t}{RT_t} \quad u_t = \sqrt{\gamma RT_t}$$

Exhaust characteristics:

$$M_e = \sqrt{\frac{2}{\gamma - 1} \left[\left(\frac{P_c}{P_e} \right)^{\frac{\gamma-1}{\gamma}} - 1 \right]} \quad T_e = \frac{T_c}{1 + \frac{\gamma-1}{2} M_e^2} \quad \rho_e = \frac{P_e}{RT_e}$$

Thus we can compute the area ratio and the thrust coefficient:

$$\frac{A_e}{A_t} = \frac{1}{M_e} \left[\frac{2}{\gamma + 1} \left(1 + \frac{\gamma - 1}{2} M_e^2 \right) \right]^{\frac{\gamma+1}{2(\gamma-1)}}$$

$$C_F = \gamma \sqrt{\left(\frac{2}{\gamma + 1} \right)^{\frac{\gamma+1}{\gamma-1}} \frac{2}{\gamma - 1} \left[1 - \left(\frac{P_e}{P_c} \right)^{\frac{\gamma-1}{\gamma}} \right]} + \frac{P_e - P_a}{P_c} \frac{A_e}{A_t}$$

Finally we can compute the exhaust velocity, throat area and the mass flow:

$$c = C_F c^* \quad A_t = \frac{F}{C_F P_c} \quad \dot{m} = \frac{P_c A_t}{c^*}$$

Thus we can write the following Matlab code to simulate:

```

1 Pc = 10; % Chamber pressure
2 Pe = 0.094; % exhaust Presssure (given RPA)
3 gamma = 1.335; % RPA
4 R = 0.3686e3; % RPA
5 Tc = 1223; % Combustion temperature given (RPA)
6
7 c = sqrt( R * Tc / gamma ) * ((gamma + 1)/2)^((gamma + 1)/2 * (gamma - 1));
8
9 % Throat characterisctics
10 Tt = Tc * (2/(gamma + 1));
11 Pt = Pc * (2/(gamma + 1))^((gamma/(gamma - 1)));
12 rho = Pt / R * Tt;
13 Ut = sqrt(gamma * R * Tt);
14
15 % Exhaust characteristics
16 Me = sqrt((2/(gamma - 1))*((Pc/Pe)^((gamma - 1)/ gamma - 1)));
17 Tebis = Tc / (1 + ((gamma - 1) / 2) * Me^2);
18 rho_e = Pe / R * Tebis;
19
20 Exp_ratio = (1 / Me) * ((2 / (gamma + 1)) * (1 + ((gamma - 1) / 2) *
21   ↳ Me^2))^((gamma + 1)/2*(gamma-1));
21 Cf = gamma * sqrt((2/(gamma + 1))^((gamma + 1)/(gamma - 1)) * (2/(gamma -
22   ↳ 1)) * (1 - (Pe/Pc)^((gamma - 1)/gamma))) + ((Pe - 1)/Pc) * Exp_ratio;
22
23 c_e = Cf * c; At = 100 / (Cf * Pc); m_flow = (Pc * At)/c;
```

From the simulation we finally have:

- Exhaust velocity: $c = 617.38 \text{ m/s}$
- Mass flow rate: $\dot{m} = 0.105 \text{ kg/s}$

The most important value for us is the mass flow rate as it allows us to compute the propellant mass needed to perform our maneuvers.

In addition of the thrusters we also need another system which is the Reaction Wheels. This system which is separated in 3 different wheels, one for each axis, and allow to rotate the entire craft on the 3 axes with the reaction motion applied by the rotation of the wheel.

10.3 Multi-usage of hydrogen peroxide

Hydrogen Peroxide as the main engines oxidizer is the main dictator of all sub-system and system design decisions. GREDER uses it for following applications:

1. Main engine oxidizer
2. ACS mono-propellant
3. Fuel cell power generation in combination with stored hydrogen
4. Oxidizer tank pressurization

Hydrogen peroxide's decomposition behavior is the reason for its multi-purpose usability, but also its major risk. If the pressure or temperature in the tank go unregulated and exceed certain boundaries, the propellant can enter critical status and endanger the tank's integrity. Therefore, extensive design and simulation was conducted to determine a tank design which allows thermal regulation based on the rotational angle of space craft, as indicated in Figure 10.4.

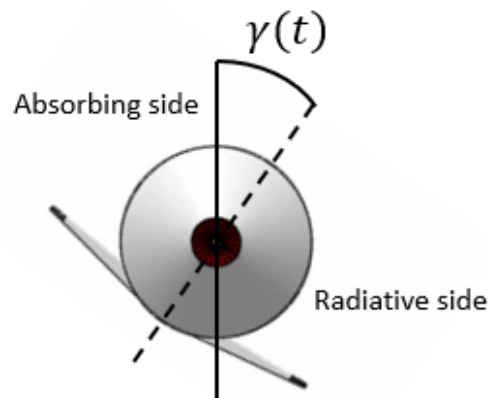


Figure 10.4: Lessons learnt

The absorbing side of the space craft is painted in a way which causes a high absorption coefficient and a low emissivity, while the radiative side is coated vice-versa. The tank materials are chosen to deliver high heat transfer while being compatible with hydrogen peroxide. Thereby, a rotation of the space craft will cause a change in the heat flux, while every hydrogen peroxide temperature can be assigned a rotational angle for neutral heat flux at which no temperature change happens. This design was simulated with some simplifications and its technological feasibility could be verified. This is detailed in section 11.3.

The usage of hydrogen peroxide is the sole reason for GREDER using electrically-driven turbo pumps, as the ease in electricity production makes this the most efficient method. The relatively low combustion chamber pressure and thrust are not a major issue, as a long mission duration is necessary anyways for electricity production in between burns. In addition, the low complexity of the electric turbo pump cycle compensates for the higher complexity of the challenge of storing hydrogen peroxide for long durations, as it is a highly reactive chemical which poses extreme risks, especially due to its decomposition behavior, which GREDER uses as an advantage.

As batteries have a low energy density compared to chemical fuels, electric cycles for main engines usually come with a mass disadvantage due to the necessity of carrying large battery masses. While GREDER needs a total main engine burn time of around 2500 seconds per mission, the battery only needs to power the turbo pumps and electrical equipment for 900 seconds at a time, because the hydrogen peroxide decomposition product oxygen powers a fuel cell in combination with hydrogen between main engine burns for additional power generation. The main trade-off to consider at this point is between bringing a fuel cell, a hydrogen tank and the additional equipment for separation of the decomposition products and dimensioning the battery large enough for powering the entire mission. As the other applications of the hydrogen peroxide are discussed in other chapters, this chapter will detail the power generation usage and detail a trade-off with respect to using a larger battery. The detailed description of how the power generation and tank pressure control work can be found in chapter 12 and the simulation model in the annex. This chapter will use analytical terms to compare the two approaches, while the simulation can be seen as a proof of concept.

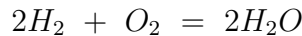
In order to determine the necessary masses for the additional components for fuel cell usage, the energy output of the fuel cell was calculated using the reaction energy multiplied with an assumed efficiency coefficient supported by literature. Following assumption for the efficiency was made:

$$\eta_{Fuel_cell} = 0.6 \quad (10.1)$$

With the theoretical reaction energy being :

$$P_{Fuel\ cell_{th}} = 286\ 000\ J/mole \quad (10.2)$$

For the reaction :



Taking the mole masses into account and assuming complete reaction, for every kilogram of hydrogen the fuel cell uses 7.937 kg of oxygen. The resulting energy per kilogram of hydrogen can then be calculated as follows:

$$E_{Fuel\ cell_{real}} = 286\ 000\ J/mole \times 0.6 \times \frac{1kg}{0.01\ kg/mole} = 47.29\ kWh \quad (10.3)$$

In order to perform a trade-off calculation between using a fuel cell for battery re-charging or installing a larger battery directly, the total masses for both systems will be compared at this point. The current mass budget for the fuel cell system is as follows:

Component	Mass (kg)
Battery	388.66
Fuel cell	202
H_2 tank	5
Other equipement	10
Total	605.66

Now, as the fuel cell allows GREDER to only be designed for a 900 s duration of not being re-powered, the battery mass can remain relatively low at a conservative battery energy density of 100 Wh/kg. During the burn duration, around 98.6% of electrical energy is used to power the turbo pumps. Therefore, as a first estimate, the necessary battery mass for powering the turbo pumps during all mission burn times, which amount to 2475.2 seconds, is calculated:

$$m_{Bat,\ onlybat} = \frac{P_{TP} \times 2475.2s}{100\ Wh/kg} = 1\ 053.9\ kg \quad (10.4)$$

This results in a **mass difference of 448.2kg in favour of the fuel-cell architecture**. Now, two possible problems can be brought up with this estimation:

1. The energy density estimate is at the lower end of current lithium battery technology and a higher density would result in a shift towards the advantages of using only a battery.
2. The fuel-cell architecture is not technologically proven in combination with hydrogen peroxide decomposition and constitutes larger technical complexity.

While these points are valid arguments for using only a battery, the trade-off analysis clearly pointed out using a fuel-cell would result in a mass reduction, the higher level of technical complexity of which is justifiable. The above-mentioned arguments can be answered as follows:

1. While lithium batteries of higher energy densities have been flight-proven, the mission itself has never been performed in a similar way. Refuelling and frequent satellite capturing are completely new territory and therefore, conservative estimates in key design criteria offer a way of compensating for the additional mission challenges.
2. Fuel cells are very well researched and very common technology in on-earth use. Therefore, the implementation of a decomposition-product recycling system, while posing some new design problems, is not comparable to the difficulty of challenges like designing a new engine. Additionally, as this mass estimate only takes turbo pump power into account, the battery-only architecture would need to either have even greater battery mass or be fitted with solar power generators to cover the system power requirements between burns. This again adds up to system complexity and poses large problems during re-entry.

10.4 Propellant tanks

The vehicle must use propellant tanks in order to carry the oxidizer and fuel, in this case H₂O₂ and RP-1, during the mission. The required total useable propellant was already found in the final mass budget calculation. This chapter describes the tank design beginning with the requirements and tank specification, afterwards the analysis of compatible materials following by the design including different options, expulsion principle, stresses, MAIT and final design. The Liner tanks are also addressed in the last part of this chapter.

10.4.1 Requirements and specification

Several parameters have to be set in prior to the propellant tank design in order to ensure that all top level vehicle and propulsion system requirements are met. Additionally it must be ensured that the propellant tank assemblies sustain launch and flight loads during all phases of the mission.

Propellant Tank masses and volumes

Table 10.1 shows the calculated values of the final propellant mass and final volumes of both oxidizer and fuel. The basis of this calculation is the final mass budget that provided the useable propellant masses. Starting at this value and calculating 1% additional propellant

for ignition, 2% for shutdown, 2% performance reserve and 2% residuals, the masses add up to 24t for H₂O₂ and 3.4t for RP-1. H₂O₂ needs a greater ullage volume than RP-1 due to the decomposition, with 20% ullage a total tank volume of $\geq 18.62 \text{ m}^3$ is necessary. For RP-1 a total tank volume of $\geq 3.99 \text{ m}^3$ needs to be accomplished.

	H ₂ O ₂	RP-1
Useable propellant [kg]	22347	3161
+ RACS propellant [kg]	90	N/A
1% ignition transus (0.2% per burn) [kg]	223.5	31.6
2% shutdown transus (0.4% per burn) [kg]	446.9	63.2
2% performance reserve [kg]	446.9	63.2
2% residuals [kg]	446.9	63.2
Final propellant mass [kg]	24001.2	3382.2
Volumes [m^3]	15.52	3.63
Ullage [m^3]	3.1 (20%)	0.36
Final volumes [m^3]	18.62	3.99

Table 10.1: Propellant masses and volumes

Driving requirements

The driving requirements for the oxidizer propellant tank assembly (PTA) are summarized in Table 10.2. MDP is taken according to ECSS¹

Subject	Requirement Description	
	Oxidizer Tank	Fuel Tank
Usable net volume	18.62 m^3	3.99 m^3
Tank dimensions	Interface diameter $\leq 2500 \text{ mm}$	Interface diameter $\leq 2500 \text{ mm}$
Tank mass	$\leq 650 \text{ kg}$	$\leq 200 \text{ kg}$
Maximum design pressure (MDP)	1.3 bar	1.3 bar
Launch pressure	1.3 bar	1.3 bar
Proof pressure	1.25 x MDP	1.25 x MDP
Burst pressure	1.5 x MDP	1.5 x MDP
Pressure drop	$\leq 50 \text{ mbar}$	$\leq 50 \text{ mbar}$
Flow rate	8.76 kg/s	1.24 kg/s
Expulsion efficiency	$\geq 99.5\%$	$\geq 99.5\%$
Accelerations	$4g_o$ in lateral direction $2g_o$ in vertical direction	$4g_o$ in lateral direction $2g_o$ in vertical direction

Table 10.2: PTA driving requirements

¹ECSS-E-ST-32-01C Rev. 1, Fracture control

Pressure loads

The ECSS² requires a safety factor of 1.25 on proof pressure and 1.5 on burst pressure. Therefore the pressure levels including safety factors are listed in Table 10.3.

	Oxidizer	Fuel
MDP	1.3 bar	1.3 bar
Proof pressure	1.63 bar	1.63 bar
Burst pressure	1.95 bar	1.95 bar

Table 10.3: PTA pressure loads

The number of pressure cycles after delivery is shown in Table 10.4. This number of pressure cycles applies for both the oxidizer and fuel tank.

	Oxidizer	Fuel
MDP	1.3 bar	1.3 bar
Proof pressure	1.63 bar	1.63 bar
Burst pressure	1.95 bar	1.95 bar

Table 10.4: PTA pressure cycles

²ECSS-E-ST-32-01C Rev. 1, Fracture control

10.4.2 Materials

The intended materials for the propellant tanks are listed in Table 10.5. For the fuel tank and liner tanks a common titanium alloy can be used with high strength and good ductility. The titanium alloy shall be heat treated to .7 status (solution treated and aged) in order to achieve the below mentioned material characteristics and to stress relieve. The liner tanks can also be winded or wrapped with CFK in order to be further strengthened and to reduce the wall thickness of the titanium.

The oxidizer tank shall be manufactured of aluminum 5254 which is long term compatible and corrosion resistant against H₂O₂. Unfortunately the aluminum alloy shows a low strength which has to be taken into account in the mechanical calculations. A higher strength option of this alloy is currently in development acc. to NASA paper.

	OX Tank	Fuel Tank	Liner Tanks
Propellant	H ₂ O ₂	RP-1	H ₂ , He
Material	Aluminum 5254	TiAl6V4 .7	TiAl6V4 .7
Reason	<ul style="list-style-type: none"> ▪ Resistant against H₂O₂ ▪ Lightweight ▪ Higher strengths option is currently in development acc. to NASA paper 	<ul style="list-style-type: none"> ▪ Typical aerospace alloy ▪ High tensile strength with good ductility ▪ Good for electron beam welding 	<ul style="list-style-type: none"> ▪ Often used for high pressure (300-500bar) applications ▪ Sometimes enforced with by CFK wrapping ▪ High tensile strength with good ductility ▪ Good for electron beam welding
R _{P0.2} (yield) [MPa]	270	1034	1034
UTS (ultimate) [MPa]	350	1103	1103

Table 10.5: Propellant tank materials

10.4.3 Concepts and options

During the process of finding the optimum propellant tank concept for the GREDER vehicle, our mission and application, several possible design option have been taken into account. Figure 10.5 shows the three most promising options.

The first option is an integrated concept with the fuel tank placed within the oxidizer tank. Integrated designs are in theory the most lightweight design option for propellant tanks because the basic idea is to reduce the wall thickness of the inner tank due to theoretically no pressure delta between fuel and oxidizer tank pressure. The downside of this option is the manufacturing. Also the use of spacecraft volume is quite attractive with this design. Manufacturing of one tank inside of another tank and then welding it is a tough task. Additionally the fuel tank also needs to be compatible with both propellants because it is in contact with the oxidizer from the outside and the fuel from the inside. Therefore option 1 is not suitable for our application due to manufacturing complexity, material compatibility and our MDP of 1.3 bar is way too low to justify the advantage of wall thickness reduction.

The second option is also an integrated option but this time with two separate tanks. This slightly increases the spacecraft volume but is still more spacecraft volume efficient than option 3. This option, especially the special shape of the oxidizer tank, is a complex geometry and therefore also complex to manufacture. The fuel tank manufacturing is simpler than in the first option due to the half sphere hemispheres and gimbal mounting. During first attempts of a detailed design of that option it was found that the vehicle diameter increased over the boundary requirement. For this reason and also due to the complex manufacturing and design this option was found to not be the most efficient design for our application.

The third option is a rather simple “two-tanks-on-top-of-each-other” design. The main advantage is here the simple design and manufacturing and assembly of all parts, the possibility of load carrying structure of the outer tank walls as well as good options for tank expulsion principles. This design was found to be the optimum for our application and is therefore the baseline for all further calculations and detailed design.

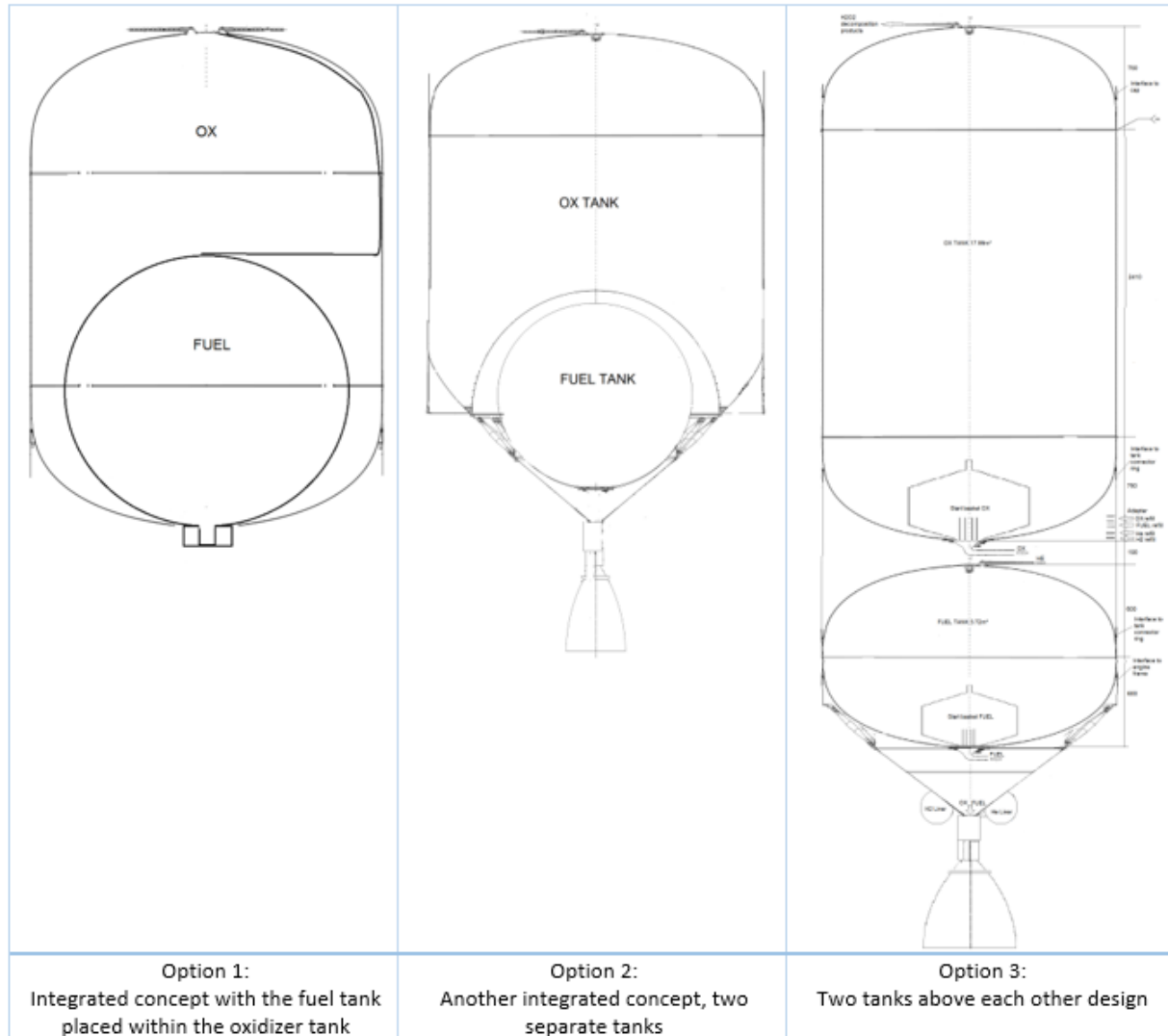


Figure 10.5: Different propellant tank design options

10.4.4 Final design

The final design is therefore an option with a stacked structure, as already mentioned in the previous chapter. ?? shows a detailed view on the final design with the major parts shown. The Oxidizer tank consists of two cassini shaped hemispheres and one large cylinder (or several smaller cylinders if easier to manufacture). The fuel tank is built with the same cassini hemispheres, but without a cylinder. This usage of the same hemispheres for both oxidizer and fuel tanks reduces costs for jigs and tools and also for development. Each tank has an inlet at the top of the tank and an outlet at the bottom. It has to be mentioned that the upper port of the oxidizer tank is used to extract the H₂O₂ decomposition products and not to pressurize the tank since the tank is self-pressurizing.

Both propellant tanks make use of start baskets, the function is explained in the subsequent chapter.

The propellant tanks are the carrying structure of the spacecraft and they are connected by interface connector rings. In the interface connector ring there are also the adapters for refueling planned.

At the bottom of the spacecraft near the engine are the liners located. There is one helium liner tank for Fuel tank pressurization and one hydrogen liner tank for the fuel cell operation. Figure 10.7 shows a full view on the final design of the propellant tanks.

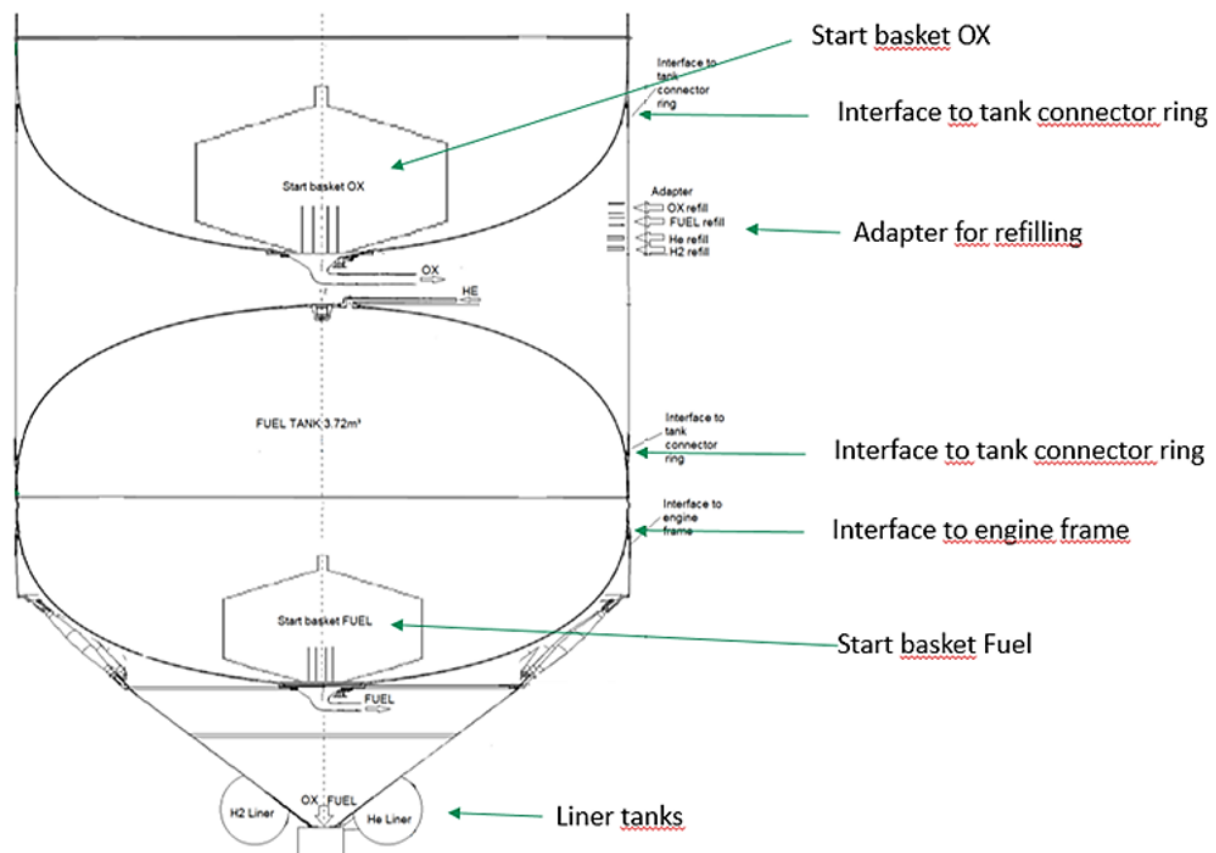


Figure 10.6: Final propellant tank design detailed view

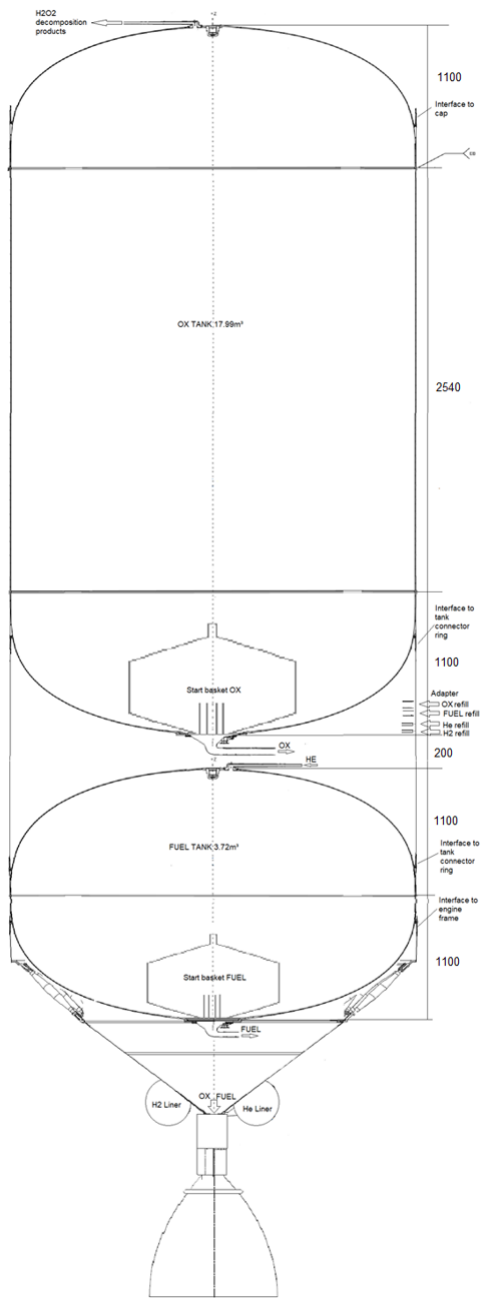


Figure 10.7: Final propellant tank design full view

10.4.5 Expulsion principle

The refillable start basket is a structure within the propellant tanks located at the outlet of the tank that is designed to ensure that there is always propellant at the outlet in zero gravity condition – at least until the spacecraft acceleration again forces the propellant towards the outlet. If the thrusting duration is sufficient to settle the liquid each time, the

start basket, is the best light weight and simple propellant management device. The start basket volume for each of the tanks must be big enough (with margin) to supply propellant to the engine until acceleration settles the liquid again. Another important aspect is that the start basket must be refillable to allow several ignitions of the engine. This principle is shown in Figure 10.8.

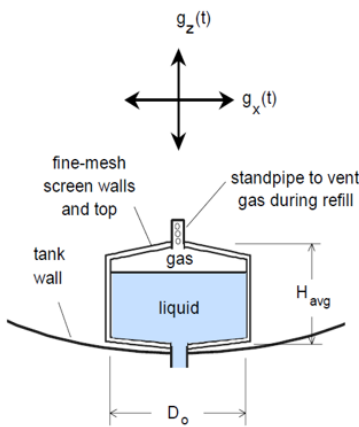


Figure 10.8: Final propellant tank design full view

Start basket design

For the start basket design, the maximum acceleration has to be defined. As already listed in the propellant tank requirements, the maximum acceleration is:

$$g_x = 4 \times g_0 \quad (10.5)$$

$$g_z = 2 \times g_0 \quad (10.6)$$

$$g_0 = 9.81 m/s \quad (10.7)$$

The first step for the start basket design is the calculation of settling acceleration, the acceleration with which the propellant moves towards the outlet

$$a_{set} = \frac{F}{m_{spacecraft}} = \frac{32860 N}{28302 kg} = 1.16 m/s^2 \quad (10.8)$$

With this acceleration the time the propellant needs to reach the ground can be calculated

$$t_{fall_{Oxidizer}} = \sqrt{\frac{h_{Ox}}{\frac{1.16}{2}}} = \sqrt{\frac{4.74}{\frac{a_{set}}{2}}} = 2.54s \quad (10.9)$$

$$t_{fall_{Fuel}} = \sqrt{\frac{1.2}{\frac{1.16}{2}}} = 2.54s \quad (10.10)$$

Since the time that the oxidizer and fuel need to reach the outlet is now known, the settling time can be calculated. The settling time is the falling time multiplied by four. This is a heritage value

$$t_{set_{Oxidizer}} = 4 \times t_{fall_{Oxidizer}} = 10.16s \quad (10.11)$$

$$t_{set_{Fuel}} = 4 \times t_{fall_{Fuel}} = 5.76s \quad (10.12)$$

With this information, the necessary start basket volume can be calculated by calculating what propellant volumes are needed to cover the settling time while still providing the requested flow rates to the engine.

$$V_{basket_{Oxidizer}} = \frac{t_{set_{Oxidizer}} \times m_{Oxidizer}}{\rho_{Oxidizer}} = 0.0618m^3 \quad (10.13)$$

$$V_{basket_{Fuel}} = \frac{t_{set_{Fuel}} \times m_{Fuel}}{\rho_{Fuel}} = 0.0079m^3 \quad (10.14)$$

It is now possible to roughly calculate size of the start basket by assuming it to be a cylinder with $d = h$

$$d_{Oxidizer} = h_{Oxidizer} = \left(\frac{V_{basket_{Oxidizer}}}{\frac{4}{\pi}} \right)^{\frac{1}{3}} = 0.36m \quad (10.15)$$

$$d_{Fuel} = h_{Fuel} = \left(\frac{V_{basket_{Fuel}}}{\frac{4}{\pi}} \right)^{\frac{1}{3}} = 0.18m \quad (10.16)$$

Afterwards the screens and screen drillings have to be dimensioned in such a way that the screens are capable to hold the propellant inside of the start basket by propellant surface tension. The if the pressure on the grids due to hydrostatic pressure by g_x (the highest acceleration) exceeds the bubble point pressure, the liquid will break through and is not captured inside the start basket anymore

$$p_{BubblePoint_{Oxidizer}} = \rho_{Oxidizer} \times g_x \times h_{Oxidizer} = 206\text{mbar} \quad (10.17)$$

$$p_{BubblePoint_{Fuel}} = \rho_{Fuel} \times g_x \times h_{Fuel} = 65\text{mbar} \quad (10.18)$$

$$(10.19)$$

In the last step the screen drillings are dimensioned in that way that the bubble point is not exceeded by the acceleration taking the surface tension into account

$$Stens_{Oxidizer} = 0.08\text{N/m} \quad (10.20)$$

$$Stens_{Fuel} = 0.028\text{N/m} \quad (10.21)$$

$$d_{drillings_{Oxidizer}} = \frac{4 \times Stens_{Oxidizer}}{p_{BubblePoint_{Oxidizer}}} = 0.0155\text{mm} \quad (10.22)$$

$$d_{drillings_{Fuel}} = \frac{4 \times Stens_{Fuel}}{p_{BubblePoint_{Fuel}}} = 0.0172\text{mm} \quad (10.23)$$

$$(10.24)$$

Therefore it has to be a very fine mesh.

10.4.6 Stresses

For the preliminary calculation of stresses and wall thicknesses several loads on the propellant tank have been identified:

- Internal tank pressure
- Hydrostatic pressure on tank walls due to accelerated propellant
- Tension and compression stress due to empty mass and propellant mass

General rules :

1. No rupture at burst pressure
2. No yield at proof pressure

The results of these calculations are listed in Table 10.6. The calculations are based on the maximum possible wall thickness that still complies with the tank mass requirement. On basis of the results the wall thickness can be further optimized.

	Oxidizer Tank	Fuel Tank
MDP	$0.13 \frac{N}{mm^2}$	$0.13 \frac{N}{mm^2}$
Proof pressure	$0.163 \frac{N}{mm^2}$	$0.163 \frac{N}{mm^2}$
Burst pressure	$0.195 \frac{N}{mm^2}$	$0.195 \frac{N}{mm^2}$
Accelerations	$g_0=9.81;$ $g_x=4*g_0;$ $g_y=2*g_0;$	$g_0=9.81;$ $g_x=4*g_0;$ $g_y=2*g_0;$
Material properties	Aluminum 5254 $Oxidizer_{yield} = 270 \frac{N}{mm^2}$ $Oxidizer_{UTS} = 350 \frac{N}{mm^2}$ $\rho_{Oxidizer} = 2700 \frac{kg}{m^3}$	Titanium TiAl6V4.7 $Fuel_{yield} = 1034 \frac{N}{mm^2}$ $Fuel_{UTS} = 1103 \frac{N}{mm^2}$ $\rho_{Fuel} = 4500 \frac{kg}{m^3}$
Tank mass	$\leq 650 \text{ kg}$	$\leq 200 \text{ kg}$
Wall thickness with given geometry at maximum mass	$s = 6.8 \text{ mm}$	$s = 3.9 \text{ mm}$
Hydrostatic pressure on tank walls		
On cylindrical parts by g_x acceleration $p_{hydro\ cylinder} = \rho_{Propellant} * g_x * h$ h is in this case the diameter of the tank	$p_{hydro\ cylinder} = 0.1413 \frac{N}{mm^2}$	N/A
On spherical parts by g_y acceleration $p_{hydro\ hemisphere} = \rho_{Propellant} * g_y * h$ h is in this case the total height of the tank	$p_{hydro\ hemisphere} = 0.1424 \frac{N}{mm^2}$	$p_{hydro\ hemisphere} = 0.0441 \frac{N}{mm^2}$
Internal tank pressure by "Kesselformel"		
Tank cylinder Tangential stresses: $\sigma_{t_{ip}} = \frac{p * d_m}{2 * s}; p = MDP + p_{hydro\ cylinder}$	$\sigma_{t_{ip}} = 49.87 \frac{N}{mm^2}$ $\sigma_{a_{ip}} = 11.95 \frac{N}{mm^2}$	N/A
Axial stresses: $\sigma_{a_{ip}} = \frac{p * d_m}{4 * s}; p = MDP$		
Tank hemispheres Axial stresses (no tangential stresses) $\sigma_{a_{ip}} = \frac{p * d_m}{4 * s}; p = MDP + p_{hydro\ hemi}$	$\sigma_{a_{ip}} = 25.04 \frac{N}{mm^2}$	$\sigma_{a_{ip}} = 16.00 \frac{N}{mm^2}$
Tension and compression stress due to empty mass and propellant mass (safety factor $sf = 3$)		
$\sigma_{tc} = \left(\frac{m_{total} * g_y}{A_{crosssection}} \right)$ with $m_{total} = mass_{Tank\ max} + mass_{prop}$	$\sigma_{tc} = 9.08 \frac{N}{mm^2}$	$\sigma_{tc} = 2.3 \frac{N}{mm^2}$
Total stresses		
Cylinder $\sigma_{axial} = (\sigma_{a_{ip}} + \sigma_{tc}) * sf$	$\sigma_{axial} = 63.09 \frac{N}{mm^2}$	N/A
Cylinder $\sigma_{tangential} = (\sigma_{t_{ip}}) * sf$	$\sigma_{tangential} = 149.61 \frac{N}{mm^2}$	N/A
Hemisphere $\sigma_{axial} = (\sigma_{a_{ip}} + \sigma_{tc}) * sf$	$\sigma_{axial} = 102.36 \frac{N}{mm^2}$	$\sigma_{axial} = 54.9 \frac{N}{mm^2}$
Check with material properties		
All $\sigma \leq$ Yield and UTS	YES	YES

Table 10.6: Preliminary tank stresses calculation

10.4.7 Liner tanks

Helium liner tank

Only the fuel tank is pressurized by Helium and only needs a tank pressure of 1.3bar. The H₂O₂ tank is self-pressurizing due to the decomposing characteristics of H₂O₂. The specification of the helium liner tank is shown in Table 10.7

Helium Liner Tank	
MDP	300 bar
Proof (1.25x MDP)	375 bar
Burst (1.25x MDP)	450 bar
Helium mass	1.07 kg
Helium tank volume	20 Liters
Radius spherical helium tank	168.2mm

Table 10.7: Helium liner tank specification

H₂ liner tank

The H₂ is needed for the fuel cell. The specification of the h2 liner tank is shown in Table 10.8.

H2 Liner Tank	
MDP	500 bar
Proof (1.25x MDP)	625 bar
Burst (1.25x MDP)	750 bar
Helium mass	6 kg
Helium tank volume	135 Liters
Radius spherical helium tank	318mm

Table 10.8: Helium liner tank specification

10.5 Catalyzer

Besides the advantages of H₂O₂ there is one major drawback that we have to take into account. This drawback is that H₂O₂ needs to be decomposed in H₂ and H₂O in order to react with RP-1.

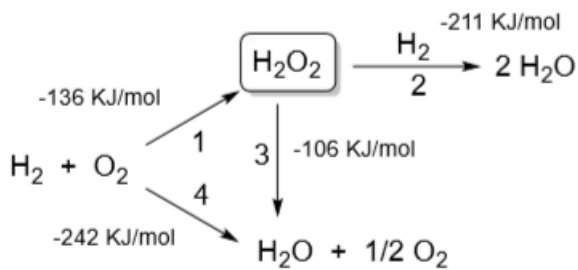


Figure 10.9: H_2O_2 chemical decomposition process

This decomposition is natural but at a low rate whereas we need a very high decomposition rate in order to feed the combustion chamber and sustain a proper flame. This decomposition is an exothermic decomposition. That's why we need a catalyser.

This catalyser needs to be placed between the turbo pump and the injectors. It allows to decompose the H_2O_2 at the last time.

The way a catalyser works is pretty simple; the H_2O_2 goes through a catalyst bed of silver pellets, reacts and generates heat. Why silver ? We chose silver because is the mostly used catalyser for H_2O_2 . However, a lot of other different material exists, like Platinum, Manganese or even Gold but these materials are rarely used due to their cost and also the fact that they need to be made in complex alloy in order to optimize the reaction.

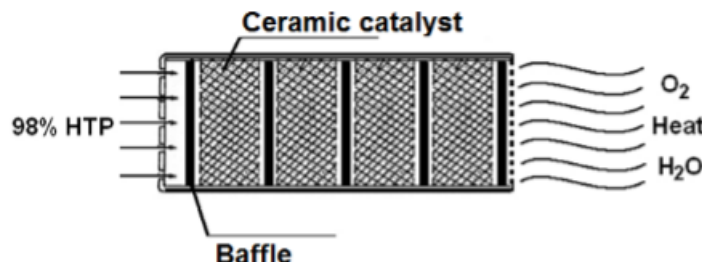


Figure 10.10: Example of catalyst bed

The figure above shows basically how a catalyser works. To have an idea of the shape of ours we just have to swap the ceramic catalyst by silver catalyst. So, it will be a steel cylinder filled with small spherical silver pellet separated by some baffles (silver grid mesh).

An important characteristic of the catalyser is the pressure drop it creates. This pressure drop influences the whole feeding system, the turbo pump sizing and even the injector design. that's why we need to characterize the pressure drop created by the catalyser. In order to do so, we are going to use the Ergun equation for packed bed reactor:

$$\frac{\Delta p}{L} = 151.2 \frac{\mu}{d^2} \frac{(1-\epsilon)^2}{\epsilon^2} u + 1.8 \frac{\rho}{d} \frac{1-\epsilon}{\epsilon^3} u^2$$

With μ the dynamic viscosity, ϵ the porosity, d the pellet diameter, ρ the density, L the length of the bed and u the velocity.

In this equation we need some important component such as ϵ . The porosity is complicated to compute and need to be model. According to a recent research we determined a porosity of 0.3802 with a pellet diameter of 5mm.

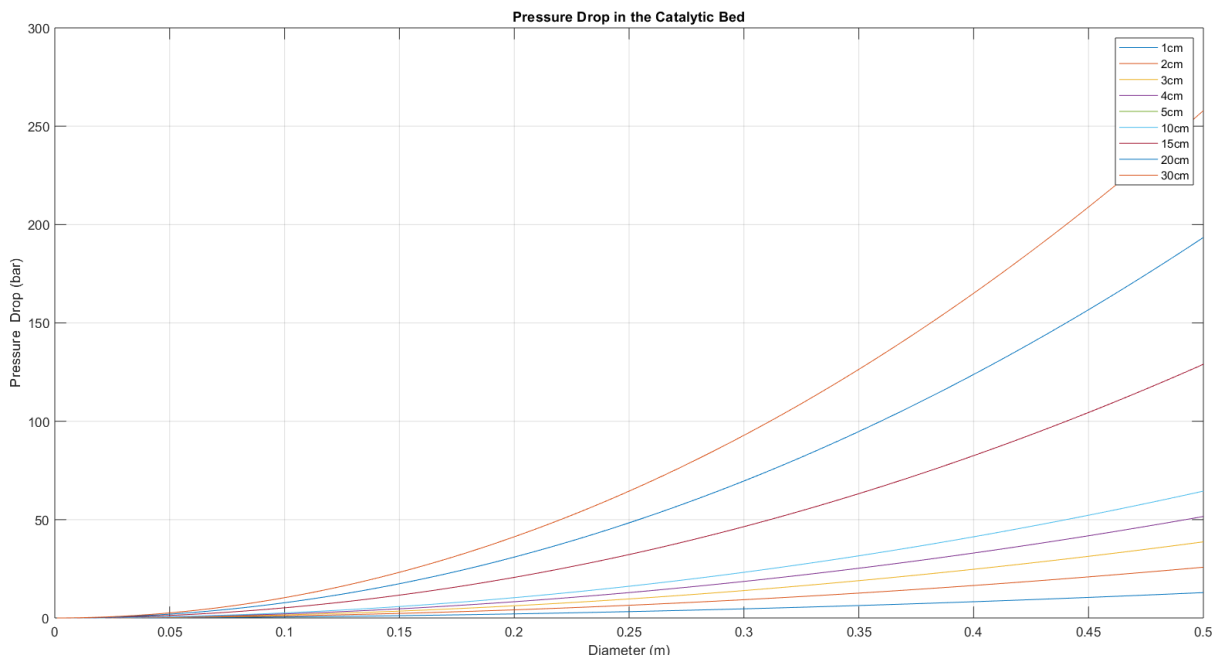


Figure 10.11: Pressure drop depending on the size of the catalyst bed

We see on the graph that the pressure drop rise quickly with the size of the bed. So we need to limit the size of our catalyser in order to not oversize the turbo pump. To do so, we chose to limit our pressure drop to around 30 bars. Finally we obtain a cylinder of 20 cm of diameter and 20 cm of length.

This geometry allows the catalyser to provide a sufficient decomposition rate, a "contained" pressure drop and size. It also generates a great heat as high as 1000K at the exit of the catalyst bed.

10.6 Injectors

To design our injectors we made some research and went through the literature about injector for hypergolic injector. We found interesting results in this paper³. Their goal was to design a small attitude control system hydrogen peroxide/RP-1 thruster, to do so they compared two main different kind of injectors; the coaxial shear injector and the coaxial-swirl injector.

After simulation the results were that coaxial shear causes the combustion chamber to be divided into three different zones, these zones are: rapid high-temperature pyrolysis, oxidization and equilibrium flow. This kind of separation can cause serious bad behaviors during the combustion process and creates issues like flame-out, explosion or very poor efficiency.

In order to avoid these kind of behaviors the use of swirl-coaxial injectors is the best choice to make.

The concept of the swirl injector is pretty simple. Indeed, it's based on a coaxial injection but instead of injecting the two propellant in the axis of the injector, here the two propellant are injected radially in what is called the vortex chamber. The radial injection combine with the chamber allows to create a vortex of H_2O_2 and RP-1 which result in a generation of a plume of propellant at the exit of the injector. In addition, due to the geometry of such an injector, the reduction of diameter at the exit, the atomization is very easy.

³The design and main performance of a hydrogen peroxide/kerosene coaxial-swirl injector in a lab-scale rocket engine (2017)

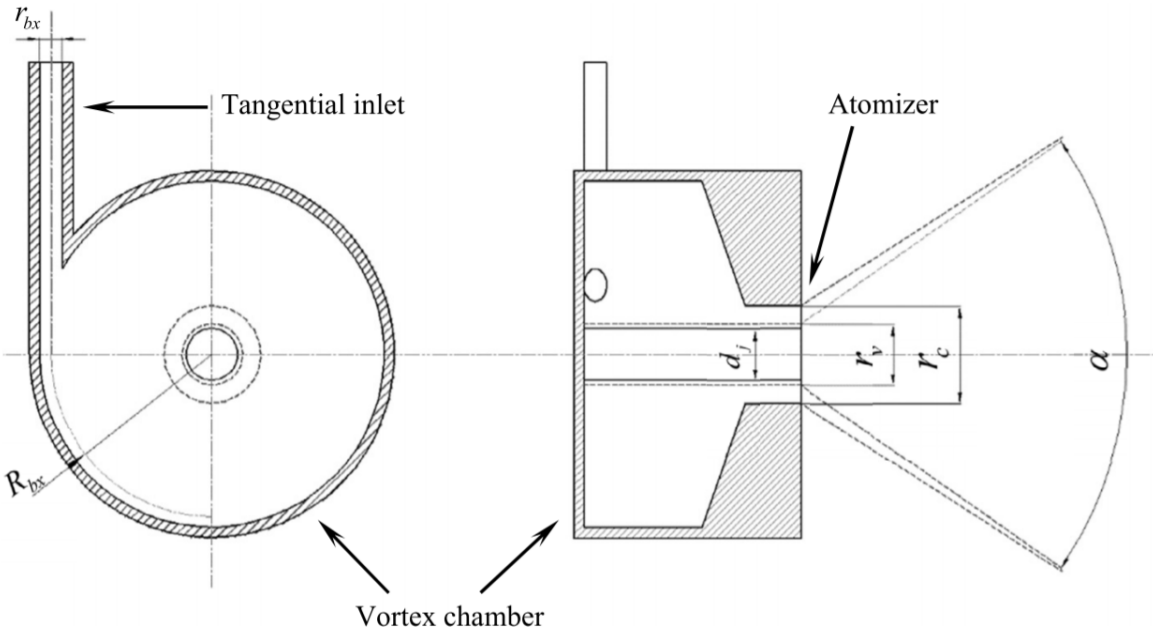


Figure 10.12: Cross section of a swirl injector

The schematic before shows how a swirl injector works. We see that there is only few parameters to take into account to design this kind of injector. These different parameters will be explain later on.

Our injection will be a liquid-gas injection but this characteristic is not really a problem for a swirl injector as the two propellant will behave the same way as a liquid or a gas.

In addition of these advantages the swirl injector offers other non-negligible advantages that it allows us to improve our efficiency. Indeed, the study shows that a swirl injector increases the combustion stability and efficiency up to 10% which result in a better fuel consumption during the operating time of the spacecraft.

10.7 Feeding system

After having designed most of our propulsion system. We need to carefully link them by designing our feeding system. The biggest challenge is to create a system that will both fit in our spacecraft and deliver the right amount of propellant from the tanks to the engine through our different, required other subsystems.

The general pressure loss in a system is given by :

$$\Delta P = K \frac{\rho}{2} w^2$$

With K depending on the type of change in system geometry as follow :

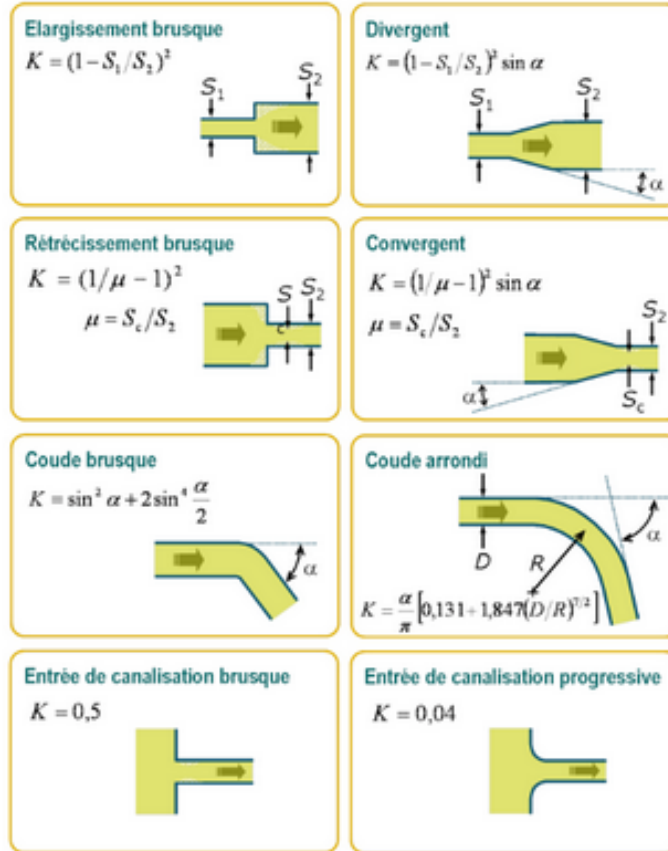


Figure 10.13: K values for geometry changes

In our case, we will use the progressive line entering loss $K = 0.04$ and the bends $K(\alpha) = \sin^2(\alpha) + 2 \sin^4 \left(\frac{\alpha}{2} \right)$. Another K will also be used for the entrance of the injector, which will be specified later on.

For manufacturing costs and simplicity purposes, we choose to only use 45° bends which will result in $K_{bends} = 0.5429$.

With that and the length measurements in mind, we designed the following feeding system layout for which we will then calculate the pressure variations along it :

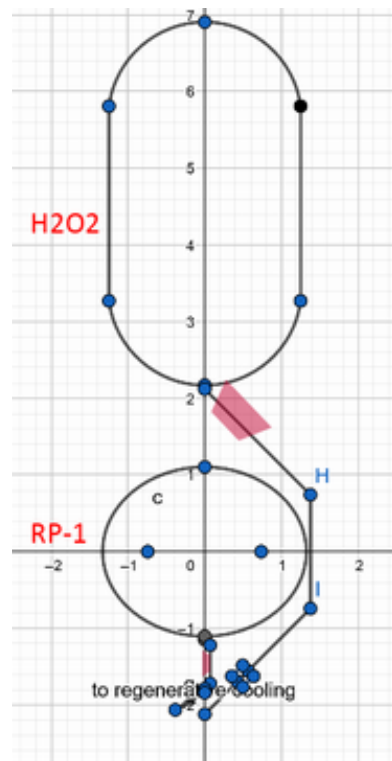


Figure 10.14: Feeding system layout (To scale)

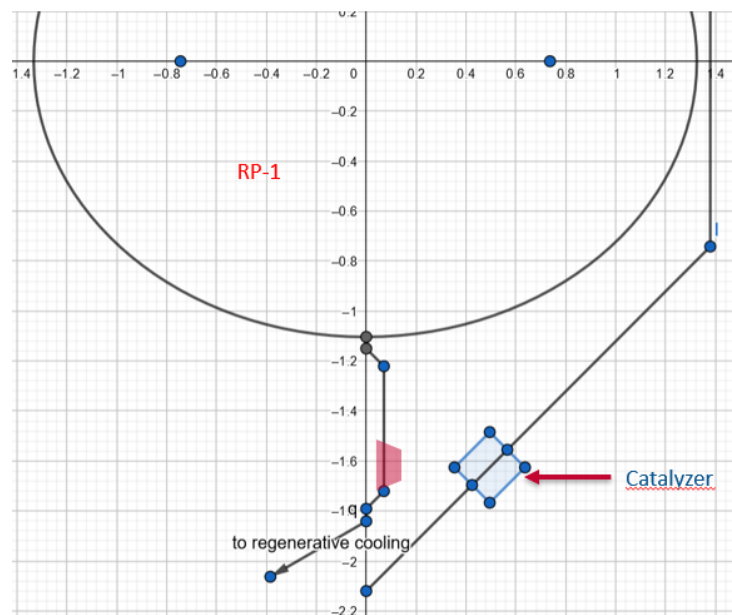


Figure 10.15: Feeding system layout - Zoomed (To scale)

10.7.1 Line diameters

In order to choose our line diameters, we can first use our volume flow and then get the line area from it and then at the end, the line diameter.

Fuel

$$\dot{V}_f = \frac{\dot{m}_f}{\rho_f} = 0.0015298 m^3/s \quad (10.25)$$

$$A_{line_f} = \frac{\dot{V}_f}{w_f} = 5.21 \times 10^{-5} mm^2 \quad (10.26)$$

$$d_{line_f} = 2\sqrt{\frac{A_{line_f}}{\pi}} = 8.1447 mm \quad (10.27)$$

As we are trying to insure a high injection velocity and to insure a certain margin in pressure and velocity, we will choose a line diameter of 7 mm for the fuel feeding system.

Oxidizer

$$\dot{V}_o = \frac{\dot{m}_o}{\rho_o} = 0.006042 m^3/s \quad (10.28)$$

$$A_{line_o} = \frac{\dot{V}_o}{w_o} = 0.000275 mm^2 \quad (10.29)$$

$$d_{line_o} = 2\sqrt{\frac{A_{line_o}}{\pi}} = 18 mm \quad (10.30)$$

In this case, we will choose a line diameter of 15 mm for the oxidizer.

10.7.2 Fuel feeding system

The following items in our fuel feeding system will cause pressure drops :

- Tank exit : $K = 0.04$
- $4 \times 45^\circ$ bends : $K = 0.5429$ for each
- Straight line losses : $\Delta P = \frac{\rho}{2} w^2 f \frac{L}{D}$
- Friction coefficient : $f = 0.02$
- Regenerative cooling : $\Delta P = 0.25$ bar
- Fuel injection : $\Delta P = 9.3843$ bars

With our current layout, we have 5 straight lines which will cause pressure losses on the fuel side. Three of them are before the turbopump which is placed at the end of the

third straight section, right before the third bend. We consider a velocity of 8 m/s before the turbopumps and of $v_{inj} = 29.363$ m/s after. The line loss for each section is given by :

$$\Delta P = \frac{810}{2} w^2 \times 0.02 \times \frac{L_{section}}{0.007}$$

1. First section ($L_{section} = 0.05m$) : $\Delta P = 0.037029$ bar
2. Second section ($L_{section} = 0.1m$) : $\Delta P = 0.074057$ bar
3. Third section ($L_{section} = 0.5m$) : $\Delta P = 0.37029$ bar
4. Fourth section ($L_{section} = 0.1m$) : $\Delta P = 0.997699$ bar
5. Fifth section ($L_{section} = 0.05m$) : $\Delta P = 0.49884$ bar

There are also two different values for the bend losses depending on the position of the bend (before or after the turbopump), we have 2 of each :

- $\Delta P_{before} = 0.14072$ bar
- $\Delta P_{after} = 1.8957$ bar

The tank exit loss is :

$$\Delta P_{exit} = K_{exit} \times \frac{\rho F}{2} \times 8^2 = 0.010368 \text{ bar}$$

10.7.3 Oxidizer feeding system

The following items in our oxidizer feeding system will cause pressure drops :

- Tank exit : $K = 0.04$
- $4 \times 45^\circ$ bends : $K = 0.5429$ for each
- Straight line losses : $\Delta P = \frac{\rho}{2} w^2 f \frac{L}{D}$
- Friction coefficient : $f = 0.02$
- Catalyzer : $\Delta P = \text{bars}$
- Oxidizer injection : $\Delta P = 4.9599$ bars

On this part of the feeding system, we also have 5 sections and 4 bends of 45° each. We also consider a velocity of 8 m/s before the turbopump and 21.971 m/s after. However, due to the larger distances (due to our tank layout), the turbopump's position in the feeding system is different and is now positioned after the first bend, right at the beginning of

the second straight line. This results in 3 bends being at high velocity and 1 at relatively slower velocity.

Here, each straight line loss section is given by :

$$\Delta P = \frac{1450}{2} w^2 \times 0.02 \times \frac{L_{section}}{0.015}$$

With :

1. First section ($L_{section} = 0.05m$) : $\Delta P = 0.030933$ bar
2. Second section ($L_{section} = 1.95m$) : $\Delta P = 9.0992$ bars
3. Third section ($L_{section} = 1.4836m$) : $\Delta P = 6.9228$ bars
4. Fourth section ($L_{section} = 1.15m$) : $\Delta P = 5.3662$ bars
5. Fifth section ($L_{section} = 0.6m$) : $\Delta P = 2.7997$ bars

For the bends, we have :

- $\Delta P_{before} = 0.2519$ bar (1 of them)
- $\Delta P_{after} = 1.0614$ bar (3 of them)

The tank exit loss is :

$$\Delta P_{exit} = K_{exit} \times \frac{\rho_o}{2} \times 8^2 = 0.01856 \text{ bar}$$

10.8 Turbo pumps

As most of our subsystems have a defined pressure drop due to their specific design, we have made the choice to use this feeding system design with all losses included to then design our turbopumps to have a pressure rise in accordance with our pressure requirements. We chose to go with electrically driven turbo pumps as we have a good amount of electrical power since we use fuel cells in our spacecraft.

Our respective turbopump required created pressures are :

- Fuel side : $\Delta P_{T_f} = P_{Chamber} + \Delta P_{feeding_f} + \Delta P_{inj_f} + \Delta P_{Regenerative cooling} - P_{Tank_f}$
- Oxidizer side : $\Delta P_{T_o} = P_{Chamber} + \Delta P_{feeding_o} + \Delta P_{inj_o} + \Delta P_{Catalyzer} - P_{Tank_o}$

Thus,

$$\Delta P_{T_f} = 54.395 \text{ bars} \quad (10.31)$$

$$\Delta P_{T_o} = 102.28 \text{ bars} \quad (10.32)$$

Considering an efficiency of 0.9×0.75 , with 0.9 for the electrical part and 0.75 for the mechanical part, we get the following powers :

$$Power_{fuelpump} = \dot{m}_f \frac{P_{T_f}}{\rho_F \eta} = 13\ 461 \text{ W} \quad (10.33)$$

$$Power_{Oxpump} = \dot{m}_o \frac{P_{T_o}}{\rho_o \eta} = 96\ 030 \text{ W} \quad (10.34)$$

Considering a maximum continuous burn time of 900 seconds, we get the following energy with a 40% margin as we are still unsure about the performance of such turbopump :

$$E_{kWh} = \frac{(Power_{fuelpump} + Power_{Oxpump}) \times 900}{3.6 \times 10^6} = 38.322 \text{ kWh} \quad (10.35)$$

We also know the following vapor pressures :

- H_2O_2 : 666.612 Pa at 30° C
- $RP - 1$: 700 Pa between 20°C and 25° C

With the information we have, we can calculate the pump head rise and the NPSH.

$$H_{p_{Fuel}} = \frac{\Delta p_{p_{Fuel}}}{g_0 \rho_{Fuel}} = 747.474 \text{ m} \quad (10.36)$$

$$H_{p_{Ox}} = \frac{\Delta p_{p_{Ox}}}{g_0 \rho_{Ox}} = 754.192 \text{ m} \quad (10.37)$$

$$NPSH_{Fuel} = \frac{p_{i_{Fuel}} - p_{v_{Fuel}}}{g_0 \rho_{Fuel}} = 6.569 \text{ m} \quad (10.38)$$

$$NPSH_{Ox} = \frac{p_{i_{Ox}} - p_{v_{Ox}}}{g_0 \rho_{Ox}} = 7.0465 \text{ m} \quad (10.39)$$

We can then get the number of stages :

$$n = 1 + \text{floor}\left(\frac{\Delta p_p}{\Delta p_{ps}}\right) \quad (10.40)$$

Thus, using $\Delta p_{ps} = 47 \times 10^6 \text{ Pa}$,

$$n_{Fuel} = 126\ 373 n_{Ox} = 228\ 256 \quad (10.41)$$

We can also get the rotation speeds :

$$N_{Fuel} = 1.636 \text{ rad/s} = 15.623 \text{ RPM} \quad (10.42)$$

$$N_{Ox} = 0.532 \text{ rad/s} = 5.079 \text{ RPM} \quad (10.43)$$

Then

$$u_{t_{Fuel}} = \sqrt{\frac{gH_{p_{Fuel}}}{n\psi}} = 0.325 \text{ m/s} \quad (10.44)$$

$$u_{t_{Ox}} = \sqrt{\frac{gH_{p_{Ox}}}{n\psi}} = 0.243 \text{ m/s} \quad (10.45)$$

$$D_{2t_{Fuel}} = \frac{u_{t_{Fuel}}}{N_{r_{Fuel}}} = 0.199 \text{ m} \quad (10.46)$$

$$D_{2t_{Ox}} = \frac{u_{t_{Ox}}}{N_{r_{Ox}}} = 0.457 \text{ m} \quad (10.47)$$

$$D_{1t_{Fuel}} = \sqrt[3]{\frac{\frac{4}{\pi}Q_{Fuel}}{\phi N_{r_{Fuel}}(1-L^2)}} = 2.197 \text{ m} \quad (10.48)$$

$$D_{1t_{Ox}} = \sqrt[3]{\frac{\frac{4}{\pi}Q_{Ox}}{\phi N_{r_{Ox}}(1-L^2)}} = 6.131 \text{ m} \quad (10.49)$$

10.9 Pressure evolution summary

10.9.1 Fuel side

Contributor	Pressure Drop (bars)	Pressure at the end of this part (bars)
Tank	NA	1.3
Tank exit	0.010368	1.29
First section	0.037	1.253
First bend	0.14	1.113
Second section	0.074	1.039
Second bend	0.14	0.899
Third section	0.37	0.529
Turbopump	54.395 (Rise)	59.924
Valve	5	54.924
Third bend	1.8957	53.0283
Fourth section	0.997	52.0313
Fourth bend	1.8957	50.1356
Fifth section	0.499	49.6366
Cooling	0.25	49.3866
Injection	9.38	40.0066
Combustion chamber	NA	40.0066

Table 10.9: Pressure evolution on fuel side

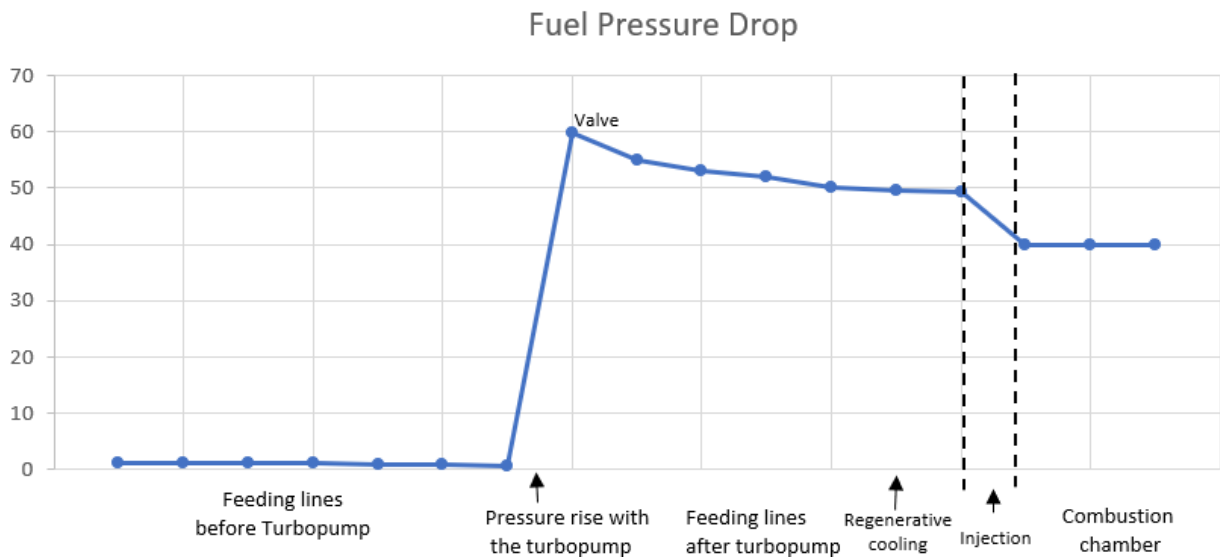


Figure 10.16: Pressure evolution on fuel side (bars)

10.9.2 Oxidizer side

Contributor	Pressure Drop (bars)	Pressure at the end of this part (bars)
Tank	NA	1.3
Tank exit	0.010368	1.29
First section	0.031	1.259
First bend	0.25	1.009
Turbo pump	102.28 (Rise)	108.289
Turbo pump	5	103.289
Second section	9.09	94.199
Second bend	1.06	93.139
Third section	6.9228	86.2162
Third bend	1.06	85.1562
Fourth section	5.366	79.7902
Fourth bend	1.06	78.7302
Fifth section	2.7997	75.9305
Catalyzer	30.95	44.9805
Injection	4.96	40.0205
Combustion chamber	NA	40.0205

Table 10.10: Pressure evolution on fuel side

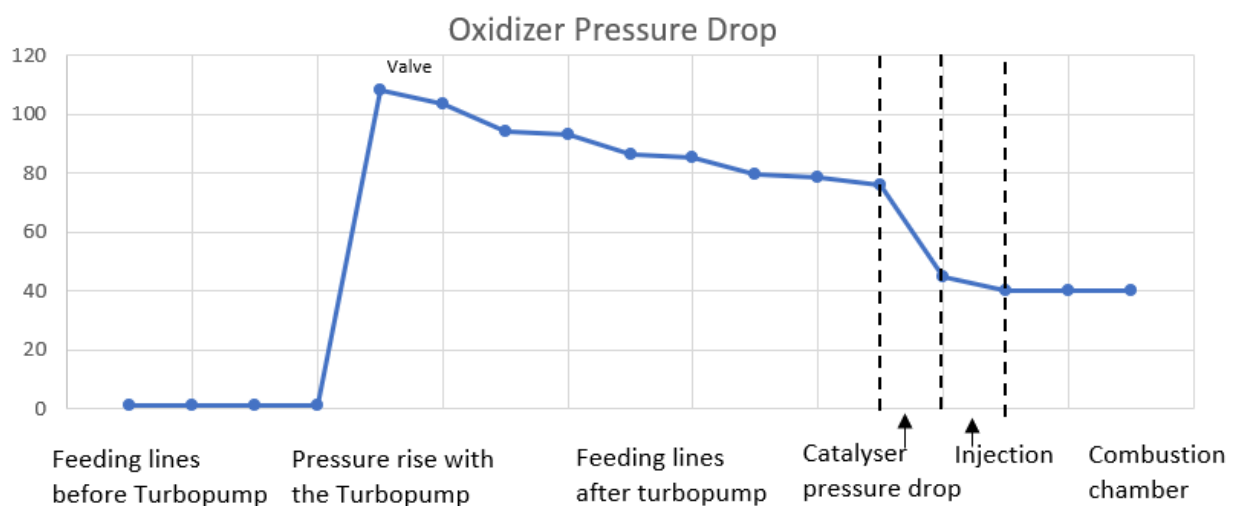


Figure 10.17: Pressure evolution on oxidizer side (bars)

10.10 Engine

10.11 Nozzle

Chapter 11

Simulations

11.1 Engine performance simulation

In order to simulate the engine performance, the largest single burn was simulated. As the initial burn for entering a Geostationary Transfer Orbit would require more than 900 s of engine burn time due to the large starting mass of the spacecraft, roughly half of this initial burn was simulated. An immediate result of the requirement to limit engine burn time to 900 s is therefore, that the first burn needs to be split into two burns. The engine simulation aims to determine thrust, acceleration, Δv and propellant masses over time. A combined MATLAB[®] / Simulink[®] was used, calculating thrust based on following equation:

$$F = \dot{m} \times C_F \times C^* \quad (11.1)$$

with :

$$C^* = \frac{p_c \times A_t}{\dot{m}}$$

and

$$C_F = \sqrt{\frac{2 \times \kappa^2}{\kappa - 1} \times \left(\frac{2}{\kappa + 1}\right) \times \left[1 - \left(\frac{p_e}{p_c}\right)^{\frac{\kappa-1}{\kappa}}\right] + \varepsilon \left(\frac{p_e - p_a}{p_c}\right)}$$

assuming a constant mass flow rate of $\dot{m} = 10 \text{ kg/s}$. Considering a constant chamber pressure after initial start-up of 40 bars and an exit pressure of 3900 Pa, which was determined using RPA, a steady-state thrust of 33.6kN was observed, as can be seen in Figure 11.1. κ was determined using RPA as well and, while varying slightly throughout the engine, assumed as constant to facilitate the simulation.

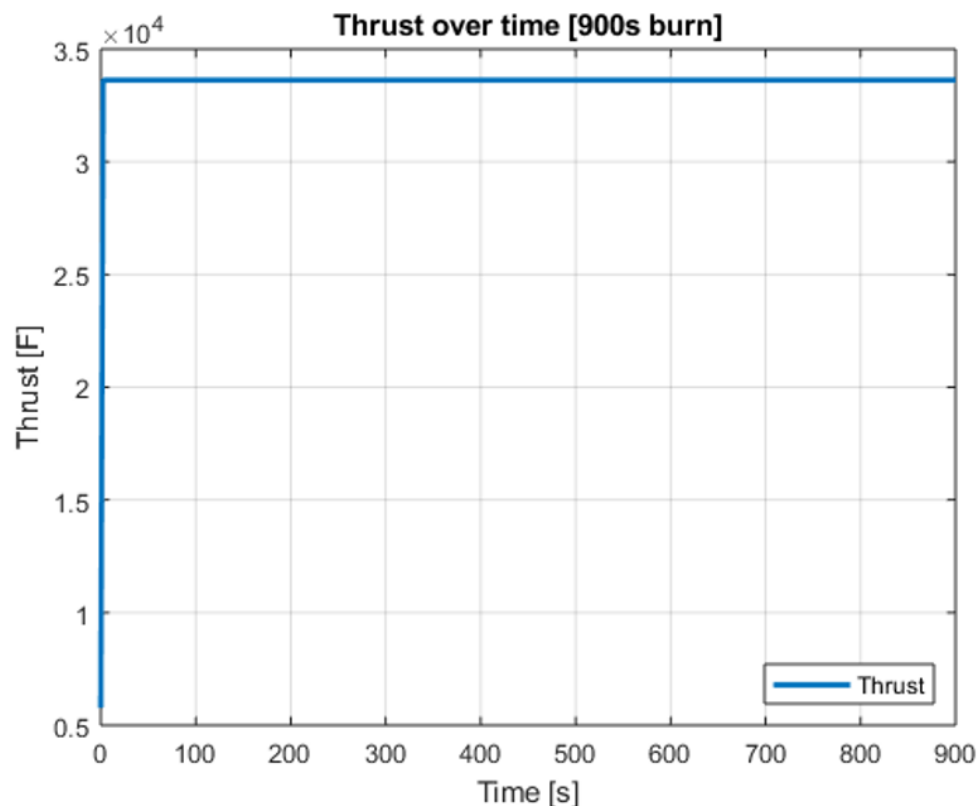


Figure 11.1: Engine simulation - Thrust over time

The resulting acceleration and Δv over time are shown in Figure 11.2.

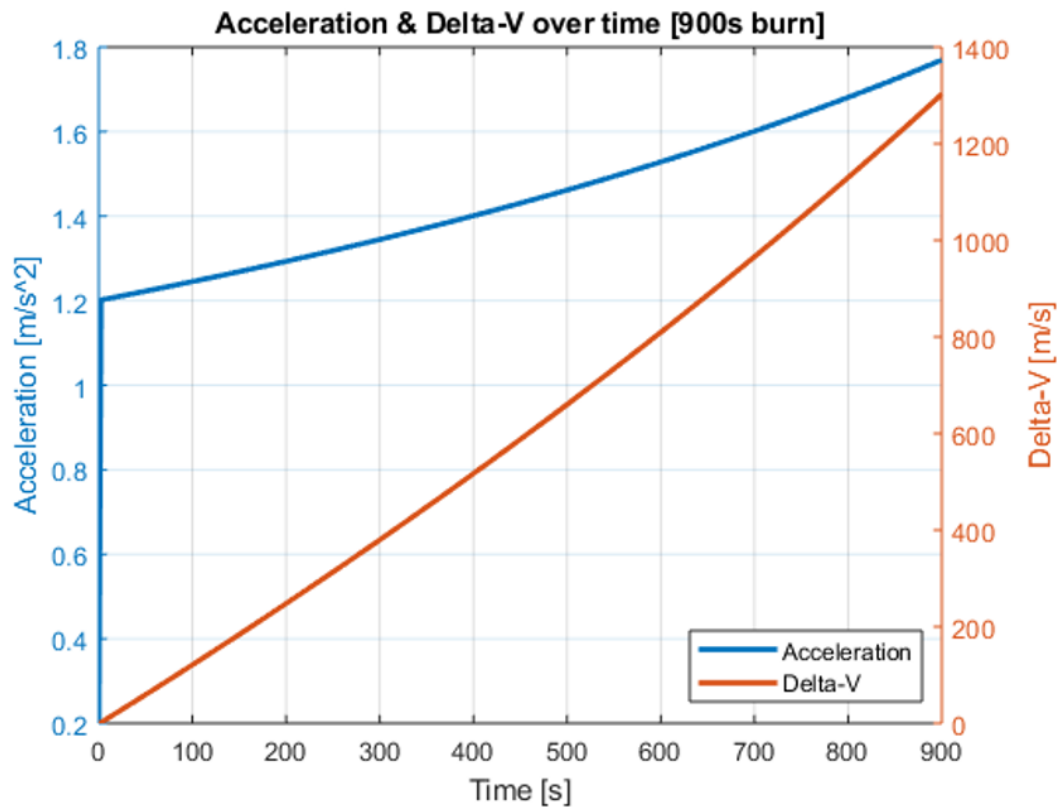


Figure 11.2: Engine simulation - Acceleration and Δv over time

The acceleration, shown in blue, starts off at around 1.2 m/s^2 , which is a value in the range of our expectations. After 900 seconds, the mass loss leads to a final acceleration of slightly below 1.8 m/s^2 , when a Δv of ca. 1300 m/s is reached. At the point of discovery of the insufficiency of 900 s, the decision to divide the first burn into two was taken. Lastly, the behavior of the propellant masses is portrayed in Figure 11.3.

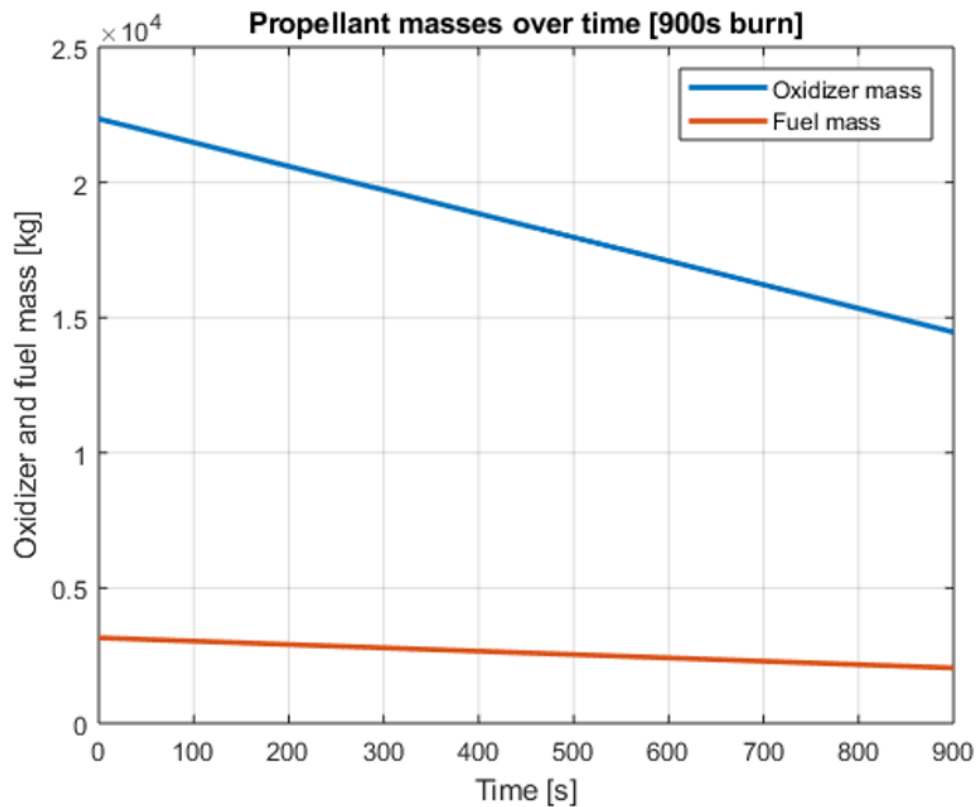


Figure 11.3: Engine simulation - Propellant masses over time

With roughly one third of the total usable propellant having been burnt throughout 900 seconds of burn time, these results are also according to expectations. The simulation of the maximum burn time is representative of the entirety of burns throughout the mission, therefore it validates the viability of the engine design for the fulfillment of mission requirements. The complete simulation script and model can be found in the annex.

11.2 Regenerative cooling simulation

The thermal loads of the engine combustion are managed by regenerative cooling of the engine, with the cooling channels running along axial lines throughout the entire length of the engine. The cooling liquid is the engine fuel (RP-1), being fed into the combustion chamber wall and running along cooling channels with varying cross-section area before exiting at the end of the nozzle. The cooling channel design was determined by simulation of the relevant wall temperatures in steady-state operation, where a temperature at a given location does not change over time, with heat flux in and out being equal. Following assumptions and design choices were made before and during the preliminary calculations:

- The inner engine wall is made of copper throughout the entire engine
- The outer wall is made of steel
- A defined number of symmetrical rectangle-shaped cooling channels run through the engine wall, with varying cross-section to allow for higher and lower thermal flux at different sections
- The cooling channels are symmetrical w.r.t. to the engine propellant flow axis
- Injection into the cooling channels takes place at the combustion chamber end of the engine, in order to create larger heat transfer at more thermally stressed areas due to lower coolant temperature
- **The RP-1 is assumed to not change phase during the regenerative cooling**
(While this decreases simulation accuracy, too little data on high-pressure RP-1 phase change behaviour was available. The temperature does however affect the liquid's heat capacity within the simulation)

In order to simulate the steady-state thermal behaviour of the engine along its length, some simplifications needed to be conducted. All coefficients (e.g. ratio of specific heat capacities) are assumed to be constant throughout each section, with three different values for the combustion chamber, throat area and nozzle respectively. In addition, all time-related values were transformed into distance-based values, so that the simulation time is actually millimetres, instead of seconds. This was achieved by limiting the simulation time to the engine length in millimetres and using switches to change constants based on what section the propellant is in at any given millimetre value, while using the flow velocity as the key parameter to transform into metres. The simulation script, model and complete results can be found in the annex. At this point, only some key conclusions will be presented and discussed.

The central aim of the iterative calculation was to determine a combination of material, wall thickness and cooling channel geometry which allows the inner wall temperature to remain below its maximum operating temperature. All other temperatures, like the coolant

and outer wall temperatures, were of secondary importance. Due to its high thermal conductivity, copper was chosen as the inner wall material.

The cooling channel cross-section was defined to always be equally sized relative to the local engine diameter, with the ratio being a function of the local engine wall cross-section area and a factor, which represents the filling grade. Figure 11.4 shows the cross-section change over the engine length. The rectangular geometry is defined by a ratio of width to height of 5.

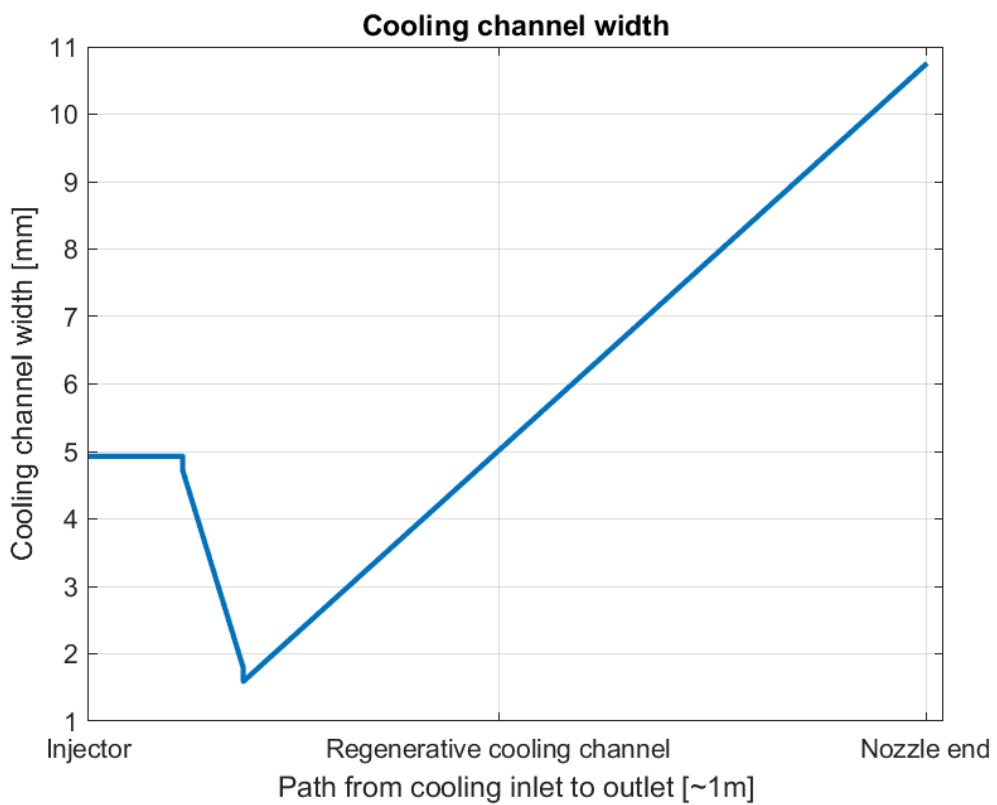


Figure 11.4: Regenerative cooling simulation - Cooling channel width over engine length

The final cooling channel system is a compromise between the copper wall temperature and minimum necessary material for weight savings. Therefore, the copper wall has a thickness of 6 mm in the combustion chamber, 7 mm in the throat area and 5 mm in the nozzle section. The resulting relevant temperatures can be seen in Figure 11.5.

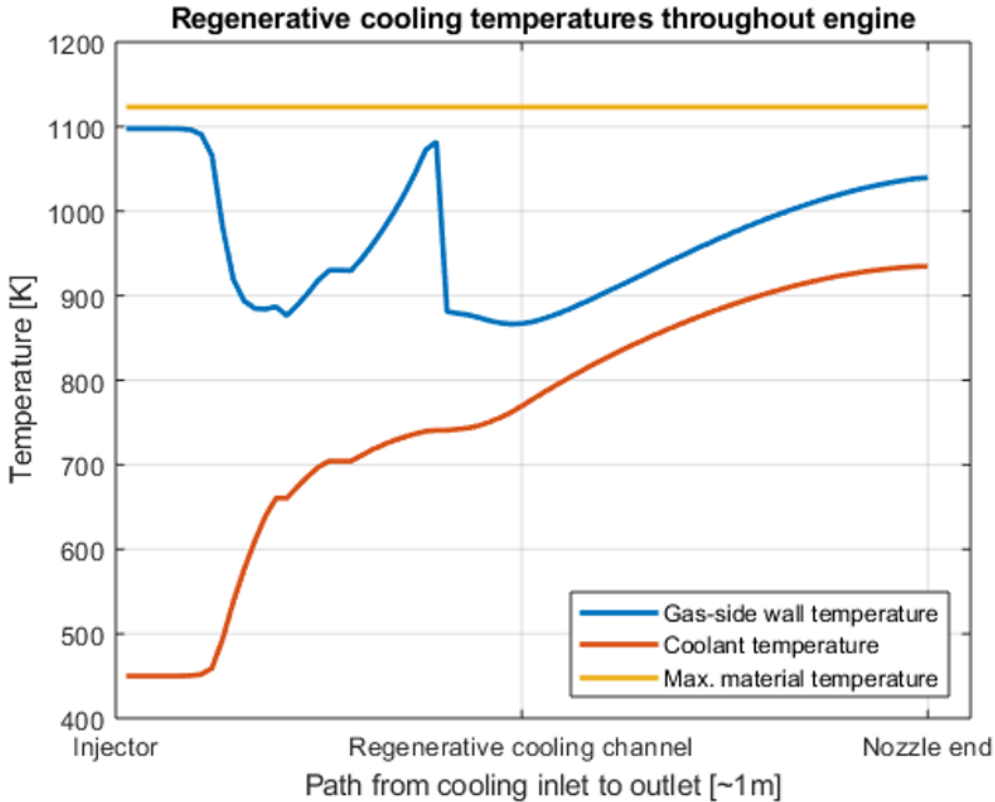


Figure 11.5: Regenerative cooling simulation - Relevant temperatures

The highest temperatures can be observed in the combustion chamber section, as low flow speeds cause less convective heat transfer to take place, reducing the overall heat flux. The gas-side wall temperature then drops in the beginning of the throat area, before rising again towards the throat. After passing the throat, the gas-side wall temperature drops sharply and then rises again towards the nozzle exit.

11.3 Hydrogen peroxide decomposition simulation

As mentioned in section 10.3, the decomposition of hydrogen peroxide is used for self-pressurization of the oxidizer tank as well as power generation in a fuel cell in combination with hydrogen. As hydrogen peroxide is not only decomposing, but the decomposition is also an exothermal process, the thermal control system needs to be well under control in order to avoid critical behavior of the hydrogen peroxide if 150° C are exceeded. Therefore, a detailed simulation has been performed, taking wall thicknesses, materials, radiative and absorbing coefficients as input parameters. The simulation is structured like a control system, calculating the temperature of the hydrogen peroxide inside the tank, the cold and hot wall temperatures. Upon reaching the specified target temperature, the control loop

rotates the spacecraft to a neutral degree for constant hydrogen peroxide temperature. Before discussing the results, an overview of the simplifications taken for facilitation of the simulation follows:

- Inside the tank, only vaporization takes place, no condensation
- The space craft can rotate to any angle instantaneously and there is no modelling of the necessary thruster activation
- The cold and hot walls are always at a homogenous temperature, only depending on heat flux between hydrogen peroxide, the walls, the sun and dark space
- As the structural calculations needed to be complete before the simulation was able to prove the technical feasibility of the decomposition regulation, **the hydrogen peroxide tank is assumed to be made of only one material throughout the rest of the documentation, while the simulation allows for two different materials**, as different heat flux coefficients are advantageous. Therefore, the results of this simulation are not exactly compatible with the final space craft design and more of a proof of concept, to be reunited with the structural design as a next step.

The simulation showed that, with the simplifications taken, a control system maintaining the hydrogen peroxide pressure at an acceptable level is technically feasible. A control reaction to raising the temperature from 310 K to 350 K has been chosen as the case for technical feasibility demonstration. As explained in section 10.3, the rotational angle of the space craft is the dictating parameter for heat input and output. Figure 11.6 shows the rotational angle, resulting H₂O₂ pressure, the relevant temperatures and the generated energy considering consumption of all generated oxygen in the fuel cell. The four graphs are outputs of the same simulation, the complete script and model for which can be found in the annex. The initial values for the integration blocks, which output temperatures, are all assumed.

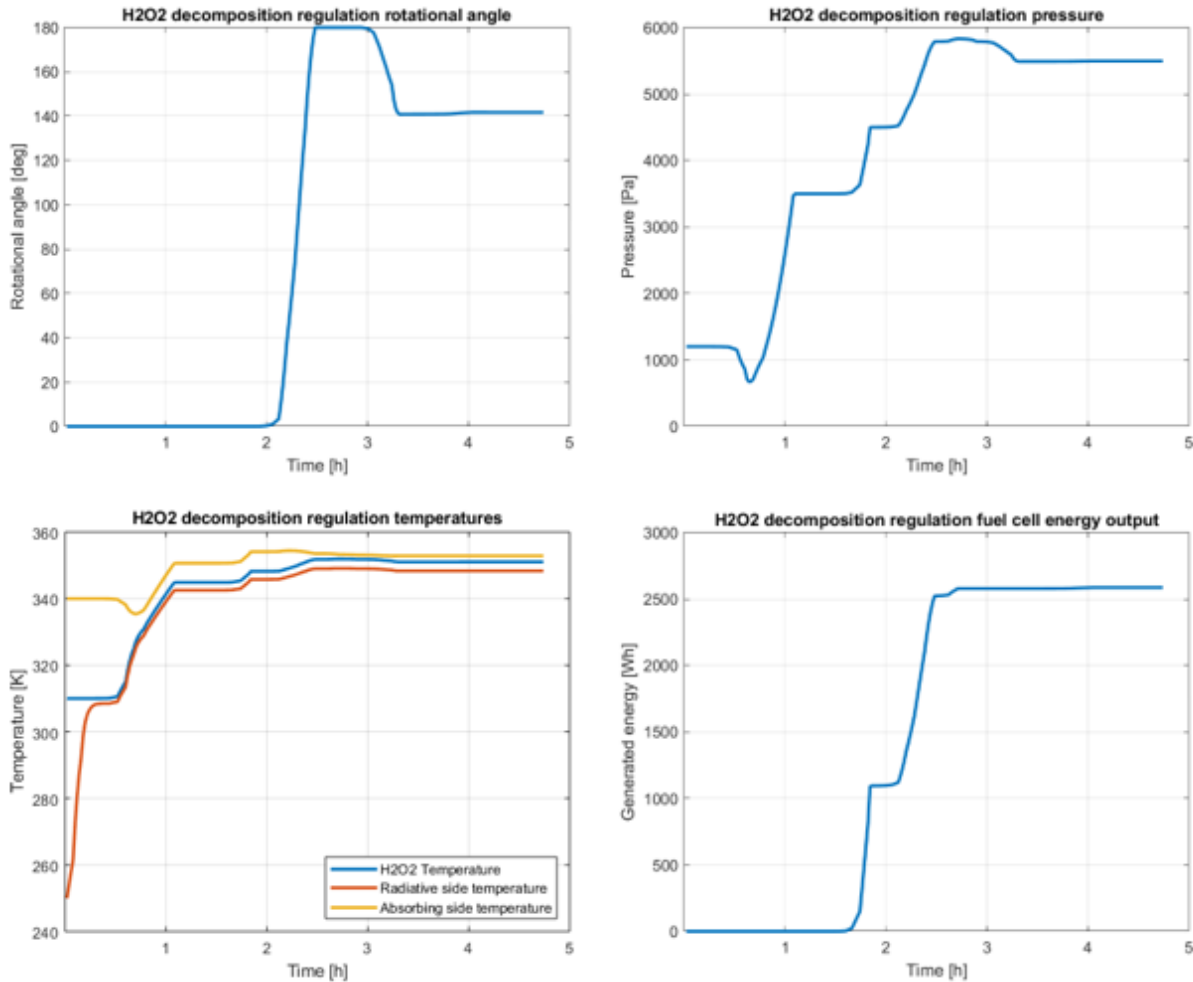


Figure 11.6: Demonstration case for technical feasibility of H_2O_2 decomposition regulation

As the simulation results show, the rotational angle is initially maintained at 0° , meaning full exposure of the more absorbing side towards the sun, with the less radiative side facing dark space. After 2 hours, the space craft turns towards the other side, decreasing the heat flux gradually while approaching the target temperature. In the end, a constant neutral rotational angle of 140° is maintained, with a final control error of around $1 - 2$ K. After this process, 2,5 kWh of energy were generated, while the pressure inside the tank has risen from around 1000 Pa to 5500 Pa. The tank pressure is determined via interpolation of temperature-dependent vaporization pressures to gain a function of pressure with respect to temperature.

Chapter 12

Evaluation

12.1 Requirement verification

The top level requirements were already defined at the beginning of the project. In the end of the project it was verified whether the requirements were fully fulfilled, partially fulfilled or not fulfilled (See Figure 12.1). Some of the requirements have to be confirmed (TBC), since the result can only be stated after first launch.

Operation		
TL-1 provide sufficient thrust for completion of the mission profile including a safety margin.	OK	Delta v and thrust match the mission
TL-2 re-ignitable at least 1000 times.	TBC	
TL-3 service life time of at least 100 missions or 25 years in orbit	TBC	
TL-4 ignition and functional reliability shall be higher than 99,5%.	TBC	
Environment		
TL-5 withstand the launch phase	OK	Accelerations were taken into account
TL-6 operate in vacuum	OK	
TL-7 withstand temperature gradients results from areas turned towards or away	OK	Simulated and used for H2O2 decomposition
TL-8 sustain space-related radiation throughout its complete life time	TBC	
TL-9 able to withstand debris impact of objects under 1cm of diameter with a maximum relative speed of 15km/s	TBC	
Vehicle		
TL-10 The engine shall be the main propulsion system of a GEO satellite recovery vehicle.	OK	
TL-11 refuelable between missions	OK	
TL-12 perform aerobreak maneuvers in earth's atmosphere	OK	
TL-13 control its flight path in earth's atmosphere using non-propulsive flight control systems	OK	
TL-14 remain within the ARIANE 6/Falcon 9 payload launch capabilities to LEO.	OK	
TL-15 remain on its guided trajectory with less than 0.1% deviation.	TBC	

Figure 12.1: Requirements for the vehicle

12.2 Lessons learnt

At the end of the project, a lessons learned session was performed to summarize the major problems and issues during the whole project work. The result can be found in Figure 12.2.

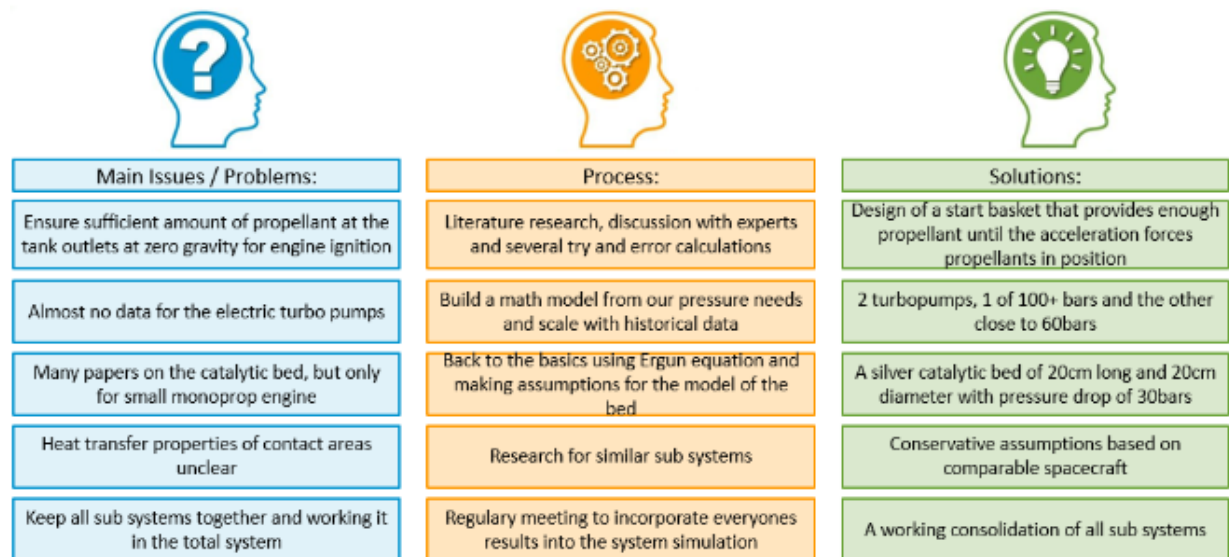


Figure 12.2: Lessons learnt

List of Figures

1.1	Initial schedule	3
1.2	Final schedule - comparison as planned and as achieved	4
3.1	Falcon 9 - Ariane 6 - combined fairing	8
4.1	Mission planning - First part	14
4.2	Mission planning - Second part	15
5.1	CAD of a capturing magnet	18
5.2	Capturing sequence (not to scale)	19
6.1	Shape effect on drag	24
6.2	Shadowgraph images of Reentry vehicles	27
6.3	Radiative cooling of the heat shield	29
6.4	GREDER Spacecraft (various views) - Heat shield sown in gray	30
8.1	Vehicle design 3D-Render	39
8.2	Vehicle architecture - Tank section	40
10.1	Flow Schematic - Pressurization system	54
10.2	Flow Schematic - Engine section	55
10.3	RCS thruster repartition	56
10.4	Lessons learnt	59
10.5	Different propellant tank design options	67
10.6	Final propellant tank design detailed view	68
10.7	Final propellant tank design full view	69
10.8	Final propellant tank design full view	70
10.9	H_2O_2 chemical decomposition process	75
10.10	Example of catalyst bed	75
10.11	Pressure drop depending on the size of the catalyst bed	76
10.12	Cross section of a swirl injector	78
10.13	K values for geometry changes	79
10.14	Feeding system layout (To scale)	80

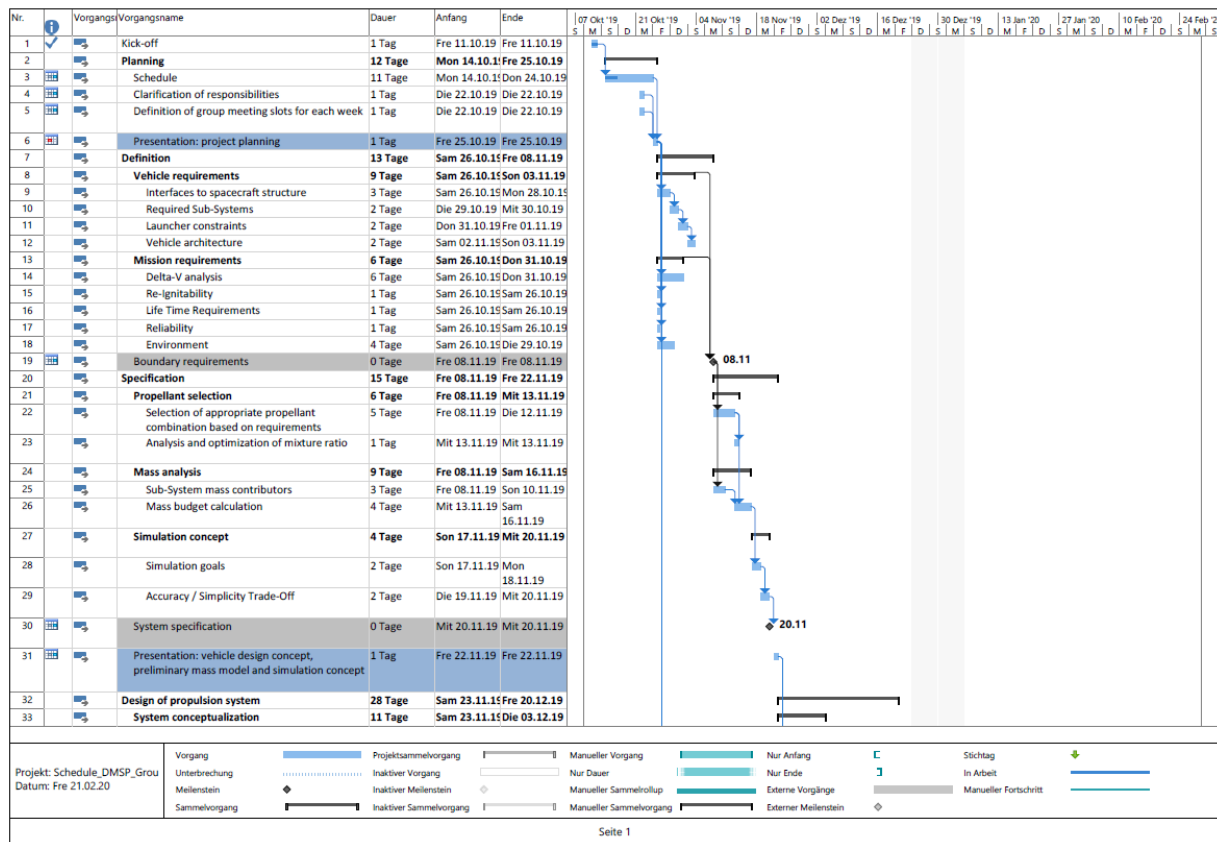
10.15 Feeding system layout - Zoomed (To scale)	80
10.16 Pressure evolution on fuel side (bars)	86
10.17 Pressure evolution on oxidizer side (bars)	87
11.1 Engine simulation - Thrust over time	90
11.2 Engine simulation - Acceleration and Δv over time	91
11.3 Engine simulation - Propellant masses over time	92
11.4 Regenerative cooling simulation - Cooling channel width over engine length	94
11.5 Regenerative cooling simulation - Relevant temperatures	95
11.6 Demonstration case for technical feasibility of H_2O_2 decomposition regulation	97
12.1 Requirements for the vehicle	98
12.2 Lessons learnt	99
12.3 Gantt Schedule	104

List of Tables

2.1 Requirements for the vehicle	6
4.1 Mission planning options	13
6.1 Comparison of materials for heat shield	22
7.1 Propellant combinations overview	33
7.2 Detailed propellant comparison MON/MMH and H ₂ O ₂ /RP-1	35
7.3 Historical data of flight H ₂ O ₂ /RP-1 engines	36
9.7 Initial mass budget	44
9.10 Frozen information	48
9.11 Coefficients and masses after steps	49
9.13 Mass budget - Electrical systems	50
9.14 Mass Budget - Attitude Control	51
9.15 Mass Budget - Propulsion	51
9.16 Final mass budget	51
9.17 Masses after step	52
10.1 Propellant masses and volumes	63
10.2 PTA driving requirements	63
10.3 PTA pressure loads	64
10.4 PTA pressure cycles	64
10.5 Propellant tank materials	65
10.6 Preliminary tank stresses calculation	73
10.7 Helium liner tank specification	74
10.8 Helium liner tank specification	74
10.9 Pressure evolution on fuel side	86
10.10 Pressure evolution on fuel side	87

Annexes

Annex I - Gantt Schedule



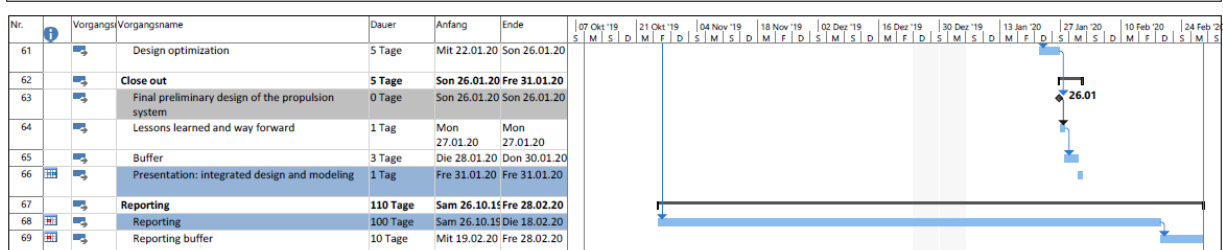
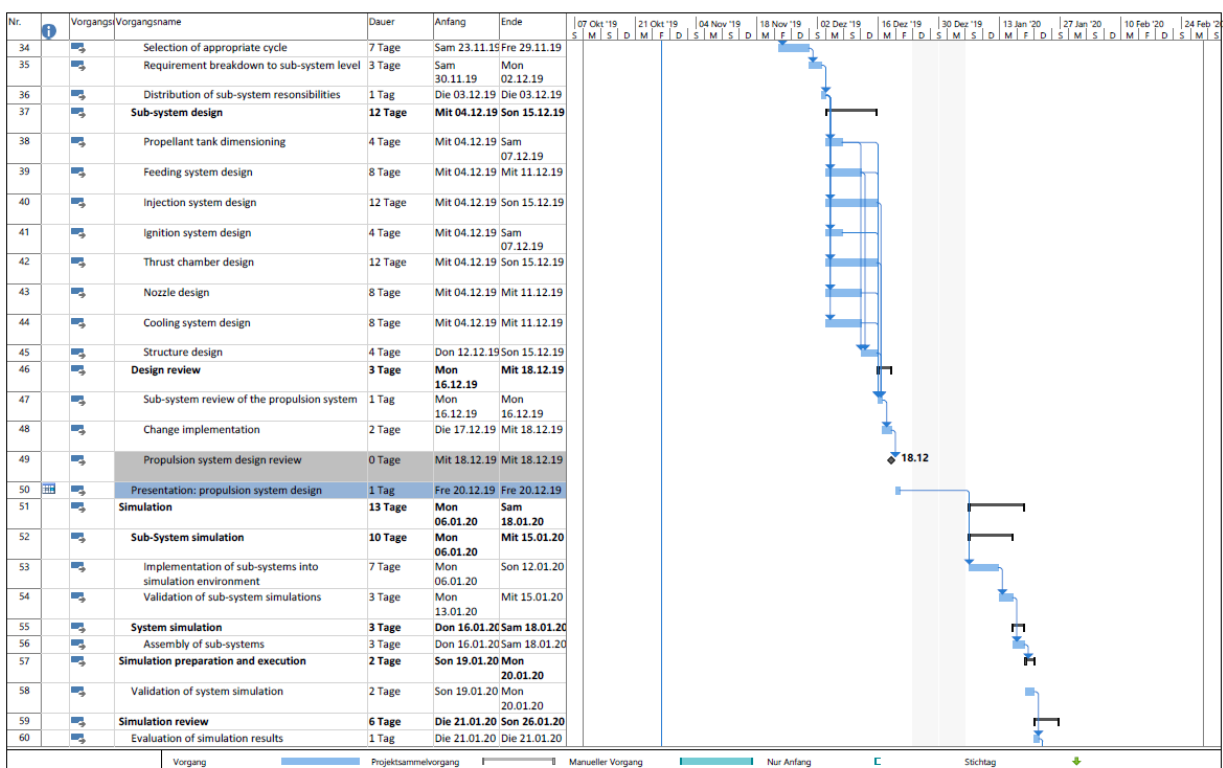


Figure 12.3: Gantt Schedule

Sources

1. <http://braeunig.us/space/propel.htm>
2. <http://astronautix.com/l/loxkerosene.html>
3. https://en.wikipedia.org/wiki/Liquid_rocket_propellant#Bipropellants
4. <http://www.astronautix.com/h/h2o2kerosene.html>
5. Hydrogen Peroxide / Kerosene, Liquid-Oxygen / Kerosene, and Liquid-Oxygen / Liquid Methane for Upper Stage Propulsion, Paper, S. Krishnan* Universiti Teknologi Malaysia
6. <https://ntrs.nasa.gov/archive/nasa/casi.ntrs.nasa.gov/19720019028.pdf>
7. https://www.nasa.gov/centers/glenn/technology/fuel_cells.html
8. <https://www.ginerinc.com/regenerative-fuel-cell-systems>
9. <https://ntrs.nasa.gov/archive/nasa/casi.ntrs.nasa.gov/19990063763.pdf>
10. <http://www.esa.int/esapub/bulletin/bullet90/b90dudle.htm>
11. <https://www.sciencedirect.com/science/article/abs/pii/S0360319904003106>
12. <http://citeseerx.ist.psu.edu/viewdoc/download?doi=10.1.1.526.3797&rep=rep1&type=pdf>
13. http://juser.fz-juelich.de/record/135459/files/HP3d_3_Ranjbari.pdf
14. <https://www.sciencedirect.com/topics/chemistry/proton-exchange-membrane-fuel-cells>
15. <http://www.dartmouth.edu/~cushman/courses/engs37/FuelCells.pdf>
16. https://ocw.mit.edu/courses/aeronautics-and-astronautics/16-851-satellite-engineering-fall-2003/lecture-notes/l3_scpowersys_dm_done2.pdf
17. Article : The design and main performance of a hydrogen peroxide/kerosene coaxial-swirl injector in a lab-scale rocket engine
18. Article : Design and Analysis of a Fuel Injector of a Liquid Rocket Engine
19. Article : The spray characteristic of gas-liquid coaxial swirl injector by experiment
20. <https://www.grc.nasa.gov/www/k-12/airplane/shaped.html>
21. TPSX NASA Material Properties Database : <https://tpsx.arc.nasa.gov/>
22. Columbia accident report : https://www.nasa.gov/columbia/home/CAIB_Vol1.html
23. An Internet Book on Fluid Dynamics - The Flat Plate Airfoil :
<http://brennen.caltech.edu/fluidbook/externalflows/lift/flatplateairfoil.pdf>
24. <https://de.wikipedia.org/wiki/Kesselformel>
25. Paper: THE NEW “DYNAMIC BEHAVIOR OF LIQUIDS IN MOVING CONTAINERS”, Franklin T. Dodge, Southwest Research Institute, 2000

Abstract

With space debris becoming increasingly problematic, the GREDER is a spacecraft based in a 55° inclination LEO orbit, designed to deorbit nonoperational satellites from GEO orbit and back to Earth. The main focus during the design of this spacecraft is the will of creating a "Green" space deorbiter which results in an organized cluster of innovations working together. Among them are a clean $RP - 1/H_2O_2$ combination with electrically driven turbopumps and a smart management and multi purpose usage of the H_2O_2 .

Keywords : Space debris, Satellite, Liquid propulsion system, LEO, GEO, Oxygen Peroxide